Relevance of the abundance and redox state of Kelch13 for the artemisinin susceptibility of *Plasmodium falciparum*

Vom Fachbereich Chemie der Technischen Universität Kaiserslautern zur Verleihung des akademischen Grades

„Doktor der Naturwissenschaften“ (Dr. rer. nat.)

genehmigte Dissertation

D 386

TECHNISCHE UNIVERSITÄT KAISERSLAUTERN

vorgelegt von

Robin Schumann

Betreuer: Prof. Dr. Marcel Deponte

Datum der wissenschaftlichen Aussprache:

31. März 2021

Promotionskommission

Vorsitzender:	Prof. Dr. Antonio Pierik
1. Berichterstatter:	Prof. Dr. Marcel Deponte
2. Berichterstatter:	Prof. Dr. Jörg Fahrer

Affidavit

Hereby I declare that I have written this thesis by my own. Furthermore, I confirm that no other sources have been used than those specified in the thesis itself.
This thesis, in same or similar form, has not been available to any audit authority yet.

Kaiserslautern, 25.02.2021

Robin Schumann

Table of contents

Acknowledgements

I wish to express my deepest gratitude to my supervisor Prof. Dr. Marcel Deponte who gave me the opportunity to work on a very hot topic in malaria research. You convincingly guided and encouraged me to be professional. Your patience, motivation, enthusiasm and deep knowledge helped me in all the time of research.

Besides my supervisor, I would like to thank the rest of the thesis committee: Prof. Dr. Jörg Fahrer and Prof. Dr. Antonio Pierik.

My sincere thanks also goes to:

Julia Flock and Kim Remans for introducing me to the insect expression system,

Frederik Sommer and Markus Räschle for mass spectrometry measurements,

Florian Mahler for CD spectrum measurements,

and Nina Seiwert for fluorescence microscopy imaging.

Thanks to the Pierik lab for letting me use your equipment and rooms.

I would like to thank my fellow labmates and friends Fabian Geissel, Gino Turra, Luzia Schneider, Eileen Bischoff, Sophie Möhring, Sandra Specht, Linda Liedgens, and Doreen Knochenhauer for your ideas and your critical input on this project. With you, I could enjoy long working days and especially some cold drinks after.

Besonderer Dank gilt meiner Familie. Danke für eure Unterstützung, den Rückhalt und die vielen lieben Zusprüche während meiner bisherigen akademischen Laufbahn. Auf euch konnte und kann ich mich stets verlassen.

Summary

Malaria is still a big problem globally causing more than 400,000 deaths each year. Although very effective antimalarial drugs are on the market, their mode of action is still not fully understood. In the last years some patients showed an increased clearance time from *Plasmodium falciparum* malaria parasites after a therapy with the most effective antimalarial compound artemisinin. It was shown that mutations in the propeller domain of a protein called *Pf*Kelch13 are directly linked to this decreased susceptibility towards the drug. To gain insights into the protein function, I produced different mutants of a truncated version of this protein containing the BTB and propeller domain in high yield and purity in insect cells. I showed a positive correlation between the solubility of the recombinant protein and the artemisinin susceptibility. Prominent *Pf*Kelch13 mutants from the field with decreased artemisinin susceptibility (I543T, R539T, C580Y) were insoluble when recombinantly expressed suggesting that improper folding of *Pf*Kelch13 leads to this decrease in sensitivity. The mutation C580Y is the most frequent mutation in South East Asia. The substitution of this cysteine residue does not allow the formation of an intramolecular disulfide bond with cysteine C532 according to an existing crystal structure. Interestingly, substitution of these cysteines to serines did not show improper folding in insect cells, arguing that rather specific substitutions than the residue position itself are responsible for the alteration of drug sensitivity. To test the impact of the disulfide bond on artemisinin susceptibility, I generated stable transgenic parasites expressing the corresponding serine mutations. Neither C580S nor C532S showed decreased artemisinin susceptibility. Therefore, it could be excluded that the formation of the intramolecular disulfide bond has an influence on artemisinin susceptibility. We further asked, if the protein abundance has an influence on the sensitivity towards the drug. I successfully generated stable transgenic parasites expressing His_8-*PFKELCH13* fused to the *glmS* riboswitch. I showed that protein levels could be efficiently down-regulated by more than 90% resulting in a very low parasite susceptibility towards artemisinin. This strain offers a basis for future experiments in the understanding of the impact of *Pf*Kelch13 protein levels on biochemical pathways in malaria parasites.

Peroxiredoxins (Prxs) play an important role in protecting the cell from high amounts hydroperoxides. Among the five known Prxs in *P. falciparum* our group took *Pf*AOP as a model enzyme to study the catalytic cycle. It has been shown that *Pf*AOP reduces hydroperoxides

like H_2O_2 or tBuOOH with fast kinetics, and that reduction of the protein is linked to the GSH/Grx system (Djuika et al. 2013). However, no direct kinetic data was available for the reductive half-reaction of *Pf*AOP and GSH. In this thesis, I qualitatively showed that oxidized *Pf*AOP can be glutathionylated and that in a next step glutathione can be transferred to *Pf*Grx. I further determined the rate constants of the glutathionylation of *Pf*AOP by stopped-flow measurements. Rate constants of around 10^5 $M^{-1}s^{-1}$ indicate a fast kinetic that is able to protect the protein from hyperoxidation and inactivation. Furthermore, I determined the activation energy, entropy and enthalpy for this reaction of 41.1 kJ/mol, -0.79 J/mol and 39.8 kJ/mol, respectively. Hence, the activation energy of the glutathionylation of oxidized *Pf*AOP suggests the break of two to three hydrogen bonds and is rather temperature-independent.

Zusammenfassung

Auch heute noch stellt Malaria ein globales Problem dar und fordert jährlich mehr als 400.000 Tote. Obwohl sehr effektive Antimalariamittel zur Verfügung stehen, ist ihr genauer Wirkungsmechanismus oft nicht völlig geklärt. In den letzten Jahren wurde bei Patienten nach einer Therapie mit dem effektivsten Antimalariamittel Artemisinin eine erhöhte *Clearance time* von *Plasmodium falciparum* Malariaparasiten beobachtet. Es konnte gezeigt werden, dass Mutationen in der Propellerregion des Proteins *Pf*Kelch13 zu einer verminderten Sensitivität gegenüber dieses Mittels führten. Um Einblicke in die Funktion des Proteins zu erhalten, wurden unterschiedliche Mutanten einer verkürzten Variante des Proteins, bestehend aus BTB und Kelch-Propeller, in hoher Ausbeute und Reinheit in Insektenzellen hergestellt. Es wurde eine Korrelation zwischen der Löslichkeit der in Insekten produzierten Konstrukte und der im Parasiten beobachteten Sensitivität gegenüber Artemisinin gezeigt. Prominente Feldmutanten von *Pf*Kelch13, die mit einer verminderten Artemisininsensitivität assoziiert sind (I543T, R539T, C580Y), waren unlöslich, wenn sie in Insektenzellen produziert wurden. Dieses Ergebnis deutet auf einen Zusammenhang zwischen korrekter Faltung des Proteins und der Artemisininsensitivität hin. Die Mutation C580Y ist die am häufigsten vorkommende in Südostasien. Diese Aminosäuresubstitution verhindert das mögliche Ausbilden einer Disulfidbrücke mit dem Cysteinrest C532 gemäß einer existierenden Kristallstruktur des Proteins. Die Produktion der entsprechenden Serinmutanten in Insektenzellen zeigte keine verminderte Löslichkeiten. Dieses Ergebnis deutet darauf hin, dass spezifische Aminosäuresubstitutionen und nicht die alleinige Position des Aminosäurerestes zu einer veränderten Sensitivität gegenüber Artemisinin führt. Um dieses Ergebnis zu stützen, wurden Malariaparasiten genetisch verändert, um *Pf*Kelch13 mit den entspechenden Serinmutationen zu exprimieren. Weder die Mutation C532S, noch C580S führte zu einer verminderten Artemisininsensitivität. Dementsprechend kann ein Einfluss der Disulfidbrücke auf die Artemisininempfindlichkeit ausgeschlossen werden. Desweiteren wurde untersucht, ob der Proteingehalt von *Pf*Kelch13 einen Einfluss auf die Artemisininempfindlichkeit hat. Hierzu wurde der *PFKELCH13*-Locus genetisch verändert, um His_8-*PFKELCH13-glmS* zu exprimieren. Über den *glms* Riboswitch konnten *Pf*Kelch13-Proteinmengen um bis zu 90% gesenkt werden. Der verminderte Proteingehalt ging mit einer sehr geringen Empfindlichkeit gegenüber Artemisinin einher. Der generierte Stamm stellt einen vielversprechenden

Ausgangspunkt für zukünftige Experimente dar, um den Einfluss des *Pf*Kelch13-Proteingehalts auf biochemische Prozesse zu untersuchen.

Peroxiredoxine (Prxs) spielen eine wichtige Rolle, die Zelle vor hohen Hydroperoxidkonzentrationen zu schützen. In *P. falciparum* sind fünf Prxs bekannt, von denen unsere Gruppe *Pf*AOP als ein Modellenzym gewählt hat, um den Katalysezyklus genauer zu untersuchen. Es konnte bereits gezeigt werden, dass *Pf*AOP die Reduktion von Hydroperoxiden wie H_2O_2 oder tBuOOH äußerst effizient katalysiert. Zudem ist die Reduktion des Proteins an das GSH/Grx-System geknüpft (Djuika et al. 2013). Zu der reduktiven Halbreaktion zwischen *Pf*AOP und GSH sind bislang jedoch keine direkten kinetischen Daten verfügbar. In dieser Arbeit wurde zunächst qualitativ gezeigt, dass oxidiertes *Pf*AOP glutathionyliert werden kann. In einem nächsten Schritt kann Glutathion auf *Pf*Grx übertragen werden. Abschließend wurden die Geschwindigkeitskonstanten der Glutathionylierung von *Pf*AOP mittels Stopped-Flow-Messungen bestimmt. Geschwindigkeitskonstanten in der Größenordnung von 10^5 $M^{-1}s^{-1}$ stellen ein schnelle Reaktion zwischen oxidiertem *Pf*AOP und GSH dar, die eine Hyperoxidation und eine damit einhergehende Inaktivierung des Enzymes verhindern könnte. Des Weiteren wurden die Aktivierungsenergie, -entropie und -enthalpie bestimmt. Eine Aktivierungsenergie von 41.1 kJ/mol sowie eine Aktivierungsenthalpie von 39.8 kJ/mol deuten auf den Verlust von zwei bis drei Wasserstoffbrücken bei der Glutathionylierung von oxidiertem *Pf*AOP hin. Eine geringe Aktivierungsentropie von nur -0.79 J/mol spricht für eine nahezu temperaturunhängige Reaktion.

List of figures

List of tables

Abbreviations and symbols

°C	degree Celsius
α	anti
#	number
Δ	delta
x g	gravitational force
%	per cent
ε	extinction coefficient
µg	microgram
µl	microliter
µm	micrometer
µM	micromolar
Å	Ångström
aa	amino acid
AB	antibody
ACT	artemisinin-based combination therapy
ALAD	aminolevulinic acid dehydratase
ALAS	aminolevulinic acid synthase
AOP	antioxidant protein
AP-2µ	adaptor protein-2µ
APS	ammonium persulfate
AS	artesunate
bp	base pair
BSA	bovine serum albumin
BTB	Broad-Complex, Tramtrack and Bric a brac
C-terminus	carboxy terminus
CCC	Coiled-coil-containing
CD	Circular Dichroism
CPO	Coproporphyrinogen oxidase
Cas9	CRISPR-associated protein 9
cm	centimeter
CRISPR	Clustered Regularly Interspaced Short Palindromic Repeats
Da	Dalton
DAPI	4',6-diamidino-2-phenylindole
ddH_2O	double-destilled water
DHA	dihydroartemisinin
DHFR	dihydrofolate reductase
DHODH	dihydroorotate dehydrogenase
DMSO	dimethyl sulfoxide
DNA	deoxyribonucleic acid
DNase	deoxyribonuclease
DOC	deoxycholic acid
dNTPS	deoxyribonucleoside triphosphate
DTPA	diethylenetriaminepentaacetic acid
DTT	dithiothreitol
EC_{50}	half maximal effective concentration
E. coli	*Escherichia coli*
EDTA	ethylendiaminetetraacetic acid
e.g.	*exempli gratia* (for example)
EGTA	ethylenbis(oxythylenenitrilo) tetraacetic acid
EHD	Eps15 homology domain protein
Eps15	Epidermal Growth Factor receptor substrate-15
ER	endoplasmic reticulum
FBS	fetal bovine serum
Fc	ferrochelatase
FF	fully folded
Fig.	figure
g	gram
GAPDH	glyceraldehyde 3-phosphate dehydrogenase
GFP	green fluorescent protein
GSH	glutathione
GSSG	glutatione disulfide
GR	glutathione reductase
Grx	glutaredoxin
h	hour
Hb	hemoglobin
HRP	horseradish peroxidase
IPTG	isopropyl β-D-1-thiogalactopyranoside
iRBC	infected red blood cell
K13	Kelch13
kb	kilobase pair
kDa	kilodalton
Keap1	Kelch-like ECH-associated protein 1
l	liter
LB	Luria Bertani
LU	locally unfolded
M	molar
mg	milligram
min	minute
ml	milliliter
mM	millimolar
mmPEG	methyl-PEG-maleimide
mRNA	messenger ribonucleic acid
MS	mass spectrometry
N-terminus	amino terminus
NADPH	nicotinamide adenine dinucleotide
nm	nanometer
nM	nanomolar
Nrf2	nuclear factor erythroid 2-related factor 2
OD	optical density
P. falciparum/ Pf	*Plasmodium falciparum*
PAGE	polyacrylamide gel electrophoresis
PBGD	porphobilinogen deaminase
PBS	phosphate buffered saline
PCR	polymerase chain reaction
PDB	Protein Data Bank
PEG	polyethylene glycol
PI3K	phosphatidylinositol-3-kinase

PI3P	phosphatidylinositol 3-phosphate
PPO	protoporphyrinogen oxidase
Prx	peroxiredoxin
PVDF	polyvinylidene difluoride
RBC	red blood cell
RNase	ribonuclease
RNS	reactive nitrogen species
roGFP2	reduction-oxidation sensitive green fluorescent protein 2
ROS	reactive oxygen species
rpm	revolutions per minute
RSA	ring-stage survival assay
RT	room temperature
s	second
SDS	sodium dodecyl sulfate
SEA	South East Asia
SLI	selection linked integraton
SOD	superoxide dismutase
tBuOOH	*tert*-Butyl hydroperoxide
TBS	Tris buffered saline
TEMED	tetramethylethylenediamine
T_m	melting temperature
Tris	Tris(hydroxymethyl)aminomethane
Trx	thioredoxin
TrxR	thioredoxin reductase
UBP1	ubiquitin carboxyl-terminal hydrolase 1
UROD	uroporphyrinogen decarboxylase
UROS	uroporphyrinogen synthase
UTR	untranslated region
UV	ultraviolet
v/v	volume to volume
w/v	weight to volume
WHO	World Health Organization
wt	wild-type

1 Introduction

1.1 Malaria

The disease malaria is caused by parasites of the genus *Plasmodium*. To date five species are known that infect humans: *P. falciparum*, *P. vivax*, *P. ovale*, *P. malariae*, and *P. knowlesi*. Among these species, *P. falciparum* is the most virulent one causing the majority of infections and also deaths. Between 2000 and 2015 the number of malaria cases declined by 27%. However, between 2015 and 2019 the reduction of malaria cases declined by just 2% with a total number of 229 million infections causing 409,000 deaths in 2019. Worldwide 87 countries are endemic for the disease (Fig. 1). The most affected continent is Africa with about 94% of all cases and deaths globally (World Health Organization 2020).

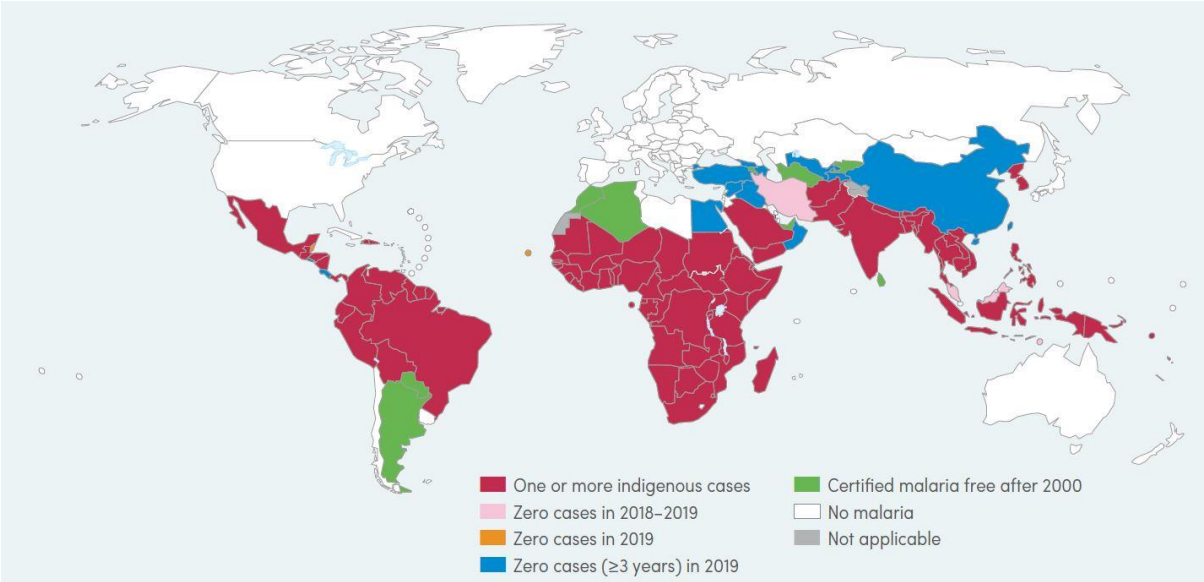

Fig. 1 Distribution of malaria worldwide

(World Health Organization 2020)

Following the infective bite of a female *Anopheles* mosquito, symptoms begin after 10-15 days. Typical symptoms are: fever, chills and headache. Since these symptoms do not specifically indicate malaria, the disease is difficult to recognize in its beginning. During the progress of the disease the fever shows up in a recurring or periodic manner. Due to the length and synchrony of the blood stage life cycles, different *Plasmodium* species result in a different rhythm of the fever. *P. falciparum* replicates asynchronously and this thereby results

in irregular fever attacks. Although the percentage of dead children aged under 5 years decreased in the last years, with 67% they still account for the highest percentage of all malaria deaths globally. Along with pregnant women and immunodeficient persons (e.g., HIV/AIDS patients) they are at higher risk to suffer from a severe course of the disease. Typical symptoms are severe anaemia, respiratory distress and/or cerebral malaria which in most of the cases leads to death (Bartoloni and Zammarchi 2012).

1.2 The life cycle of *Plasmodium falciparum*

Plasmodium falciparum exhibits a complex life cycle with a whole develeptomental cycle in two hosts (Fig. 2). After the bite of a female mosquito of the genus *Anopheles*, sporozoites actively pass through the dermis and are transported via the blood vessels to reach the liver. The sporozoites pass through Kupffer cells to finally infect a hepatocyte (Mota and Rodriguez 2004; Prudêncio et al. 2006). After the formation of a parasitophorous vacuole, the parasite starts to replicate resulting in thousands of daughter merozoites. These merozoites are released in membranous bundles of so-called merosomes into the blood vasculature where they infect red blood cells (Sturm et al. 2006). Usually one merozoite infects one red blood cell. However, infections with more than one merozoite are possible. After the formation of the parasitophouros vacuole, the parasite starts to replicate. At the end of an intraerythrocytic cycle the merozoites are released by the rupture of the red blood cell leading to the release of pro-inflammatory proteins and the typical symptoms of the desease. The merozoites infect red blood cells and the cycle starts anew. A proportion of parasites is reprogrammed and develops to the sexual stages. Once the transcriptional factor *AP2-G* is expressed, gametocytogenesis is initiated (Kafsack et al. 2014). Recently, it was shown that a conditional expression of this master regulator in a genetically modified parasite strain led to conversion rates into sexual forms of around 90% (Llorà-Batlle et al. 2020). The exact triggers and mechanisms leading to this process are not known or poorly understood (Josling und Llinás 2015). The percentage of parasites undergoing gametocytogenesis depends on the genetic background (Roncalés et al. 2012), the host lysophosphatidylcholine levels (Brancucci et al. 2017) as well as antimalarial drug pressure (Peatey et al. 2009). After around two weeks, the parasites passed 5 intra-erythrocytic gametocyte stages resulting in mature male and female gametocytes.

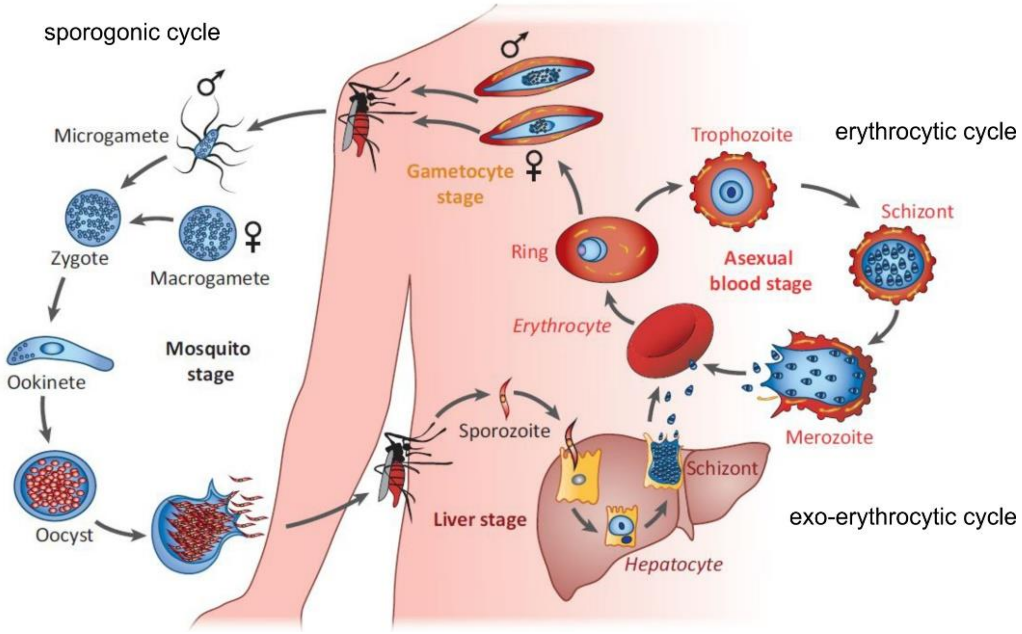

Fig. 2 The life cycle of *P. falciparum.*

Upon a bit of a female *Anopheles* mosquito, sporozoites are injected into the human body from where they travel to the liver to infect a hepatocyte. Thousands of merozoites develop, are released in merosomes and infect red blood cells to start the asexual blood stage cycle. A low percentage (< 10%) of parasites commit to gametocyte stages, the sexual stages in the human body, and are taken up by a mosquito. In the midgut of the mosquito, gametocytes develop into gametes. After fertilization, the zygote matures into an ookinete, which penetrates the midgut wall and arrests beneath the basal lamina. Hundreds of sporozoites develop and are released into the hemolymph. After reaching the salivary gland, parasites can be transmitted to a human upon a mosquito bite starting the next parasite life cycle (Maier et al. 2019).

These gametocytes are taken up by a female mosquito and are transported to the midgut. Through the increase in pH and a drop in temperature (Billker et al. 1997; Ogwan'g et al. 1993) as well as the presence of xanthurenic acid (Billker et al. 1998; Garcia et al. 1998), gametocytes develop into gametes, a process calles gametogenesis. A female gametocyte exits the red blood cell in a protein kinase G-dependent process and produces a haploid female gamete called macrogamete (Billker et al. 2004; McRobert et al. 2008). A male gametocyte first replicates the DNA to octoploid and forms eight male gametes called microgametes which egress from the red blood cell in an actin-dependent process (Deligianni et al. 2011). The process of the development from a male gametocyte to a gamete is called exflagellation. A microgamete fertilizes a macrogamete leading to a diploid zygote. After meiotic division, the zygote develops into a motile parasite stage called ookinete. Especially the elongated shape of this stage makes it possible that the parasite passes through the midgut epithelium to reach the basal lamina of the midgut wall. The ookinete arrests and develops into a oocyst, a process that takes around 10 days leading to hundreds of motile sporozoites. After egress, the sporozoites are released into the hemolymph and are

transported to the salivary glands from where they can be transmitted to a human host upon a blood meal of the mosquito (Aly et al. 2009).

1.2.1 Asexual blood stages of *P. falciparum*

After the invasion of a merozoite into a red blood cell, the asexual cycle begins (Fig. 3). The parasite enters the ring stage by forming a parasitophorous vacuole and extensive remodeling of the host cell. After around 4 h, vesicular structures in the host cell cytosol, termed Maurer's clefts, become apparent. The Maurer's clefts have diverse functions but are mainly used as structures to route parasite proteins through the host cell cytosol to the erythrocytic surface (Lanzer et al. 2006). The ring stage lasts for around 18 h (Grüring et al. 2011). The transition to the trophozoite stage is characterized by the appearance of the food vacuole and the formation of red blood cell surface protrusions (knobs) mediating cytoadherence and therefore protecting the parasites from clearance by the spleen (Leech et al. 1984; Sharma 1991). At the trophozoite stage, the parasite intensively grows. In order to guarantee enough nutrients but also space in the host cell, the parasite takes up around 75% of the host cell cytosol containing a high percentage of hemoglobin. It is quite likely that structures called cytostomes are involved and directly appose and fuse with the food vacuole (Lazarus et al. 2008; Spielmann et al. 2020). The hemoglobin is digested by different proteases supplying the parasite with essential amino acids for metabolic processes. The resulting free heme is toxic to the parasite and therefore crystallized to a black polymer called hemozoin (Pagola et al. 2000). After around 34 h post infection, the parasite enters the schizont stage, which is characterized by nuclear division by schizogony (Gerald et al. 2011). Following the formation of daughter cells, a sequential activation of different proteases leads to the disruption of the parasitophorous vacuole and the plasma membrane of the erythrocyte (Blackman and Carruthers 2013; Wirth and Pradel 2012) releasing up to 32 daughter merozoites (Bannister et al. 2000). The merozoites invade red blood cells and the asexual blood stage cycle starts anew. The whole cycle takes around 48 h.

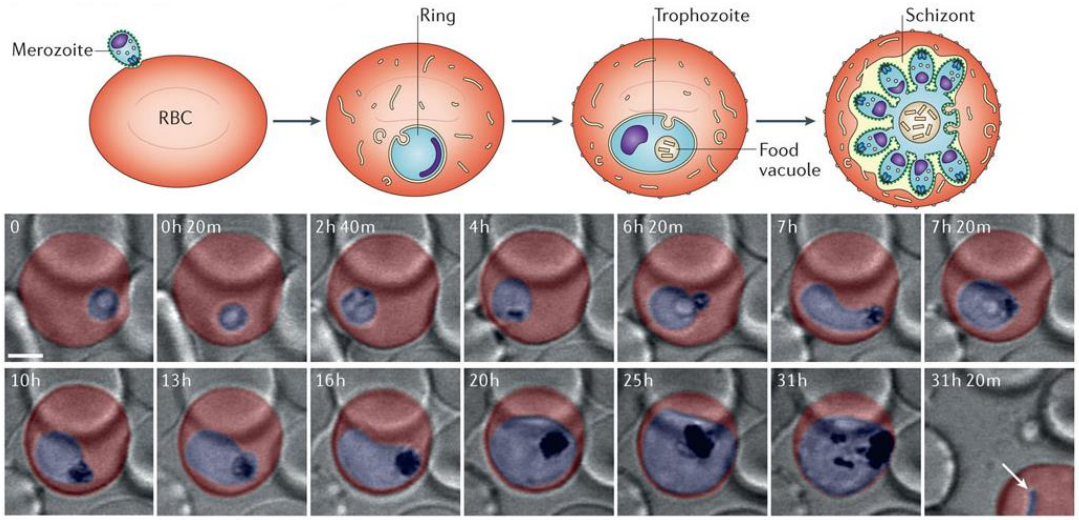

Fig. 3 Asexual blood stages of *Plasmodium falciparum.*

After invasion of a merozoite into a red blood cell, the parasite enters the ring stage. In this stage, the parasite remodels the host cell. Characteristic structures are so-called Maurer's clefts in the cytosol of the red blood cells. The transition to the trophozoite stage is characterized by the appearance of surface protrusions (knobs) of the host cell and the formation of a food vacuole. Extensive endocytosis guarantees enough nutrients for biosynthesis processes. Resulting free heme upon the digestion of hemoglobin is crystallized to the insoluble black pigment hemozoin. In the trophozoite stage the parasite increases its volume intensively. In the schizont stage up to 32 merozoites are formed and released to infect new red blood cells (arrow in the last picture). The upper panel shows a scheme of the developmental stages, the lower a 4D imaging of the asexual cycle (Niz et al. 2017). Scale bar: 2 µm.

1.2.2 Cellular biology of *P. falciparum*

Besides the typical organelles of eukaryotic cells like a nucleus, an endoplasmic reticulum (ER), a Golgi and mitochondrion (Fig. 4), *P. falciparum* merozoites pocesses secretory organelles that are important for the invasion of and egress from red blood cells. Hence, proteins present in these organelles, termed rhoptries, micronemes, exonemes, and dense granules (Cowman and Crabb 2006; Kats et al. 2006; Yeoh et al. 2007), are possible drug targets. In addition to these specialized secretory organelles, the parasite contains a plastid and a lysosome-like organelle, the apicoplast and the food vacuole, respectively. The apicoplast was acquired by secondary endosymbiosis of a red algae (Fast et al. 2001; Köhler et al. 1997) therefore containing four membranes. In contrast to the closely related algae *Vitrella brasicaformis,* which shares the same ancestor (Oborník et al. 2012), apicomplexan parasites lost their photosynthetic activity (Oborník and Lukeš 2015). Less than 10% of the proteins of the apicoplast of *P. falciparum* are encoded by a plastid genome of 35 kb (Wilson et al. 1996). The remaining coding sequences were transferred to the nucleus. Specific N-terminal signal sequences guide the proteins to the apicoplast (Waller et al. 2000). With the discovery of

these targeting sequences, a total number of apicoplast proteins of around 500 was predicted (Foth et al. 2003). Proximity biotinylation-based proteomics resulted in a similar number of 346 proteins (Boucher et al. 2018). These proteins take part in diverse biochemical pathways such as biosynthesis of fatty acids (Tarun et al. 2009), isoprenoids (Guggisberg et al. 2014), iron-sulfur clusters (Gisselberg et al. 2013) and heme (Fig. 5). Due to the essential role of the apicoplast and the unique sequences and structures of proteins, the apicoplast was of special interest as a drug target (Chakraborty 2016; Soldati 1999). However, for blood stages of *P. falciparum* just the isoprenoid biosynthesis seems to be essential (Yeh and DeRisi 2011) making this pathway the only current one as a drug target of the apicoplast (Wiesner and Jomaa 2007).

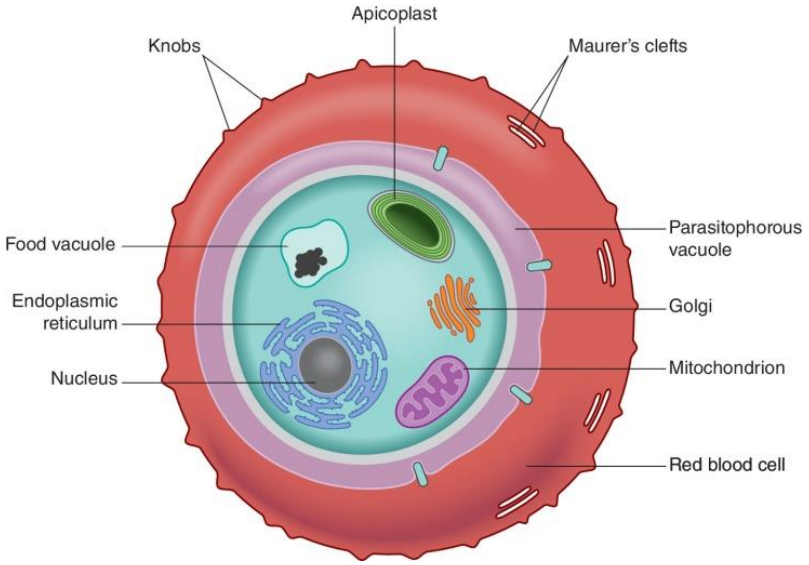

Fig. 4 *P. falciparum* infected red blood cell.

Characteristic organelles of a trophozoite stage parasite in a red blood cell (Florentin et al. 2020).

The acidic food vacuole is fundamental for the digestion of hemoglobin to supply the parasite with amino acids for biosynthesic processes (Goldberg 2005). This catabolic process results in the formation of toxic heme, which the parasite crystallizes to hemozoin. The mechanism leading to the formation of hemozoin is still controversially discussed. It was shown that histidine-rich proteins (Sullivan et al. 1996) and/or lipids are involved (Huy et al. 2013; Pandey et al. 2003), but also the involvement of a protein complex containing a heme detoxification protein was suggested (Chugh et al. 2013). Although the exact mechanism of hemozoin formation is not solved yet, compounds disrupting this detoxification process are of special

interest as antimalarial drugs (Hempelmann 2007). In contrast to other organelles, the food vacuole is formed *de novo* in every asexual blood stage cycle since it is disposed after egress of the parasites from the red blood cell. In the late ring stage, cytostome-derived invaginations results in acidified vesicular structures that coalesce and form the food vacuole (Abu Bakar et al. 2010).

1.2.3 Heme metabolism in *P. falciparum*

Malaria parasites contain a mitochondrion with all the classical known components of the electron transport chain. Proteins carrying heme as a cofactor are: cytochrome *b* and c_1 (Complex III), soluble cytochrome *c* and the CoxI subunit of ComplexIV. Since heme has an essential role in the electron transport chain, heme generation pathways have been considered as possible antimalarial drug targets. Heme generation is achieved by two pathways: 1. Heme biosynthesis, 2. Hemoglobin digestion. Heme biosynthesis takes place in the liver, mosquito and blood stage, whereas hemoglobin digestion only occurs in the blood stage. Therefore, heme biosynthesis is essential in the liver and mosquito stage (Ke et al. 2014; Nagaraj et al. 2013). The heme biosynthesis takes part in three compartments of the parasite (Fig. 5). In the mitochondrion, aminolevulinic acid synthase (ALAS) catalyzes the reaction of succinyl-CoA and glycine to 5-aminolevulinic acid, the common precursor for all tetrapyrroles. The synthesis to coproporphyrinogen III takes place in the apicoplast. After oxidation in the cytoplasm, the synthesized protoporhyrinogen IX is dehydrogenated and the iron ion is inserted by the ferrochelatase (Fc) in the mitochondrion. The generation of a Fc knock-out strain clearly showed that heme biosynthesis is dispensable in blood stage parasites. Furthermore, no growth alteration was observed (Ke et al. 2014). Therefore, heme has to be transported from the food vacuole into the mitochondrion. The mechanisms that lead to efficient transport to the mitochondrion are still unclear. However, heme levels in the cytoplasm of the parasite were estimated to be around 1.6 µM (Abshire et al. 2017) which could be assumed to be enough to fulfill the essential functions of the mitochondrion. The cytoplasmic heme levels were not altered during asexual development and strongly dependended on the heme sequestration in the food vacuole (Francis et al. 1997). Although heme biosynthesis is not essential in blood stage parasites and therefore unlikely to use components as possible drug targets, they can have an impact on artemisinin resistance as

recently shown. Knock-out of the mitochondrial protease DegP2 resulted in reduced porphyrin and heme levels leading to decreased susceptibility towards artemisinin (Harding et al. 2020).

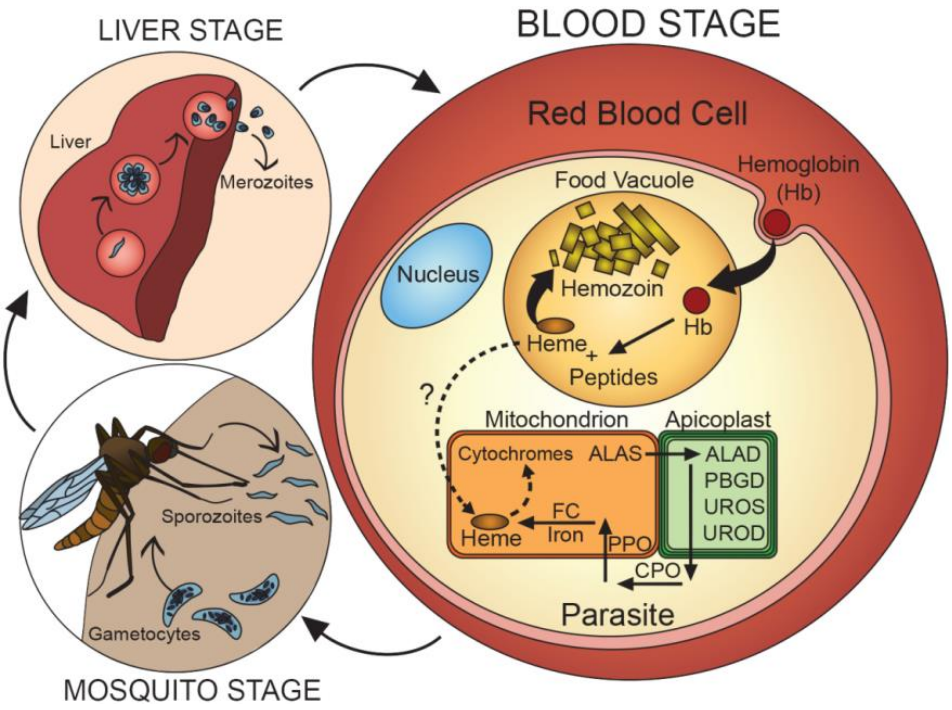

Fig. 5 Heme metabolism in *P. falciparum.*

Heme generation is achieved by two pathways: 1. Heme biogenesis, 2. Hemoglobin digestion. See text above for further information. ALAS: aminolevulinic acid synthase, ALAD: aminolevulinic acid dehydratase, PBGD: porphobilinogen deaminase, UROS: uroporphyrinogen synthase, UROD: uroporphyrinogen decarboxylase, CPO: coproporphyrinogen oxidase, PPO: protoporphyrinogen oxidase, Fc: ferrochelatase (Goldberg and Sigala 2017).

The second pathway to generate heme is the digestion of hemoglobin. More than 90% of all proteins of a red blood cell are hemoglobins, which make up around 5 mM. *P. falciparum* endocytose up to 80% of this whole content (Ginsburg 1990). The vesicles are then transferred to the acidic food vacuole. The exact components and delivery process are still not known (Spielmann et al. 2020). However, the involvement of *Pf*Kelch13 in a clathrin-independent pathway seems to play a crucial role to initiate endocytosis (Birnbaum et al. 2020). In the food vacuole, different peptidases digest hemoglobin into heme and the amino acids, which the parasite can use for metabolic processes. The liberation of heme in high concentrations is toxic for the parasite. To solve this problem heme is biocrystallized to hemozoin. Both, drugs targeting hemoglobin digestion or the crystallization of heme are under intense investigation (Olafson et al. 2017).

1.3 Fighting against malaria

To fight against malaria, one strategy is the development and use of antimalarial drugs. The first used antimalarial drug in the western world was quinine, a natural compound extracted from the bark of the cinchona tree (Achan 2011). It has been used since the beginning of the 17th century and was the most used antimalarial drug until the 1920s when more effective synthetic drugs were developed. The first complete synthetic structurally related analog was chloroquine. The toxic effect of both compounds is caused by the accumulation in the food vacuole (Yayon et al. 1984) inhibiting the crystallization of heme to hemozoin (Herraiz et al. 2019). However, in the 1950s a chloroquine resistant phenotype emerged spreading rapidly in Asia, South America as well as Africa (Payne 1987). The high tolerance of malaria parasites towards the most used antimalarial drug argued for the need of the discovery of a new drug to overcome this problem. Since 2001, the World Health Organization recommends an artemisinin-based combination therapy (ACT) to prevent resistance and to treat patients suffering from malaria. Such ACTs combine the high efficiency but short-lived nature of artemisinin or a derivate (e.g., artesunate) and a partner drug that acts over a longer time scale (World Health Organization 2020).

1.3.1 Artemisinin as the first-line antimalarial drug

Due to the emergence of a chloroquine-resistant phenotype in the 1950s (Payne 1987), the Chinese government set up a plant screening research program (Project 523) to discover new antimalarial chemicals. A variety of different extraction methods from the plant *Artemisia annua* finally resulted in a highly active antimalarial compound called artemisinin. Main work was done by Tu Youyou (Tu 2011) who was honored in 2015 with the Nobel Prize of physiology or medicine (Liu and Liu 2016). Nowadays, different derivates of artemisinin are available with artemether and artesunate being the most prominent ones. These derivates differ in their site chain group (Fig. 6a). They show different solubilities and stabilities in the human body, thereby having different half-life times and also efficiencies in killing malaria parasites (Vries 1996). All compounds have an endoperoxide in common. This functional group is responsible for the high efficiency in killing malaria parasites, since the endoperoxide bond is cleaved by heme (Fe^{2+}-FPIX), a degradation product of hemoglobin. It was shown that inhibition of either the hemoglobinase or the cysteine protease falcipain-2 decreases artemisinin susceptibility

(Klonis et al. 2011; Xie et al. 2016). The generated primary carbon-centered radicals alkylate either heme or other proteins in the cell (Fig. 6b), and are thought to tackle different biochemical pathways (Bridgford 2018; Ismail et al. 2016; Wang et al. 2015). Since artemisinin activation is heme-dependent, the efficiency of this antimalarial drug is directly linked to the uptake and digestion of hemoglobin by the parasite (Klonis et al. 2011). This correlation results in a stage-dependent profile of artemisinin susceptibility, with the highest sensitivity at later asexual stages (Sutherland 2017). Although in South East Asia a phenotype emerged that shows increased clearance times upon artemisinin treatment, the described dependency between heme uptake and artemisinin susceptibility makes it unlikely that a complete resistance towards artemisinin will arise.

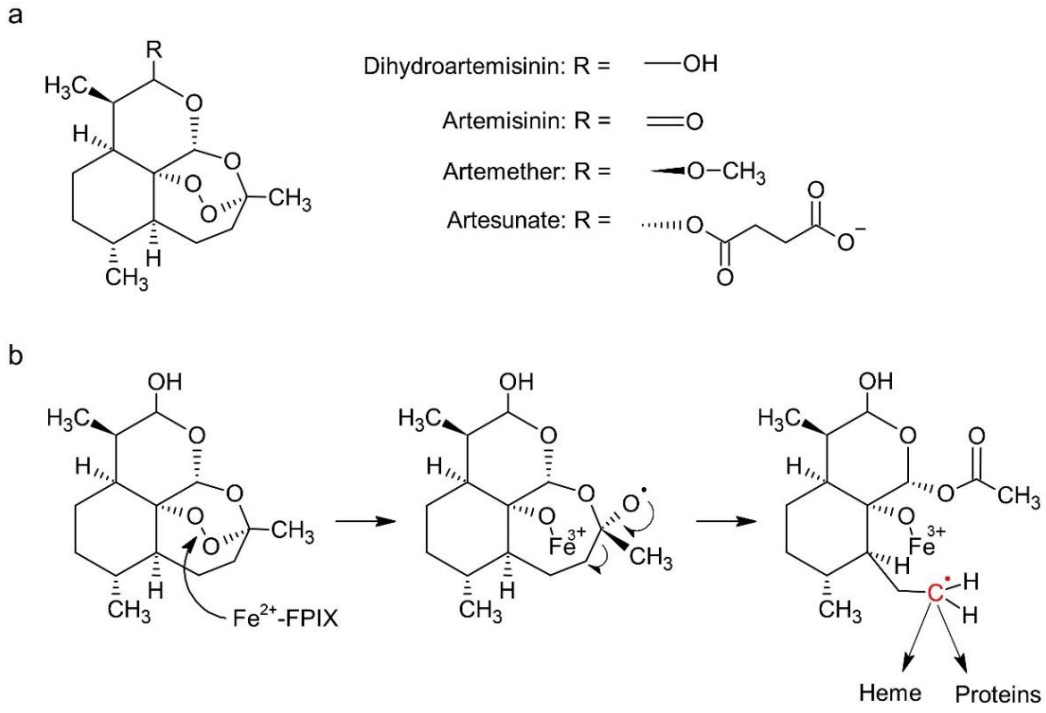

Fig. 6 Artemisinins and their activation by heme.

(a) Structure of artemisinin and some derivates used as antimalarial drugs. **(b)** Activation of dihydroartemisinin (DHA). Heme (Fe^{2+}-FPIX) breaks the endoperoxide group of DHA. In the end, a carbon-centered radical is generated, that damages heme and proteins through alkylation processes. Modiefied after Rosenthal and Ng 2020.

1.3.2 *Pf*Kelch13: architecture, localization and proposed function

The *Pf*Kelch13 protein consists of 726 amino acids (Fig. 7a). It contains an apicomplexan-specific region and three known domains: 1 CCC, 1 BTB, and 6 kelch domains. The six kelch domains form a six-bladed kelch propeller.

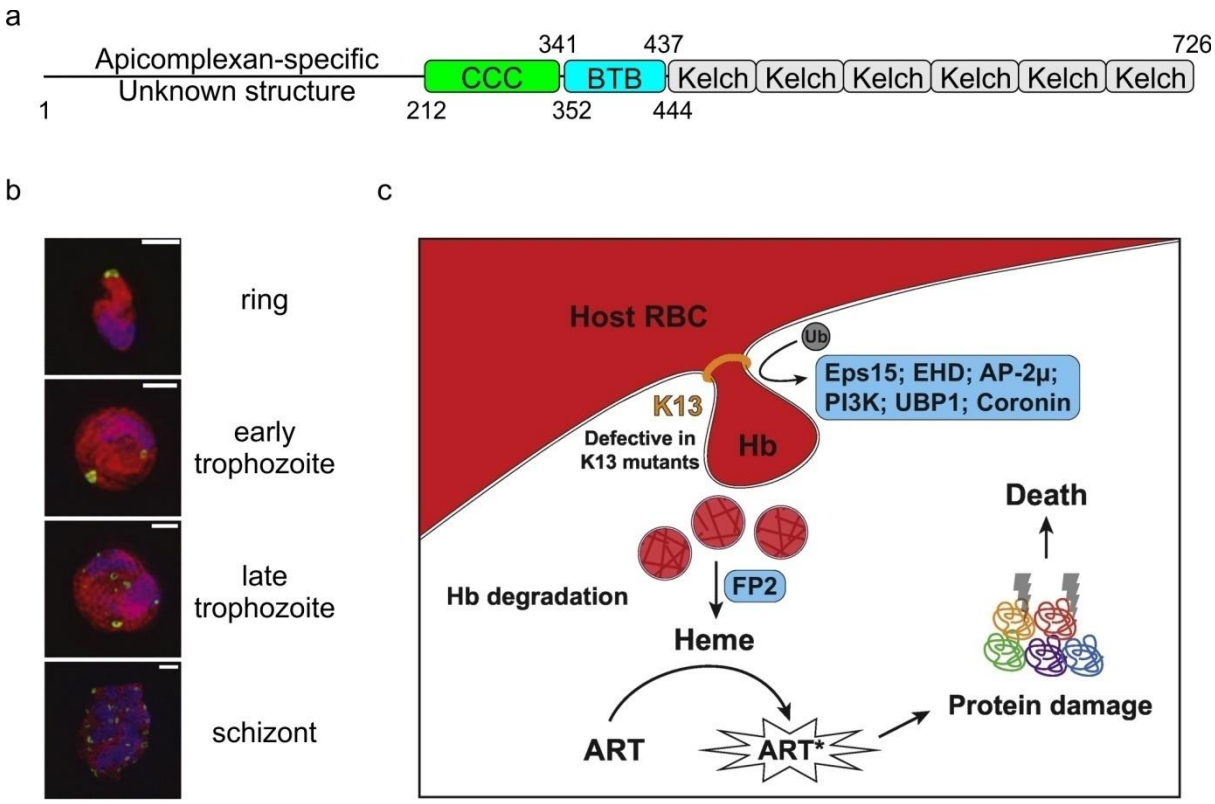

Fig. 7 Features of *Pf*Kelch13.

(a) Architecture of *Pf*Kelch13. The protein consists of four domains: 1 Aplicomplexa-specific unknown region, 1 CCC, 1 BTB, and 6 kelch domains. The six kelch domains form a propeller. **(b)** Localization of *Pf*Kelch13 (N-terminally GFP-tagged, green). *Pf*Kelch13 is expressed throughout the whole asexual blood stage cycle localizing near the periphery of the parasite. Anti-*Pf*GAPDH (cytoplasm, red), DAPI (nucleus, blue); Scale bars: 2 µm (Yang et al. 2019). **(c)** Proposed function of *Pf*Kelch13. *Pf*Kelch13 is essential for the hemoglobin (Hb) uptake and thereby regulates the activation of artemisinin (ART) leading to the toxic effect of the drug. Specific mutations in *Pf*Kelch13 lead to a decreased hemoglobin uptake. Another proposed function of the protein is its role as a substrate adaptor for ubiquitination processes. Hence, it is regulating the protein level of these interaction partners in the cell (Xie et al. 2020).

The whole protein belongs to the top 5% of the most conserved proteins in *P. falciparum* and also the single domains show high conservation levels (Coppée et al. 2019). It is expressed throughout the whole asexual life cycle (Gnädig et al. 2020; Siddiqui et al. 2020) and localizes near the plasma membrane, close to cytostomes (Xie et al. 2020), to the endoplasmic reticulum and Rab-positive vesicles (Gnädig et al. 2020) as well as to PI3P tubules/vesicles associated with trafficking processes (Bhattacharjee et al. 2018). The number of the *Pf*Kelch13

ring-structures that are close to cytostomes increases with the development of the parasite (Fig. 7b). Recently, it has been shown that mislocalization of *Pf*Kelch13 from its site of action drastically reduces hemoglobin uptake in the ring stage (Birnbaum et al. 2020). High levels of mislocalization resulted in complete growth inhibition and the arrest of the parasite in the ring stage (Birnbaum et al. 2017). Therefore, *Pf*Kelch13 is essential in a hemoglobin uptake process in the ring stage and directly influences the activation of artemisinin by heme (Fig. 7c).

Since 2014, *Pf*Kelch13 has been used as a molecular marker for artemisinin resistance (Ariey et al. 2014). Different mutations leading to an increased clearance time upon artemisinin treatment were found in Asia (Group 2019). The most dominant mutation in South East Asia is the substitution of C580 to tyrosine (Zaw et al. 2020). Recently, the first mutation (R561H) leading to an increased survival rate upon artemisinin was found in Rwanda (Uwimana et al. 2020). However, if this mutation will spread to other countries like C580Y in Asia, cannot be predicted yet. Besides its essential role in hemoglobin uptake, *Pf*Kelch13 shares high structural similarity to the human protein Keap1, which plays an important role in stress sensing via the interaction to the transcriptional factor Nrf2, the master regulator of the antioxidant response in mammals (Paloque et al. 2016). Under normal conditions, Keap1 interacts with Nrf2, which leads to the ubiquitination and proteasomal degradation of Nrf2. Upon oxidative stress, this interaction is broken via the formation of an intramolecular disulfide bond in Keap1. Nrf2 enters the nucleus and initiates the expression of stress response genes (Kobayashi et al. 2006). A similar function was predicted for *Pf*Kelch13. *Pf*Kelch13^{wt} coprecipitated with PI3K whereas *Pf*Kelch13^{C580Y} did not, arguing for a possible redox regulation of C580 and the involvement of PI3P in artemisinin resistance (Mbengue et al. 2015). However, pull-down experiments using an anti *Pf*Kelch13 antibody (Gnädig et al. 2020) as well as proximity biotinylation labeling (Birnbaum et al. 2020) did not find this kinase but proteins involved in folding processes or proteins with a so far unknown function. Interestingly the ubiquitin carboxyl-terminal hydrolase 1 (UBP1) was found, indicating a possible role in ubiquitination processes.

1.4 The antioxidant system of *P. falciparum*

The term “oxidative stress” is defined as an imbalance of oxidants and antioxidants in favor of the former that lead to cellular damage (Sies 1997). Since the 1980s it is intensively used in the context of cellular damaging processes in which reactive oxygen species (ROS) and/or reactive nitrogen species (RNS) are involved. Such species can damage lipids, membranes, proteins and nucleic acids. However, ROS can also take part in cellular signaling processes (Schieber and Chandel 2014). One of the most dominant ROS are superoxide ions ($O_2^{\bullet-}$). The respiratory chain is considered to be a major source of $O_2^{\bullet-}$ in eukaryotes (Zhao et al. 2019). Another source of such ions comes from the oxidation of the iron ion of hemoglobin, which in *Plasmodium* takes place in the food vacuole (Fig. 8). Due to the low pH in this organelle, the rate of disproportionation of superoxide ions is relatively high (Baker and Gebicki 1984). Therefore, it could be assumed that low amounts of $O_2^{\bullet-}$, if any, can cross the food vacuole to reach the cytosol. There, efficient disproportionation is achieved by the catalysis via superoxide dismutase (SOD) generating molecular oxygen and hydrogen peroxide. *P. falciparum* expresses two SODs: the cytosolic SOD1 (Bécuwe et al. 1996) and the mitochondrial SOD2 (Sienkiewicz et al. 2004). Moreover, it was shown that during the erythrocytic cycle, the parasites import a human SOD (Fairfield et al. 1983). Hydrogen peroxide is finally reduced to water by peroxiredoxins. Since *P. falciparum* expresses neither a catalase nor a glutathione peroxidase, peroxiredoxins represent an efficient reducing system of hydrogen peroxides that is coupled to the NADPH-dependent Trx/TrxR and/or the Grx/GR/GSH system. The low redox potential of the cytosol with a value of -309 mV (Mohring et al. 2017) is mainly set by a high glutathione concentration that is approximiated to be around 2 mM (Becker et al. 2003). By assuming a standard redox potential of E^0_{GSH} = -240 mV at pH = 7.0 and a pH effect of -59.1 mV/pH unit (Schafer and Buettner 2001), the GSH:GSSG ration is calculated to be ~36000:1. Hence, the cytosol displays a highly reducing environment that is mainly influenced by the ratio between reduced and oxidized glutathione.

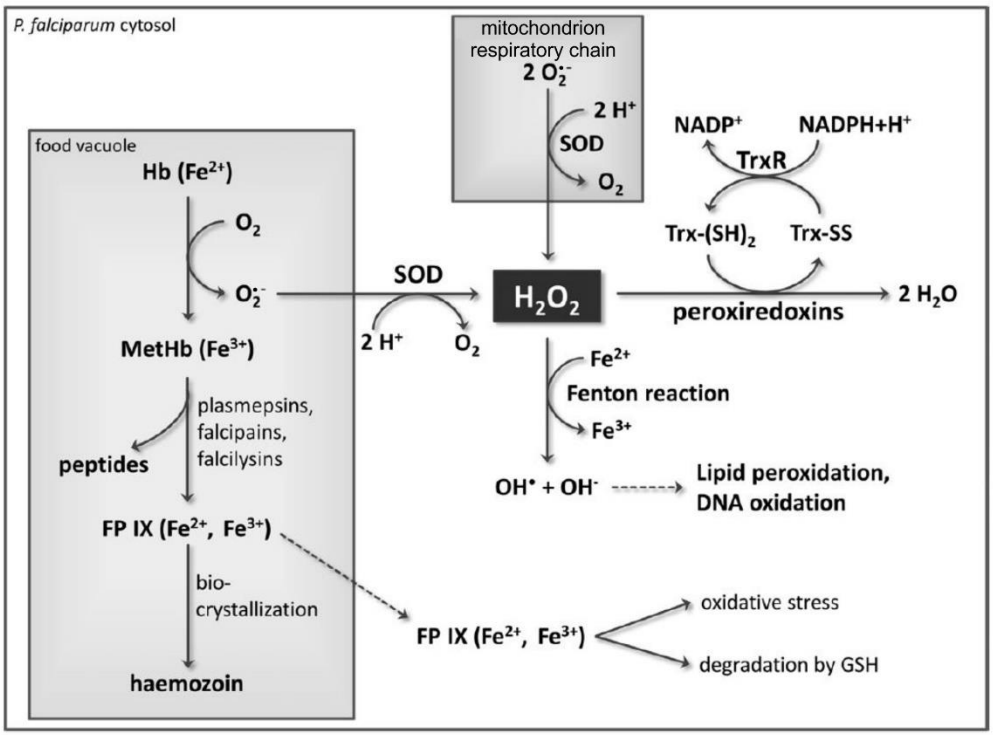

Fig. 8 Sources of reactive oxygen species in *P. falciparum.*

Superoxide ions that can damage lipids, membranes and nucleic acids are supposed to be produced by the respiratory chain and heme oxidation in hemoglobin (Hb). In *P. falciparum* two superoxide dismutases (SODs) catalyze the disproportionation to molecular oxygen and hydrogen peroxide. H_2O_2 is reduced by peroxiredoxins, which are coupled to the NADPH-dependent Trx/TrxR system. MetHb: methemoglobin, FP IX: ferriprotoporphyrin IX, Trx: thioredoxin, TrxR: thioredoxin reductase (Jortzik and Becker 2012).

Peroxiredoxins (Prxs) are ubiquitonously found in eukaryotic cells and belong to the most abundant proteins in a cell (Wood et al. 2003). They play an important role in the antioxidant protection system of a cell via the reduction of hydroperoxides and peroxynitrites to the corresponding harmless alcohols and nitrites, respectively. Moreover, they can take part in diverse signaling processes using H_2O_2 as a second messenger (Stone and Yang 2006). Due to their sequence similarity, they are grouped into six structural classes: AhpC/Prx1, BCP/PrxQ, Prx5, Prx6, Tpx, and AhpE. Tpx and AhpE were found exclusively in bacteria whereas the other subfamilies are also found in eukaryotes (Soito et al. 2011). Peroxiredoxins can also be grouped according to their catalytic cycle in 1-Cys, 2-Cys or atypical 2-Cys Prxs (Rhee 2016). In *P. falciparum* five Prxs have been indentified so far: Prx1a, Prx1m, Prx5/AOP, Prx6, and PrxQ/nPrx (Jortzik and Becker 2012). nPrx displays an unusual Prx that localizes exclusively to the nucleus and interacts with chromatin (Richard et al. 2011). Moreover, during its

erythrocytic cycle, *P. falciparum* imports and uses human Prx2 for hydroperoxide detoxification (Koncarevic et al. 2009).

The catalytic cycle follows a common sequence among all known Prxs (Fig. 9). **1** The cycle starts with the nucleophilic attack of the peroxidatic thiolate (S_p^-) on a hydroperoxide (ROOH). Thereby, the peroxidatic cysteine (C_p) is oxidized to the sulfenic acid (S_pOH) releasing the corresponding alcohol. **4** If high amounts of hydroperoxides are present, the sulfenic acid can be further oxidized to the sulfinic acid (S_pO_2H) leading to the inactivation of the Prx. **5** Some cells harbor a sulfiredoxin (Srx) that can reduce the sulfinic acid back to the sulfenic acid, thereby reactivating the Prx (Rhee et al. 2007). **2** A local unfolding (LU) in the surrounding of C_p allows the attack of a resolving thiol (S_rH) resulting in the formation of a disulfide intermediate. Depending on the Prx, S_rH can be located on the same subunit (atypical 2-Cys), on the opposite subunit (2-Cys) or on another protein/small molecule. **3** Another thiol can attack the disulfide bond resulting in the local refolding of the surrounding of C_p (FF). The thiolate can attack a hydroperoxide and enter a new round of the catalytic cycle.

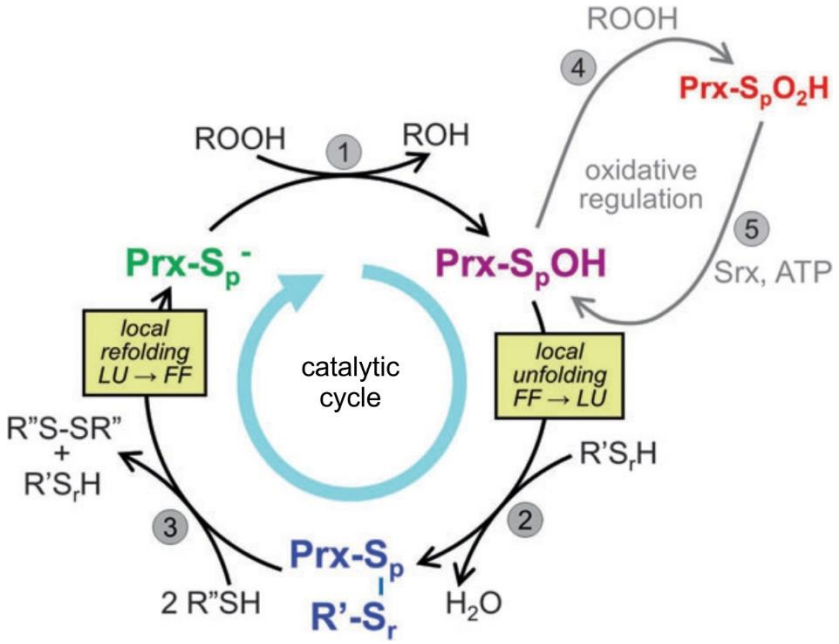

Fig. 9 Catalytic cycle of a Peroxiredoxin (Prx).

1 In the fully folded (FF) conformation, the thiolate of the peroxidatic cysteine attacks a hydroperoxide. The hydroperoxide is reduced to the corresponding alcohol, and the Prx oxidized to the sulfenic acid. **4** Further oxidation leads to the formation to the sulfinic acid **5** which can be reduced by a sulfiredoxin (Srx). **3** Upon locally unfolding (LU) a resolving thiol attacks the oxidized Prx generating a disulfide intermediate. The attack of another thiol reduces Prx leading to the fully folded conformation. In Choi 2018, adapted from Hall et al. 2011.

1.4.1 The AntiOxidant Protein of *P. falciparum* (*Pf*AOP)

The AntiOxidant Protein (*Pf*AOP) was identified as a candidate from a gene locus with around 50 genes that alters artemisinin susceptibility. However, neither deletion nor overexpression of *PFAOP* altered the artemisinin susceptibility (Djuika 2017). *Pf*AOP contains 240 amino acids with two predicted domains: an N-terminal signal peptide and a thioredoxin-like domain (Prx5 domain). The signal peptide was predicted to guide the protein to the apicoplast (Sarma et al. 2005). It was shown that GFP-tagged *Pf*AOP localizes to the apicoplast (Kehr et al. 2010). Immunofluorescence microscopy as well as subcellular fractionation and western blot analyses revealed, however that *Pf*AOP is dually localized in the apicoplast and cytosol, arguing for an independent translation initiation downstream of the targeting sequence (Djuika et al. 2015). The protein is expressed during the whole erythrocytic cycle but is dispensable (Djuika et al. 2017). Heterologous expression of the Prx5 domain showed that the protein homodimerizes in a crystal (Sarma et al. 2005) as well as in solution (Djuika et al. 2013). Moreover, the crystal structure showed that C143 was buried by a β-sheet indicating a monothiol mechanism via C117. It was demonstrated that *Pf*AOP reduces hydroperoxides like tBuOOH and H_2O_2 effectively and that Grx as well as Trx1 are able to function as electron donors (Nickel et al. 2006). However, in contrast to the cytosol, so far neither a Grx nor a Trx was identified in the apicoplast. A later study, using the Grx system clearly demonstrated, that C117 is the peroxidatic cysteine and that its oxidation can be resolved without the need of C143. However, due to the use of a steady-state assay that acquires the whole catalytic cycle, including the oxidative and the reductive half-reaction, two mechanisms of the reductive half-reaction are theoretically possible: First, oxidized *Pf*AOP could form a *Pf*AOP-Grx intermediate before it is reduced by GSH or second, oxidized *Pf*AOP is glutationylated and then reduced by Grx (Djuika et al. 2013). The C143S mutant showed slower kinetics indicating a modulatory role in the catalytic cycle of *Pf*AOP. Interestingly, mutations of the residue L109 that separates both cysteines alters the kinetic values (Staudacher et al. 2015). These results indicate that residue 109 in *Pf*AOP controls the kinetics to form an intramolecular disulfide bond between C143 and C117. Although the formation of the disulfide bond is not essential for the reduction of hydroperoxides *in vitro*, it might have a regulatory role *in vivo,* like protecting C117 from hyperoxidation or the resolving of disulfide intermediates of C117 and other peptides/proteins (Djuika et al. 2013). Intracellular activity measurements with a fused redox-

sensitive GFP-2 (roGFP2) revealed a reduced hyperoxidation-dependent inactivation of *Pf*AOP^{L109M} (Staudacher et al. 2018).

1.5 Aim of the study

This PhD thesis aimed to study a putative Keap1-like redox-dependent function of *Pf*Kelch13 and its influence on the parasite's susceptibility towards the endoperoxide artemisinin. Since the mutation of cysteine residue C580 to tyrosine showed a decreased artemisinin susceptibility (Ghorbal et al. 2014), the goal was to study the relevance and a potential influence of a disulfide bond with C532 on artesmisnin susceptibility. Therefore, serine substitutions of C532 and C580 were generated and analyzed by ring-stage survival assays in *Plasmodium falciparum*. To test a possible role of *Pf*Kelch13 protein stability on artemisinin susceptibility, *Pf*Kelch13 knock-down strains were generated by using the *glmS* riboswitch system. Growth determination and ring-stage survival assays were used to test the effect of the protein abundance on artemisnin susceptibility. To analyze a possible redox regulation of *Pf*Kelch13 *in vitro*, single cysteine to serine mutantions (C447, C469, C473, C532, C542, C580, C696) were recombinantly expressed in prokaryotic (*E. coli*) as well as eukaryotic cells (*P. pastoris*, *L. tarentolae*, Sf21). Different expression conditions were tested to generate a protocol for the production of recombinant *Pf*Kelch13. The protein was characterized with different biochemical methods to analyze its stability, the oligomeric state in solution, and the accessibility of the cysteine residues.

The second aim of this study was to determine the kinetic values of the reductive half-reaction of the peroxiredoxin *Pf*AOP. First, Western blots and mobility shift assays were used to show if oxidized *Pf*AOP can be glutathionylated. Second, stopped-flow measurements were performed to determine the rate constants of this reaction.

2 Materials and Methods

2.1 Materials

2.1.1 Equipment

Table 1 Laboratory equipment.

Equipment	Manufacturer
ÄKTA FPLC system	GE Healthcare
Analytical balance	Kern
Benchtop centrifuge Mikro 220R	Hettich
Benchtop centrifuge Rotina 380 R	Hettich
Bright-field microscope AXIO Lab.A1	Zeiss
CCD digital gel imaging system Fusion SL	Vilbert Lourmat
Cell counting chamber improved Neubauer	Marien Field
Duomax 1030	Heidolph
Floor centrifuge j2-21	Beckman
Horizontal agarose minigel system	Biostep
Incubator shaker Innova 44R	New Brunswick
Incubator shaker MaxQ4450	Thermo Scientific
Laminar flow hood for *P. falciparum* Safe 2020	Thermo Scientific
Laminar flow hood, *E. coli* MSC-Advantage	Thermo Scientific
Magnetic stirer-hot plate Hei-Standard	Heidolph
Metal block thermostat MBT 250	Kleinfeld Labortechnik
Micropippette PIPETMAN (p2,P10, p20,p50,p200,p1000)	Gilson
Microplate spectrophotometer CLARIOstar	BMG
Microwave	Severin
Mini-PROTEAN electrophoresis cell	Bio-Rad
Mini-PROTEAN Tetra Cell	Bio-Rad
Mini-Trans blot cell system	Bio-Rad
NanoDrop 1000 Spectrophotometer	Thermo Scientific
Peristaltic pump P1	GE Healthcare
Personal-sized incubator	VWR
pH-meter PB-11	Sartorius
Pippette controler Accu-jet pro	Brand

Portable spectrophotometer Ultrospec 10	Amersham Biosciences
Power Supply Mini 300V	Major Science
Semi-Dry PerfectBlue system	Peqlab
Stopped-flow spectrofluorometer SX-20	Applied Photophysics
Thermal Cycler Mastercycler Nexus	Eppendorf
Thermomixer shaker incubator block	Eppendorf
Transfection Device Nucleofector II/2b	Lonza
Ultrasonic laboratory homogenizer Sonopuls HD 2070	Bandelin electronic
Vertical autoclave V-65	Systec
Vortex-mixer Genie 2	Heidolph
Water bath Aqualine 5 l	Carl Roth

2.1.2 Disposables

Table 2 Disposables.

Disposables	Source
6-well plates	Greiner
Amicon Ultra 15 ml centrifugal filters	Merck
Centrifuge tubes (15 and 50 mL)	Greiner
Cryovials 2 mL	Greiner
Cuvettes (Polystyrol)	Sarstedt
Durapore sterile filters PVDF (0.22 µm)	Merck
Electroporation Cuvettes plus 2 mm gap	BTX
Falcon 96 well black/clear flat bottom plate	Corning
Micro reaction tubes (1.5 and 2 mL)	Sarstedt
Parafilm	Bemis
PCR reaction tubes	Sarstedt
PD-10 desalting column	Merck
Petri dishes	Greiner
Pipette tips	Steinbrenner
Poly-Prep chromatography columns	Bio-Rad
PVDF membrane	Merck
Scalpel	Braun
Serological pipettes (1, 5, 10 and 25 mL)	Sarstedt
Spin chromatography columns	Bio-Rad
Stericup sterile vacum filter PVDF (0.22 µm)	Merck

Sterile syringes	BD Plastipak
SuperFrost microscope slides	Buddeberg
Whatman paper	GE Healthcare

2.1.3 Chemicals

Table 3 Chemicals.

Reagents	Source
Acetic acid	Merck
Acetone	Honeywell
Acrylamide/Bis Solution, 37.5:1 (30 % w/v)	Serva
Agarose	Serva
AlbuMAXII	Gibco
Ammonium persulfate (APS)	Sigma Aldrich
Ammonium sulfate	Merck
Ampicillin	AppliChem
Artesunate	Sigma Aldrich
Beta-Mercaptoethanol	Sigma Aldrich
Blasticidin S	Invivogen
Bluo-Gal	Thermo Fisher Scientific
Boric acid	Sigma Aldrich
Bradford reagent	Bio-Rad
Bromophenol blue	Waldeck
Bovine serum albumin (BSA)	Serva
Calcium chloride	Merck
Chorampenicol	AppliChem
CNBr-activated sepharose 4b	Merck
Cobalt(II) chloride	Carl Roth
cOmplete EDTA-free protease Inhibitor	Roche
Coomassie Brilliant Blue G 250	AppliChem
Copper(II) chloride	Carl Roth
D-(+)-Galactose	Carl Roth
D-(+)-Glucosamine hydrochloride	Sigma Aldrich
D-(+)-Glucose	Merck
D-(+)-Sorbitol	Sigma Aldrich

Deoxyribonucleoside triphosphate (dNTPs)	Thermo Fisher Scientific
Diamide	Sigma Aldrich
Dimethylformamid (DMF)	Carl Roth
Dipotassium hydrogen phosphate	Merck
Disodium hydrogen phosphate	Merck
Dithiothreitol (DTT)	Sigma Aldrich
Dimethyl sulfoxide (DMSO)	Sigma Aldrich
DNA ladder (100 bp, 1kb)	New England Biolabs
DNase I	Roche
DSM1	BEI Resources
DTNB/Ellman's reagent (5,5'-dithiobis-(2-nitrobenzoic acid)	Thermo Fisher Scientific
DTPA (diethylenetriaminepentaacetic acid)	Sigma Aldrich
EDTA (ethylenediaminetetraacetic acid)	Sigma Aldrich
EGTA (triethylene glycol diamine tetraacetic acid)	AppliChem
Ethanol (absolute)	VWR
Fetal bovine serum (FBS heat inactivated)	Gibco
Gel loading dye, purple 6×	New England Biolabs
Gel Red dye, 6X	Biotium
Gentamicin	Gibco
Giemsa stock solution	Carl Roth
Glycerol	AppliChem
Glycine	Merck
GSH (glutathione)	Sigma Aldrich
GSSG (glutathione disulfide)	Sigma Aldrich
HEPES (4-(2-hydroxyethyl)-1-piperazineethanesulfonic acid)	Merck
Hydrochloric acid	VWR
Hydrogen peroxide (30%)	Merck
Hypoxanthine	c.c.pro
Imidazole	Merck
IPTG (Isopropyl β-D-1-thiogalactopyranoside)	Merck
Iron(III) chloride	Sigma Aldrich
Isopropanol	Merck
Kanamycin	AppliChem
Luria Bertani (LB) agar	Carl Roth
Luria Bertani (LB) medium	Carl Roth

Manganese(II) chloride	Merck
Magnesium chloride	Merck
Magnesium sulfate	Merck
Methanol	Merck
mmPEG (Methyl-PEG-maleimide;MeO-dPEG(24)-mal)	Iris Biotech
Milk powered, skimmed blotting grade	Carl Roth
Ni-NTA-Agarose	QIAGEN
Niquel(II) chloride	Sigma Aldrich
Pepton	Merck
PonceauS	Serva
Potassium acetate	Sigma Aldrich
Potassium chloride	AppliChem
Potassium dihydrogen phosphate	Merck
Potassium hydroxide	Carl Roth
Roti-Lumin plus	Carl Roth
Prestained protein ladder	Thermo Scientific
Proteinase K	Roche
RNAse A	Sigma Aldrich
RPMI 1640 (HEPES, glutamine)	Gibco
Saponin	Sigma Aldrich
Sf-900 III	Thermo Scientific
Sodium acetate	Sigma Aldrich
Sodium chloride	Sigma Aldrich
Sodium dihydrogen phosphate	Merck
Sodium dodecyl sulfate (SDS)	Serva
Sodium fluoride	Merck
Sodium hydrogen carbonate	Carl Roth
Sodium hydroxide	Carl Roth
Sodium molybdate	Strem chemicals
Sodium selenite	Sigma Aldrich
Tert-butyl hydroperoxid	Sigma Aldrich
Tetracyclin	Carl Roth
Tetramethyl ethylenediamine (TEMED)	Serva
TRIS (tris(hydroxymethyl)aminomethane)	Carl Roth
Triton X-100	Merck

Trypan blue	Thermo Fisher Scientific
Tween-20	Sigma Aldrich
Urea	AppliChem
WR99210	Jacobus Pharmaceutical
X-tremeGENE HP DNA Transfection Reagent	Merck
Yeast extract	Merck
Zinc sulfate	Merck

2.1.4 Drugs used for selection

Table 4 Antibiotics

Drug	Stock	Working concentration	Supplier
Ampicilin	100 mg/ml in 50% ethanol	100 µg/ml	AppliChem
Kanamycin	50 mg/ml in ddH_2O	50 µg/ml	AppliChem
Choramphenicol	34 mg/ml in 100% ethanol	34 µg/ml	AppliChem
Tetracyclin	10 mg/ml in 100% ethanol	10 µg/ml	Carl Roth
Gentamicin	50 mg/ml in ddH_2O	10 µg/ml	Gibco
Blasticidin S	10 mg/mL in HEPES buffer	10 µg/mL	Invivogen
WR99210	20 µM in RPMI medium (0.1% DMSO)	4 nM	Jacobus Pharmaceutical
DSM1	3.75 mM in 95% DMSO/ 5% PBS	900 nM	BEI Resources

2.1.5 Enzymes

Table 5 Enzymes.

Enzyme	Manufacturer
Phusion DNA polymerase	New England Biolabs
Restriction enzymes	New England Biolabs
T4 DNA ligase	New England Biolabs
Taq DNA polymerase	New England Biolabs

2.1.6 Kits

Table 6 Kits.

Kit	Manufacturer
QIAprep Midiprep Kit	QIAGEN
QIAprep Spin Miniprep Kit	QIAGEN
Wizard SV Gel and PCR Clean-Up System	Promega

2.1.7 Software

Table 7 Software.

Software/ Bioinformatics tools	Developer
2StrucCompare	https://2struccompare.cryst.bbk.ac.uk/index.php
Benchling (2020)	https://www.benchling.com/
Citavi	Swiss Academic Software
Coreldraw	Corel
ImageJ	Wayne Rasband (NIH)
Inkscape 1.0 (2020)	https://inkscape.org/
JustBio	https://www.justbio.com
K2D2	(Perez-Iratxeta and Andrade-Navarro 2008)
MARS	BMG Labtech
MS Office	Microsoft
NCBI databases	https://www.ncbi.nlm.nih.gov/
PlasmoDB	https://plasmodb.org/plasmo/app
PrimerX	https://www.bioinformatics.org/primerx/
Pro-data SX	Applied Photophysics
ProtParam tool	https://web.expasy.org/protparam/
PyMOL Version 1.2r3pre	Schrödinger, LLC
SigmaPlot 13.0	Systat Software, Inc.

2.1.8 Antibodies

Table 8 Antibodies.

Antibody	Host species	Source	Dilution
Anti 6x-His Tag (Monoclonal)	Mouse	Thermo Fisher Scientific	1:1000
Anti Glutathione (Monoclonal)	Mouse	Thermo Fisher Scientific	1:1000
α-*Pf*Kelch13 (Polyclonal)	Rabbit	This study	1:2000
α-Mouse IgG (H+L)-HRP conjugate	Goat	Bio-Rad	1:10000
α-Rabbit IgG (H+L)-HRP conjugate	Goat	Bio-rad	1:10000

2.1.9 Oligonucleotides

All primers were purchased from Metabion, desalted and dissolved in ddH_2O (100 µM). Restriction sites are underlined. Mutations are indicated in red.

Table 9 List of primers.

Number	Name	Sequence (5´ → 3´)
Cloning primers		
P1	PfK13/337-726/KpnI/s	GATCGGTACCGATAAAAAGAAAATCGTGGACGCG
P2	PfK13/AvrII/as	GATCCCTAGGTTAGATATTCGCAATCAGAA
P3	PfK13/BamHI/s	GATCGGATCCATGGAAGGCGAGAAGGTTAAGACC
P4	PfK13/HindIII/as	GATCAAGCTTTTAGATATTCGCAATCAGAACGCTATG
P5	PfK13/BamHI/337-726/s	GATCGGATCCGATAAAAAGAAAATCGTGGACGCGAAC
P26	PfK13/XbaI/337-726/s	GATCTCTAGAGATAAAAAGAAAATCGTGGACGCGAAC
P27	PfK13/XbaI/s	GATCTCTAGAATGGAAGGCGAGAAGGTTAAGACC
P28	BglII/ATG6xHis/KpnI/NcoI/s	GATCTATGCACCATCATCACCATCACGGTACCC
P29	BglII/ATG6xHis/KpnI/NcoI/as	CATGGGGTACCGTGATGGTGATGATGGTGCATA
P30	PfK13/NotI/as	GATCGCGGCCGCTTAGATATTCGCAATCAGAACGCTATG
P31	PfK13/KpnI/s	GATCGGTACCATGGAAGGCGAGAAGG
P32	PfK13/NdeI/s	GATCCATATGGAAGGCGAGAAGGTTAAGACC
P33	PfK13/337-726/NdeI/s	GATCCATATGGATAAAAAGAAAATCGTGGACGCG
P38	PfK13_XbaI_N8Hisup_s	GATCTCTAGACCACCACCACCATCACCACCATCACATGGAAGGCGAGAAGG
P39	PfK13_EcoRI_N8Hisup_s	GATCGAATTCACCACCACCATCACCACCATCACATGGAAGGCGAGAAGG
P50	BamHI/ATG8xHis/XbaI/s	GATCCATGCATCATCATCATCATCATCATT
P51	BamHI/ATG8xHis/XbaI/as	CTAGAATGATGATGATGATGATGATGCATG
P52	PfK13/XbaI/s	GATCTCTAGAGAAGGCGAGAAGGTTAAG
P60	NheI/ATG8xHis/SalI/s	CTAGCATGCATCATCATCATCATCATCATG
P61	NheI/ATG8xHis/SalI/as	TCGACATGATGATGATGATGATGATGCATG
P62	BglII/L3rest/SalI/s	GATCTGCTGCTGCTGGTGCTGGTGGTGCTGCTAGAGCTGCTG
P63	BglII/L3rest/SalI/as	TCGACAGCAGCTCTAGCAGCACCACCAGCACCAGCAGCAGCA
P64	pSLI-PfK13$^{337-726}$/SalI/s	GATCGTCGACGACAAGAAGAAGATAGTAGACGC
P65	pSLI-PfK13$^{337-726}$loxP/XhoI/as	GATCCTCGAGTCATAATAACTTCGTATAATG
P69	pSLI-K13/SalI/s	GATCGTCGACGAGGGTGAGAAGGTTAAGACTAAAG
P88	StuI_glmS_s	GATCAGGCCTGTCCAGACCTGCAG
P89	glmS_XhoI_as	GATCCTCGAGAGATCATGTGATTTCTCTTTG
P90	GFP/speI/s	GATCACTAGTATGAGTAAAGGAGAAGAACTTTTCACTG
P91	L3/BamHI/as	GATCGGATCCAGCAGCTCTAGCAGCACC
P92	K13/SacI/as	GATCGAGCTCTTAGATATTCGCAATCAGAACGC

Mutagenesis primers

P6	PfK13/C447S/s	GTTTCCGCTGGTGTTCAGCATCGGTGGCTTTG
P7	PfK13/C447S/as	CAAAGCCACCGATGCTGAACACCAGCGGAAAC
P8	PfK13/C469S/s	GACATTAGCCAGCAAAGCTGGCGTATGTGCAC
P9	PfK13/C469S/as	GTGCACATACGCCAGCTTTGCTGGCTAATGTC
P10	PfK13/C473S/s	CAATGCTGGCGTATGAGCACCCCGATGAGC
P11	PfK13/C473S/as	GCTCATCGGGGTGCTCATACGCCAGCATTG
P12	PfK13/C532S/s	CGCGTCGTAACAACAGCGGTGTGACCAGCAAC
P13	PfK13/C532S/as	GTTGCTGGTCACACCGCTGTTGTTACGACGCG
P14	PfK13/C542S/s	CAACGGCCGTATCTACAGCATTGGTGGCTATG
P15	PfK13/C542S/as	CATAGCCACCAATGCTGTAGATACGGCCGTTG
P16	PfK13/C580S/s	GTAGCAGCGCGATGAGCGTGGCGTTTGACAAC
P17	PfK13/C580S/as	GTTGTCAAACGCCACGCTCATCGCGCTGCTAC
P18	PfK13/C696S/s	GAGGTTCTGAACAGCAGCCACTTCTTTAGCC
P19	PfK13/C696S/as	GGCTAAAGAAGTGGCTGCTGTTCAGAACCTC
P20	PfK13/C580F/s	GTAGCAGCGCGATGTTCGTGGCGTTTGACAAC
P21	PfK13/C580F/as	GTTGTCAAACGCCACGAACATCGCGCTGCTAC
P22	PfK13/C580Y/s	GCGTAGCAGCGCGATGTATGTGGCGTTTGACAACAAG
P23	PfK13/C580Y/as	CTTGTTGTCAAACGCCACATACATCGCGCTGCTACGC
P71	pSLI-K13C580S/s	GGTCTAGTGCAATGTCCGTAGCATTCGACAAC
P72	pSLI-K13C580S/as	GTTGTCGAATGCTACGGACATTGCACTAGACC
P73	pSLI-K13C580Y/s	GGTCTAGTGCAATGTACGTAGCATTCGACAAC
P74	pSLI-K13C580Y/as	GTTGTCGAATGCTACGTACATTGCACTAGACC
P75	pSLI-K13C532S/s	CAAGGAGGAACAACTCCGGAGTAACCTCTAAC
P76	pSLI-K13C532S/as	GTTAGAGGTTACTCCGGAGTTGTTCCTCCTTG
P84	pSLI-K13C469S/s	GACATATCACAGCAGAGTTGGCGAATGTGC
P85	pSLI-K13C469S/as	GCACATTCGCCAACTCTGCTGTGATATGTC
P86	pSLI-K13C473S/s	CAGCAGTGTTGGCGAATGAGTACTCCAATGTCAACTAAG
P87	pSLI-K13C473S/as	CTTAGTTGACATTGGAGTACTCATTCGCCAACACTGCTG
P95	PfK13/R539T/s	GTGACCAGCAACGGCACTATCTACTGCATTG
P96	PfK13/R539T/as	CAATGCAGTAGATAGTGCCGTTGCTGGTCAC
P97	PfK13/I543T/s	CCGTATCTACTGCACTGGTGGCTATGATG
P98	PfK13/I543T/as	CATCATAGCCACCAGTGCAGTAGATACGG

Sequencing primers

P24	PfK13/sequencing1/s	CCTGGACGCGGCGAACC
P25	PfK13/sequencing2/as	GCTGCCATCATAGCCACC
P40	T7promoter	TAATACGACTCACTATAGGG
P53	pUC/M13 Forward	CCCAGTCACGACGTTGTAAAACG

P54	pUC/M13 Reverse	AGCGGATAACAATTTCACACAGG
P55	pVL1392.seqF	AAATGATAACCATCTCGC
P66	pSLI-N-loxP/s	GTTCTTTGTTGACTTGTG
P67	pSLI-N-loxP/as	CAGTTATAAATACAATCAATTGG
P68	GFPseq.end/s	GTAACAGCTGCTGG
P70	pSLI-K13/s	CAAGGACAAAAAGGAGC
P83	K13-SLI/seq/s	CTCACCTTCTATAATGAACAC
P93	pHBIRH/seq/s	CCTACATACATATACAAACCTAC
P94	pHBIRH/seq/as	CATATGTATTTTTTTTGTAATTTCTGTG

Genotyping primers (*Pf*Kelch13 SLI)

P79	K13_int_check_5/s	CAATTATGAATACCAACAAAAAAGAG
P80	K13_int_check_3/as	GTTTCAAAAATAGCTCCACC
P81	pArl sense 55	GAGCGGATAACAATTTCAC
P82	yDHODH/as	GAGTGTAAAATGCACGAAC

2.1.10 Plasmids

Table 10 Plasmids.

Plasmid	Characteristics	Reference
***E. coli* expression constructs**		
pQE30	AmpR. T5 promotor/lac operator. For production of N-terminal His_6-tagged proteins.	QIAGEN
pQE30-*PFKELCH13*$^{337\text{-}726}$	Production of *Pf*Kelch13$^{337\text{-}726}$	This study
PQE30-*PFKELCH13*	Production of *Pf*Kelch13	This study
pET45b-*PFKELCH13*	AmpR. T7 promotor/lac operator. Production of N-terminal His_6-tagged *Pf*Kelch13 (*E. coli* codon optimized).	GenScript
pET45b-*PFKELCH13*$^{337\text{-}726}$	Production of *Pf*Kelch13$^{337\text{-}726}$	This study
pET45b-*PFKELCH13*^{C447S}	Production of *Pf*Kelch13^{C447S}	This study
pET45b-*PFKELCH13*^{C469S}	Production of *Pf*Kelch13^{C469S}	This study
pET45b-*PFKELCH13*^{C473S}	Production of *Pf*Kelch13^{C473S}	This study
pET45b-*PFKELCH13*^{C532S}	Production of *Pf*Kelch13^{C532S}	This study
pET45b-*PFKELCH13*^{C542S}	Production of *Pf*Kelch13^{C542S}	This study
pET45b-*PFKELCH13*^{C580S}	Production of *Pf*Kelch13^{C580S}	This study
pET45b-*PFKELCH13*^{C696S}	Production of *Pf*Kelch13^{C696S}	This study
pET45b-*PFKELCH13*^{C580F}	Production of *Pf*Kelch13^{C580F}	This study

pET45b-*PFKELCH13*^{C580Y}	Production of *Pf*Kelch13^{C580Y}	This study
pET45b-*PFKELCH13*$^{337-726/C447S}$	Production of *Pf*Kelch13$^{337-726/C447S}$	This study
pET45b-*PFKELCH13*$^{337-726/C469S}$	Production of *Pf*Kelch13$^{337-726/C469S}$	This study
pET45b-*PFKELCH13*$^{337-726/C473S}$	Production of *Pf*Kelch13$^{337-726/C473S}$	This study
pET45b-*PFKELCH13*$^{337-726/C532S}$	Production of *Pf*Kelch13$^{337-726/C532S}$	This study
pET45b-*PFKELCH13*$^{337-726/C542S}$	Production of *Pf*Kelch13$^{337-726/C542S}$	This study
pET45b-*PFKELCH13*$^{337-726/C580S}$	Production of *Pf*Kelch13$^{337-726/C580S}$	This study
pET45b-*PFKELCH13*$^{337-726/C580Y}$	Production of *Pf*Kelch13$^{337-726/C580Y}$	This study
pET45b-*PFKELCH13*$^{337-726/C580F}$	Production of *Pf*Kelch13$^{337-726/C580F}$	This study
pET45b-*PFKELCH13*$^{337-726/C696S}$	Production of *Pf*Kelch13$^{337-726/C696S}$	This study
pGEX-4T-1	AmpR. tac promoter. For production of N-terminal GST-tagged proteins. Thrombin cleavage site between tag and protein.	GE Healthcare
pGEX-4T-1-*PFKELCH13*$^{337-726}$	Production of *Pf*Kelch13$^{337-726}$	This study
pGEX-4T-1-*PFKELCH13*	Production of *Pf*Kelch13	This study
pMAL-c5x-TEV	AmpR. tac promoter. For production of N-terminal MBP-tagged proteins. TEV cleavage site between tag and protein.	AG Pierik (TU Kaiserslautern)
pMAL-c5x-TEV-*PFKELCH13*	Production of *Pf*Kelch13	This study
pMAL-c5x-TEV-*PFKELCH13*$^{337-726}$	Production of *Pf*Kelch13$^{337-726}$	This study
pQE30-*PFGRX*$^{C32/88S}$	Production of *Pf*Grx$^{C32/88S}$	(Djuika et al. 2013)
pQE30-*PFAOP*^{wt}	Production of *Pf*AOP^{wt}	(Djuika et al. 2013)
pQE30-*PFAOP*^{C117S}	Production of *Pf*AOP^{C117S}	(Djuika et al. 2013)
pQE30-*PFAOP*^{C143S}	Production of *Pf*AOP^{C143S}	(Djuika et al. 2013)
pGroEL/GroES	CamR. Production of GroEl/GroES	AG Pierik (TU Kaiserslautern)

Sf21 expression constructs

pCoofy41	AmpR, GmR. Polyhedrin promotor. For production of proteins in insect cells.	(Scholz 2013) Addgene: Plasmid #55184
pCoofy41-Nterm8xHis	AmpR, GmR. Polyhedrin promotor. For production of N-terminal His_8-tagged proteins in insect cells.	This study
pCoofy41-*PFKELCH13*	Production of *Pf*Kelch13	This study
pCoofy41-*PFKELCH13*$^{337-726}$	Production of *Pf*Kelch13$^{337-726}$	This study
pCoofy41-*PFKELCH13*$^{337-726/C447S}$	Production of *Pf*Kelch13$^{337-726/C447S}$	This study

pCoofy41-*PFKELCH13*$^{337\text{-}726/C469S}$	Production of *Pf*Kelch13$^{337\text{-}726/C469S}$	This study
pCoofy41-*PFKELCH13*$^{337\text{-}726/C473S}$	Production of *Pf*Kelch13$^{337\text{-}726/C473S}$	This study
pCoofy41-*PFKELCH13*$^{337\text{-}726/C532S}$	Production of *Pf*Kelch13$^{337\text{-}726/C532S}$	This study
pCoofy41-*PFKELCH13*$^{337\text{-}726/C542S}$	Production of *Pf*Kelch13$^{337\text{-}726/C542S}$	This study
pCoofy41-*PFKELCH13*$^{337\text{-}726/R539T}$	Production of *Pf*Kelch13$^{337\text{-}726/R539T}$	This study
pCoofy41-*PFKELCH13*$^{337\text{-}726/I543T}$	Production of *Pf*Kelch13$^{337\text{-}726/I543T}$	This study
pCoofy41-*PFKELCH13*$^{337\text{-}726/C580S}$	Production of *Pf*Kelch13$^{337\text{-}726/C580S}$	This study
pCoofy41-*PFKELCH13*$^{337\text{-}726/C580Y}$	Production of *Pf*Kelch13$^{337\text{-}726/C580Y}$	This study
pCoofy41-*PFKELCH13*$^{337\text{-}726/C580F}$	Production of *Pf*Kelch13$^{337\text{-}726/C580F}$	This study
pCoofy41-*PFKELCH13*$^{337\text{-}726/C696S}$	Production of *Pf*Kelch13$^{337\text{-}726/C696S}$	This study

pSLI contructs for genomic modification in *P. falciparum*

pSLI-N-GFP-2xFKBP-loxP(K13)	AmpR. Selectable marker: *h*DHFR for plasmid selection and *y*DHODH for integrant selection in *P. falciparum*. Disruption of *PFKELCH13* expression and expression of N-terminal GFP-2xFKBP-tagged *PFKELCH13* under the endogenous *PFKELCH13* promoter.	(Birnbaum et al. 2017) Addgene: Plasmid #85792
pSLI-His_8-*PFKELCH13*^{wt}	Disruption of *PFKELCH13* expression and expression of N-terminal His_8-tagged *PFKELCH13* under the endogenous *PFKELCH13* promoter.	This study
pSLI-His_8-*PFKELCH13*^{C469S}	Disruption of *PFKELCH13* expression and expression of N-terminal His_8-tagged *PFKELCH13* ^{C469S} under the endogenous *PFKELCH13* promoter.	This study
pSLI-His_8-*PFKELCH13*^{C473S}	Disruption of *PFKELCH13* expression and expression of N-terminal His_8-tagged *PFKELCH13* ^{C473S} under the endogenous *PFKELCH13* promoter.	This study
pSLI-His_8-*PFKELCH13*^{C532S}	Disruption of *PFKELCH13* expression and expression of N-terminal His_8-tagged *PFKELCH13* ^{C532S} under the endogenous *PFKELCH13* promoter.	This study
pSLI-His_8-*PFKELCH13*^{C580S}	Disruption of *PFKELCH13* expression and expression of N-terminal His_8-tagged *PFKELCH13* ^{C580S} under the endogenous *PFKELCH13* promoter.	This study
pSLI-His_8-*PFKELCH13*^{C580Y}	Disruption of *PFKELCH13* expression and expression of N-terminal His_8-tagged *PFKELCH13* ^{C580Y} under the endogenous *PFKELCH13* promoter.	This study

pSLI-His_8-*PFKELCH13-glmS*	Disruption of *PFKELCH13* expression and expression of N-terminal His_8-tagged *PFKELCH13-glmS* under the endogenous *PFKELCH13* promoter.	This study
pSLI-His_8-*PFKELCH13-M9*	Disruption of *PFKELCH13* expression and expression of N-terminal His_8-tagged *PFKELCH13-M9* under the endogenous *PFKELCH13* promoter.	This study
pSLI-His_8-$PFKELCH13^{337-726}$	Disruption of *PFKELCH13* expression and expression of N-terminal His_8-tagged $PFKELCH13^{337-726}$ under the endogenous *PFKELCH13* promoter.	This study

Plasmids for episomal expression in *P. falciparum*

pHBIRH	AmpR. Bidirectional promotor for expression of the selection marker bsd and the transgene in *P. falciparum*.	(Epp 2008)
pHBIRH-*GFP-PFKELCH13*	Expression of *PFKELCH13* in *P. falciparum.*	This study

2.1.11 Bacterial strains

Table 11 Bacterial strains.

***E. coli* strain**	**Genotype**	**Application**	**Source**
XL1-Blue	recA1 endA1 gyrA96 thi-1 hsdR17 supE44 relA1 lac [F´ proAB laclq ZΔM15 Tn10 (Tetr)]	Cloning, Protein production	Stratagene
SHuffle T7 Express	*fhuA2 lacZ::T7 gene1* [lon] *ompT ahpC gal λatt::*pNEB3-r1-*cDsbC* ($Spec^R$, $lacI^q$) Δ*trxB sulA11 R(mcr-73::miniTn10*--Tet^S)2 [dcm] *R(zgb-210::Tn10* --Tet^S) *endA1 Δgor Δ(mcrC-mrr)114::IS10*	Protein production	New England Biolabs
BL21(DE)pLysS	F^- *ompT hsdS*$_B$(r_B^- m_B^-) *gal dcm* (DE3) pLysS (Cam^R)	Protein production	Merck
Rosetta-gamiB(DE)pLysS	F^- *ompT hsdS*$_B$ (r_B^- m_B^-) *gal dcm lacY1 ahpC* (DE3) *gor522*::Tn*10 trxB* pLysSRARE (Cam^R, Kan^R, Tet^R)	Protein production	Merck
DH10EMBacY	F^-*mcr*A Δ(*mrr*-hsdRMS-*mcr*BC) Φ80*lac*ZΔM15 Δ*lac*X74 *rec*A1 *end*A1 *ara*D139 Δ(*ara*, *leu*)7697 *gal*U *gal*K λ^- *rps*L *nup*G/pMON14272/pMON7124	Production of bacmid DNA	Geneva Biotech

2.1.12 *P. falciparum* strains

Table 12 *P. falciparum* strains.

***P. falciparum* strain**	**Characteristics**	**Source/reference**
Wild-type strains		
NF54		(Ghorbal et al. 2014)
3D7	Derived from NF54	(Walliker et al. 1987)
Stable transgenic strain		
NF54K13^{C580Y}	Harbors K13^{C580Y}, shows artemisinin resistance	(Ghorbal et al. 2014)
3D7_His$_8$-*PFKELCH13*	N-terminal His$_8$-tagged Kelch13	This work
3D7_His$_8$-*PFKELCH13*^{C532S}	N-terminal His$_8$-tagged Kelch13^{C532S}	This work
3D7_His$_8$-*PFKELCH13*^{C580S}	N-terminal His$_8$-tagged Kelch13^{C580S}	This work
3D7_His$_8$-*PFKELCH13*^{C469S}	N-terminal His$_8$-tagged Kelch13^{C469S}	This work
3D7_His$_8$-*PFKELCH13-glms*	N-terminal His$_8$-tagged Kelch13. Expression is regulated by *glmS* (active riboswitch).	This work
3D7_His$_8$-*PFKELCH13-M9*	N-terminal His$_8$-tagged Kelch13. Negative control for *glmS* (*M9*: inactive riboswitch).	This work
Transiently transgenic strain		
3D7_His$_8$-*PFKELCH13*; pHBIRH-GFP-*PFKELCH13*	N-terminal His$_8$-tagged Kelch13, episomal expression of GFP-*PFKELCH13*.	This work
3D7_pSLI-His$_8$-*PFKELCH13*^{C580Y}; pHBIRH-GFP-*PFKELCH13*	Harbors pSLI-His$_8$-*PFKELCH13*^{C580Y} for integration; expresses GFP-*PFKELCH13* episomally.	This work
3D7_pSLI-His$_8$-*PFKELCH13*^{C473S}; pHBIRH-GFP-*PFKELCH13*	Harbors pSLI-His$_8$-*PFKELCH13*^{C473S} for integration; expresses GFP-*PFKELCH13* episomally.	This work
3D7_pSLI-His$_8$-*PFKELCH13*$^{337-726}$	Harbors pSLI-His$_8$-*PFKELCH13*$^{337-726}$ for integration.	This work

2.2 Molecular biology methods

2.2.1 Amplification of DNA by Polymerase chain Reaction (PCR)

In order to amplify DNA fragments used for cloning, primers with overhangs for sticky end restriction were designed (Table 9). All primers started with the nucleotide sequence GATC followed by the restriction site sequence. The annealing temperature ranched from 45-65°C and was calculated with the following formula: $T_a = 4°C\ (G/C) + 2°C\ (A/T) - 5°C$. Reaction conditions are listed in Table 13.

Table 13 PCR conditions for the amplification of DNA fragments.

Reaction mixture	
Component	Volume (µl)
ddH_2O	36
5x Phusion HF Buffer	10
10 mM dNTPs	1
100 µM forward primer	0.5
100 µM reverse primer	0.5
Template DNA	1 (~60 ng)
Phusion HF DNA Polymerase	1
Final volume	50

Thermocycling conditions		
Temperature (°C)	Time (s)	
95	30	
95	30	
45-65	30	X 35 cycles
72	1 kb/20 s	
72	300	
4	hold	

2.2.2 Agarose gel electrophoresis

DNA fragments were separated by agarose gel electrophoresis. Agarose (1-2% (w/v)) was dissolved in TAE buffer by boiling in a microwave. GelRed (10000x in water) was added and the gel was casted into a horizontal installed gel chamber. After curing, the gel was transferred to a horizontal installed electrophoresis tank filled with TAE buffer. Samples were mixed with 6x loading dye and loaded in gel pockets. As size references a 1 kb or 100 bp DNA ladder was used depending on the expected sizes of DNA fragments. Gels were run at 90-150 V until the pink dye ran around two third of the total gel length. Stained DNA was visualized by UV light using a gel imaging system (Vilber).

TAE buffer 40 mM Tris, 20 mM acetic acid, 1 mM EDTA, pH = 8.0

2.2.3 Digestion of DNA fragments

To generate DNA fragments for ligation or to check correct insertion of an insert in a vector, DNA was double-digested (Table 14). All enzymes and buffers were purchased from NEB. A buffer was chosen in which both enzymes showed highest activity. The reaction took place at 37°C for a minimum of 2 h up to overnight. Digested plasmids were separated by agarose gel electrophoresis and then purified. Digested PCR products were directly cleaned.

Table 14 Reaction mixture to digest DNA.

Reaction mixture	
Component	Volume (µl)
ddH_2O	39/28
10x Restriction Buffer	5
Vector/PCR product	4/15
Enzyme 1	1
Enzyme 2	1
Final volume	50

2.2.4 Purification of DNA fragments

PCR products as well as digested PCR products were purified using the Wizard SV Gel and PCR Clean-Up System (Promega) according to the manufacturer's protocol. If a fragment was excised from a plasmid, fragments were first separated by agarose gel electrophoresis and then purified according to the instructions. DNA was eluted in 35 µl ddH_2O and stored at -20°C until further used.

2.2.5 DNA quantification

DNA concentration was determined using a NanoDrop1000. The concentration was directly calculated by the related software by measuring the absorbance at 280 nm. Quality was checked by determining the ratio of A_{260}/A_{280} which should be between 1.7 and 2.0.

2.2.6 Ligation of DNA fragments

Digested and purified vectors and PCR products were ligated using a standard reaction mixture (Table 15). For some cloning processes, the His-tag encoding sequence was directly inserted as a "primer-sandwich". For this 2 µl of each primer were mixed with 46 µl ddH_2O

and heated at 95°C for 5 min in a metal block. The metal block was slowly cooled to RT to result in correct annealing. The sandwich was designed in a way that it already contains restriction overhangs. To ligate DNA fragments, ddH_2O, vector and inserts were mixed and cooled in a metal block on ice for 5 min. Afterwards, T4 ligase buffer and T4 DNA ligase were added. The metal block was transferred to RT. When the block reached RT (usually 2 h), 5 µl of the reaction mixture was transformed into 50 µl chemically competent XL1-Blue cells.

Table 15 Reaction mixture for the ligation of DNA fragments.

Reaction mixture	
Component	Volume (µl)
10x T4 Ligase Buffer	2
Inserts	á 4
Vector	4
T4 DNA Ligase	1
ad ddH_2O	20

2.2.7 Mutagenesis of DNA

Nucleotides were mutated by mutagenesis PCRs. For the design of mutagenic PCR primers the web-based program PrimerX was used. All PCR reactions were performed using a standard protocol (Table 16).

Table 16 PCR conditions for site-directed mutagenesis.

Reaction mixture	
Component	Volume (µl)
ddH_2O	36.6
5x Phusion HF Buffer	10
10 mM dNTPs	1
100 µM forward primer	0.2
100 µM reverse primer	0.2
Template DNA	1 (~60 ng)
Phusion HF DNA Polymerase	1
Final volume	50

Thermocycling conditions		
Temperature (°C)	Time (s)	
95	30	
95	30	
55	60	X 16 cycles
72	1 kb/20 s	
72	300	
4	hold	

Template DNA was digested by adding 1 µl DpnI. After an incubation for 1 h at 37°C, 5 µl of mutated plasmid DNA were transformed into 50 µl chemically competent XL1-Blue cells.

2.2.8 Sanger sequencing

DNA sequences were confirmed by Sanger sequencing performed by Seq-It (Kaiserslautern). Samples and primers were prepared according to the company's instructions.

2.2.9 Transformation of *E. coli* cells

In order to amplify a plasmid or prepare cells for protein production, XL1-Blue cells were transformed with plasmid DNA. To transform *E. coli* cells, 50 µl chemically competent cells were thawed on ice. After the addition of 1 µl purified plasmid DNA, cells were incubated for 30 min on ice. The cells were heat-shocked for 90 s (XL1-Blue) or 30 s (all other *E. coli* strains) at 42°C and transferred back on ice for 5 min. After the addition of 1 ml LB medium, cells were shaked in an Eppendorf Thermomixer at 600 rpm for 1 h. All *E. coli* strains used in this thesis were incubated at 37°C expect T7 SHuffle Express. For this strain a temperature of 30°C was used. Depending on the plasmid concentration and transformation efficiency, different volumes were spread on LB agar plates containing the appropriate antibiotics for plasmid selection. Usually 50 µl were used. Plates were incubated at 37°C or 30°C overnight and then stored at 4°C for up to 3 weeks.

LB medium	25 g LB medium powder in 1 l ddH_2O, autoclaved
LB agar	40 g LB agar powder in 1 l ddH_2O, autoclaved

2.2.10 Isolation and purification of plasmid DNA from *E. coli*

Plasmid DNA from *E. coli* was usually isolated and purified by the alkaline extraction method (Birnboim and Doly 1979). A single colony of transformed *E. coli* cells was picked and transferred into 3 ml LB medium containing the appropriate antibiotic. The culture was grown in a MaxQ4450 shaker at 220 rpm and 37°C overnight. Cells were harvested by centrifugation at 13000 x g for 30 s. The cell pellet was resuspended in 100 µl ice-cold buffer P1. Cells were lysed with 200 µl buffer P2 by inverting the tube 5 times and incubating for 5 min at RT. After neutralization with 150 µl ice-cold buffer P3, cell debris and genomic DNA were centrifuged at 13000 x g for 10 min at 4°C. The supernatant was transferred to a new tube. Plasmid DNA was precipitated with 600 µl 100% isopropanol by inverting the tube 5 times and

centrifugation at 13000 x g for 5 min at 4°C. Precipitated DNA was washed with 70% ethanol, air-dried and dissolved in 30 µl ddH_2O. For higher amounts and purity for transfections of *P. falciparum*, DNA was extracted and purified with the QIAGEN Plasmid Midi Kit according to the manufacture's protocol. DNA was stored at -20°C.

Buffer P1	50 mM Tris, 10 mM EDTA, 0.1 mg/ml RNase A, pH = 8
Buffer P2	0.2 M NaOH, 1% (w/v) SDS
Buffer P3	1.8 M potassium acetate/acetic acid, pH = 5.2

2.3 Plasmid construction

2.3.1 Cloning of pET45b-*PFKELCH13* plasmids

The original plasmid pET45b-*PFKELCH13* contains a codon-optimized (*E.coli*) *PFKELCH13* sequence that encodes for His_6-*Pf*Kelch13 and was synthesized by a company (GenScript). The plasmid was used as a template to generate a plasmid encoding for a truncated version of *Pf*Kelch13 (*Pf*Kelch13$^{337-726}$). The primers P1 and P2 were used to amplify this DNA fragment with the restriction sites KpnI and AvrII. The fragment was inserted into pET45b. To generate constructs that encode for single cysteine mutations, all seven cysteines of *Pf*Kelch13 were mutated by site-directed mutagenesis. All mutations were generated for the truncated version. The following primer pairs were used (Table 17).

Table 17 Primer pairs for site-directed mutagenesis in *PFKELCH13* in pET45b plasmids.

Primer pair	Encoded *Pf*Kelch13 mutation
P6/P7	C447S
P8/P9	C469S
P10/P11	C473S
P12/P13	C532S
P14/P15	C542S
P16/P17	C580S
P22/P23	C580Y
P20/P21	C580F
P18/P19	C696S

2.3.2 Cloning of pQE30-*PFKELCH13* plasmids

The primers P3 and P4 were used to amplify full length *PFKELCH13* from pET45b-*PFKELCH13* with the restriction sites BamHI and HindIII. The truncated version was amplified using the primers P5 and P4 and pET45b-*PFKELCH13*$^{337\text{-}726}$ as a template. Fragments were inserted into pQE30.

2.3.3 Cloning of pSLI-His$_8$-*PFKELCH13* plasmids

As a template to generate pSLI-His$_8$-*PFKELCH13* plasmids, the plasmid pSLI-N-GFP-2xFKBP-loxP(K13) (kindly provided by Tobias Spielmann, addgene: plasmid #85792) was used. GFP-2xFKBP-K13 was excised using the restriction sites NheI and XhoI. The *PFKELCH13* gene was amplified using primers P65 and P69 with SalI and XhoI restriction sites. Primers P60 and P61 were annealed resulting in the restriction sites NheI and SalI. All DNA fragments were ligated resulting in the replacement of GFP-2xFKBP-K13 for N-terminal His tagged *PFKELCH13*. To introduce mutations in *PFKELCH13*, the gene was first subcloned into the plasmid pET45b using the restriction sites AvrII and XhoI. All mutations were introduced by site-directed mutagenesis using the following primer pairs (Table 18). The mutated *PFKELCH13* genes were amplied and cloned into pSLI-N-GFP-2xFKBP-loxP(K13) as described above.

Table 18 Primer pairs for site-directed mutagenesis in *PFKELCH13* in pSLI plasmids.

Primer pair	Encoded *Pf*Kelch13 mutation
P75/P76	C532S
P84/P85	C469S
P86/P87	C473S
P71/72	C580S
P73/74	C580Y

A construct encoding for a truncated version of His$_8$-tagged *Pf*Kelch13 (His$_8$-*Pf*Kelch13$^{337\text{-}726}$) was generated by using P64 and P69 instead of P65 and P69.

2.3.4 Cloning of pSLI-His$_8$-*PFKELCH13-glmS* and pSLI-His$_8$-*PFKELCH13-M9*

The *glmS* and *M9* (inactive riboswitch) sequences were amplified from pCR 2.1 TOPO-mCherry-glmS and pCR 2.1 TOPO-mCherry-M9 (Turra et al. 2021) respectively using the

primers P88 and P89 with the restriction sites StuI and XhoI. The loxP site was excised from pSLI-His_8-*PFKELCH13* using the same restriction sites and replaced with the *glmS* and *M9* sequence.

2.3.5 Cloning of pHBIRH-*GFP-PFKELCH13*

The *GFP* sequence was amplified from the plasmid pSLI-N-GFP-2xFKBP-loxP(K13) (kindly provided by Tobias Spielmann, addgene: plasmid #85792) using primers P90 and P91 with restriction sites SpeI and BamHI. The *PFKELCH13* sequence was amplified from pET45b-*PFKELCH13* using primers P3 and P92 with the restriction sites BamHI and SacI. The gene *PFERV* in the plasmid pHBIRH-*PFERV* (provided by Sandra Specht) was excised with SpeI and SacI and replaced with the generated inserts *GFP* and *PFKELCH13*.

2.3.6 Cloning of pCoofy-His_8-*PFKELCH13*$^{337-726}$ plasmids

The plasmid pCoofy41 (kindly provided by the EMBL, Heidelberg, addgene: plasmid #55184) was digested with BamHI and HindIII. A truncated version of the *PFKELCH13* gene encoding *Pf*Kelch13$^{337-726}$ was amplified from pET45b-*PFKELCH13* plasmids encoding for different mutations of *Pf*Kelch13 using primers P26 and P4 with the restriction sites XbaI and HindIII. Primers P50 and P51 encoding the His_8 tag were annealed resulting in the restriction sites BamHI and XbaI. All DNA fragments were ligated resulting in pCoofy-His_8-*PFKELCH13*$^{337-726}$ plasmids encoding for different mutations in *Pf*Kelch13. Two further mutations were introduced by site-directed mutagenesis (P95/P96: R539T and P97/P98: I543T) using pCoofy-His_8-*PFKELCH13*$^{337-726}$ as a template.

A construct encoding for the full-length His_8-tagged *Pf*Kelch13 was generated by using P52 and P4 instead of P26 and P4.

2.4 Cell culture of Sf21 cells

2.4.1 Thawing of Sf21 cells

A cryovial containing 1 ml frozen Sf21 cells (1×10^7 cells) were thawed in the hand and immediately transferred into a falcon tube containing 9 ml pre-warmed Sf-900 III insect medium (Gibco). After centrifugation at 200 x g for 10 min, the supernatant was discarded, the cell pellet resuspended in 20 ml insect medium and transferred to a 100 ml shaker flask that was sealed with aluminum foil. Cells were cultured under standard conditions as outlined below. Cells recovered usually within one week indicated by a normal doubling time of ~24 h/day and a viability greater than 95%.

2.4.2 Standard culture of Sf21 cells

Sf21 cells were cultured as suspensions in Sf-900 III medium in standard Erlenmeyer flasks in an Innova 44R shaker at 120 rpm and 27°C. The volume of the culture was one fifth of the maximal flask volume (e.g. 20 ml culture in a 100 ml flask). Cultures were kept between a density of 0.5-2 x 10^6 cells/ml. Cells were counted every day. Viability was determined by staining cells with trypan blue. For this, 100 µl of the cell suspension were mixed with an equal volume of trypan blue solution and directly transferred to a Neubauer chamber and analyzed by microscopy. The viability was usually higher than 97%. Cells were cultured until the viability dropped below 95%, the doubling time was more than 30 h or a maximal culturing time of 2 months.

Trypan blue solution	0.4% (w/v) trypan blue in PBS
PBS	1.84 mM KH_2PO_4, 10 mM Na_2HPO_4, 137 mM NaCl, 2.7 mM KCl, pH = 7.3 (HCl)

2.4.3 Cryo-preservation of Sf21 cells

Sf21 cells with a doubling time of ~24 h and a viability higher than 98% were cryo-preserved. For this, 20 ml of a culture with a density of 2 x 10^6 cells/ml were centrifuged at 400 x g for 10 min. The supernatant was discarded and the cell pellet resuspended in 4 ml freezing

medium. The suspension was transferred to four cryovials, 1 ml each. The vials were placed at -20°C for 1 h and then stored at -80°C for 48 h. For long-term storage, the vials were transferred to liquid nitrogen.

Freezing medium 60% (v/v) Sf-900 III medium, 30% (v/v) FBS, 10% (v/v) DMSO

2.4.4 Generation of bacmid DNA

The generation of bacmid DNA for the transfection of Sf21 cells was carried out in *E. coli* strain DH10EMBacY. These cells contain a bacmid with a kanamycin resistance and a beta-galactosidase gene and a helper plasmid for efficient transposition with a tetracycline resistance. 50 µl cells were thawed on ice and 1 µl of a pCoofy vector with a gentamicin resistance marker was added. The mixture was incubated for 20 min on ice. Cells were heat-shocked for 45 s at 42°C and placed back on ice for 2 min. After addition of 400 µl LB medium, cells were shaken at 600 rpm in an Eppendorf Thermomixer at 37°C over night. A serial 1 to 10 dilution using LB medium was prepared with a maximal dilution of 1 to 100,000. 100 µl of each dilution was spread on LB agar plates containing the appropriate antibiotics (Table 4) plus 200 µg/ml BluOGal and 1 mM IPTG. Plates were incubated at 30°C for 2 days and for 1 day at 4°C. IPTG addition was used to induce beta-galactosidase production and therefore reaction with BluOGal resulting in a blue compound. White colonies indicate the disruption of the beta-galactosidase gene as a course of successful transposition of the targeting gene delivered by the pCoofy plasmid. Plates were blue/white screened and 4 single white colonies were restreaked on new LB agar plates and incubated for 3 days at RT. Two white clones were picked and transferred to 2 ml LB medium containing the appropriate antibiotics. Cells were grown at 220 rpm in a MaxQ4450 shaker at 37°C over night. Cells were harvested by centrifugation at 4000 x g for 10 min. The bacmid was purified using buffers from the QIAprep Spin Miniprep Kit. The *E. coli* pellet was resuspended in 300 µl buffer P1. Lysis was induced by the addition of 300 µl buffer P2. The tube was inverted several times until the sample had a homogeneous blue color. After the addition of buffer N3, the tube was inverted until no blue color was visible anymore. The tube was centrifuged at 20000 x g for 10 min. The supernatant was transferred to a new tube and centrifuged again. The supernatant was transferred to a new tube and DNA was precipitated by the addition of 700 µl 100% isopropanol. The tube

was centrifuged at 20000 x g for 10 min. Precipitated bacmid DNA was washed with 70% ethanol. After centrifugation at 20000 x g for 5 min the supernatant was discarded under a sterile bench and the DNA was air-dried for 10 min and dissolved in 40 µl sterile ddH_2O by tapping the tube 10 times on the hood bench. Successful transposition was validated by analytical bacmid PCRs using the primer pair P53/P54. Bacmid DNA was immediately used to transfect Sf21 cells.

2.4.5 Transfection of Sf21 cells to generate baculovirus

Sf21 cells were diluted to a density of 0.8 x 10^6 cells/ml. One ml insect medium was pipetted into each well of a 6-well plate. Then, 1 ml of the diluted cell suspension were evenly added to each well. The plate was left for a minimum of 15 min at 27°C to let the cells settle down. During this time, bacmid DNA was mixed with the transfection reagent: To 50 µl insect medium 10 µg bacmid DNA (e.g., in 5 µl water) were added. In another tube 50 µl insect medium were mixed with 5 µl X-tremeGENE HP DNA transfection reagent. DNA and transfection reagent were combined and incubated for 10 min. The mixture (100 µl) was added dropwise to the insect cells (2 ml). The plate was gently rotated and subsequently incubated without shaking at 27°C. After exactly 5 h, 1 ml insect medium was added to the well to dilute the transfection reagent. Cells were incubated at 27°C for 72 h without shaking. The supernatant (2.5 - 3 ml) containing the virus V_0 was transferred to a sterile tube and directly used for the infection of a new batch of Sf21 cells.

2.4.6 Virus amplification used for protein expression

A 25 ml Sf21 cell suspension with a density of 0.6 x10^6 cells/ml was infected by the addition of 2 ml of the V_0 supernatant. Cells were cultured under standard conditions and counted every day. Cells were kept between 1-1.5 x 10^6 cells/ml. If the cell density was higher, cells were diluted. When cells stopped dividing (usually after four days), they were cultured for further 24 h. The culture was centrifuged at 800 x g for 3 min. The supernatant containing the virus V_1 was transferred to a new tube and stored at 4°C for several weeks. This virus was used to infect Sf21 cells for recombinant protein production.

2.5 Cell culture of *P. falciparum* blood stages

2.5.1 Thawing of cryo-preserved *P. falciparum*

Cryovials containing normally 1 ml cryo-preserved *P. falciparum* were thawed in a water bath at 37°C and transferred into a 15 ml tube. After the dropwise addition of 0.2 volumes of thawing solution I, cells were incubated for 2 min. Then, 10 volumes of thawing solution II was slowly added and centrifuged at 300 x g for 5 min. The supernatant was discarded and the cell pellet resuspended in 10 ml thawing solution III. After centrifugation, the cell pellet was washed with complete medium. The cell pellet was resuspended in 14 ml complete medium. Red blood cells were added to set the hematocrit to 3.6%. Infected red blood cells were continuously cultured under standard conditions.

Thawing solution I	12% (w/v) NaCl
Thawing solution II	1.6% (w/v) NaCl
Thawing solution III	0.9% (w/v) NaCl, 0.2% (w/v) glucose
Complete medium	RPMI 1640, 0.45% AlbuMAX II, 200 µM hypoxanthine, 5 µg/ml gentamicin

2.5.2 Giemsa staining and parasitemia estimation

Parasite stages, morphology as well as parasitemia were analyzed by staining infected red blood cells with Giemsa. With a 1 ml serological pipet red blood cells were scrapped from the bottom of a culture containing petri dish and transferred to a microscope slide. With a second slide the blood drop was smeared to generate a blood cell monolayer, and air-dried. Smeared cells were fixed in 100% methanol for 30 s at RT and dried again. Staining was carried out in a 10% (v/v) Giemsa solution for a minimum of 30 min. Slides were washed wish deionized water to remove unspecific Giemsa staining and dried. Cells were analyzed using a light microscope with high magnification (100x, oil-immersion). Parasitemia was expressed as the percentage of infected red blood cells to the total number of red blood cells.

2.5.3 Continuous cultivation of *P. falciparum*

All *P. falciparum* strains were cultured according to a modified standard protocol (Trager and Jensen 1976) at 37°C, 5% O_2, 5%CO_2, 90% N_2 and min. 90% humidity in RPMI 1640 containing 0.45% AlbuMAX II, 200 µM hypoxanthine and 5 µg/ml gentamicin. Infected A^+ erythrozytes were suspended in 14 ml medium and cultured in petri dishes. The hematocrit was set to 3.6%. The parasitemia was kept between 0.1 and 10% to guarantee optimal growth conditions. Depending on the parasitemia, 10 ml culture medium was replaced every one to two days. Cultures with a parasitemia higher than 5% were diluted with red blood cells to maintain a hematocrit of 3.6%. Cells were usually cultured for up to 2 months.

2.5.4 Cryo-preservation of *P. falciparum*

Cultures with a parasitemia of ring stages of > 3% were cryo-preserved. A 14 ml standard culture with a hematocrit of 3.6% was centrifuged at 300 x g for 5 min. The supernatant was discarded and the cell pellet was dropwise resuspended in 500 µl freezing solution. After transferring to a cryovial, cells were immediately frozen in liquid nitrogen.

Freezing solution 28% (v/v) glycerol, 0.65% (w/v) NaCl, 3% (w/v) sorbitol

2.5.5 Synchronization of *P. falciparum*

In order to obtain synchronized parasites, cultures were treated with sorbitol according to a standard procedure by Lambros and Vanderberg 1979. Treatment with sorbitol leads to osmotic lysis of red blood cells infected with more mature parasite stages whereas red blood cells infected with ring stage parasites stay intact. Usually, a 14 ml culture with a hematocrit of 3.6% and a parasitemia of minimum 0.5% was centrifuged at 300 x g for 5 min. The cell pellet was resuspended in 5 ml prewarmed sorbitol solution and incubated for 5 min at RT. After centrifugation the cell pellet was washed with 10 ml complete medium, resuspended in 14 ml complete medium and continuously cultured.

Sorbitol solution 5% (w/v) sorbitol in ddH_2O

Complete medium RPMI 1640, 0.45% AlbuMAX II, 200 µM hypoxanthine, 5 µg/ml gentamicin

2.5.6 Sterilization of plasmid DNA for *P. falciparum* transfections

To sterilize plasmid DNA used for *P. falciparum* transfections 100 µg pure plasmid DNA from a midi-preparation were acidified with 0.1 volumes NaAc buffer and precipitated with 2.5 volumes 100% ethanol. For efficient precipitation the mixture was stored at -20°C over night. After centrifugation at 20000 x g for 30 min at 4°C the DNA was washed with 500 µl 70% ethanol. The supernatant was discarded under sterile conditions and the DNA dried for 10 min. The DNA was directly used to transfect *P. falciparum*.

NaAc buffer 3 M sodium acetate/acetic acid, pH = 4.7

2.5.7 Transfection of *P. falciparum*

In order to genetically modify *P. falciparum*, parasites were transfected by the spontaneous uptake of DNA from preloaded red blood cells (Deitsch et al. 2001). In this thesis all tranfections were performed into a 3D7 strain. First, parasites were sorbitol-synchronized. The next day, mature parasites were diluted to a parasitemia of 1%. After centrifugation at 300 x g for 5 min, 100 µl infected red blood cells and 8 ml complete medium were transferred to a petri dish.

Red blood cells (2 ml) were washed with 6 ml ice-cold cytomix twice (centrifugation: 300 x g, 5 min). Then, 400 µl of washed red blood cells were mixed with 100 µg DNA dissolved in 400 µl cytomix. The mixture was transferred to two electroporation cuvettes and incubated on ice for 5 min. Cells were transfected by electroporation using program U-033 of the Nucleofector 2b (Lonza). After electroporation, cuvettes were immediately transferred on ice and incubated for 5 min. DNA loaded red blood cells were transferred to a 15 ml tube by rinsing each cuvette with 4 ml complete medium. After centrifugation at 300 x g for 5 min, the supernatant was discarded and the remaining cell pellet was resuspended in 5 ml complete medium and pipetted to the infected red blood cells. The next day, smears were prepared. Usually, parasites were in the ring stage indicating successful invasion. To remove lysed red blood cells, infected erythrocytes were washed with 10 ml complete medium, resuspended in 14 ml complete medium and transferred to a new petri dish. The hematocrit was adjusted to 3.6% and the drug for plasmid selection was applied. For *h*DHFR selection 5 nM WR99210 and for BSD 2 µg/ml Blasticidin S were applied. In the first week 10 ml

complete medium were replaced with fresh medium containing the appropriate selection drug. Usually, parasites disappeared within this time. Thenceforth, the medium was exchanged every second day. Once a week 50 µl fresh red blood cells were added to the cultures. Parasites appeared 3-5 weeks post transfection.

Cytomix	120 mM KCl, 0.15 mM $CaCl_2$, 2 mM EGTA, 5 mM $MgCl_2$, 10 mM K_2HPO_4, 10 mM KH_2PO_4, 25 mM HEPES, pH = 7.6 (KOH)
Complete medium	RPMI 1640, 0.45% AlbuMAX II, 200 µM hypoxanthine, 5 µg/ml gentamicin

2.5.8 Selection linked integration of *P. falciparum*

Successfully transfected and selected parasites containing pSLI plasmids were used to further select for integration. All used pSLI vectors encodes for the selection marker *yDHODH*, which is expressed upon successful integration under the control of the endogenous promoter in the *PFKELCH13* locus. Parasites carrying pSLI vectors were grown to a parasitemia of around 5% and 900 nM DSM1 were applied. The medium containing the selection drug was exchanged every day. Usually parasites disappeared after 4 days and reemerged after around 2 weeks. Integration into the correct locus was confirmed by genotyping PCRs.

2.5.9 Extraction of genomic DNA from *P. falciparum*

To isolate genomic DNA from *P. falciparum,* a fast and low-cost protocol was used (Seesui et al. 2018). This protocol does not result in pure genomic DNA. However, it resulted in DNA that led to reproducible results for genotyping PCRs.

A 14 ml standard culture with a parasitemia of 1-3% was centrifuged at 300 x g for 5 min. After discarding the medium, 100 µl of infected red blood cells were resuspended in 1.9 ml EDTA solution. To lyse the red blood cells the suspension was vortexed vigorously, incubated on ice for 10 min and centrifuged at 12000 x g for 5 min. The supernatant was discarded and the remaining pellet was resuspended in 40 µl TE buffer. Parasite lysis and release of DNA was initiated by the addition of 10 µl proteinase K solution. The mixture was shaken at 400 rpm in an Eppendorf Thermomixer heating block at 56°C for 1 h. Proteinase K was inactivated at 80°C

for 10 min. After centrifugation at 12000 x g for 5 min the supernatant was transferred to a new tube and centrifuged again to remove insoluble material. The supernatant containing genomic DNA was stored at -20°C until further used.

EDTA solution	500 µM EDTA in ddH_2O
TE buffer	10 mM Tris, 1 mM EDTA, pH = 7.6 (HCl)
Proteinase K solution	22 mg/ml proteinase K in TE buffer

2.5.10 Genotyping of *P. falciparum* by PCR

Successful integration of SLI cassettes into the correct locus were analyzed by genotyping PCRs. Integration was confirmed from the 5' as well as the 3' of the cassette. We further checked the absence of the endogenous non-modified gene elsewhere in the genome by a primer pair binding inside the gene but outside the homology region (Fig. 18).
As the template, genomic DNA was used. All modified *P. falciparum* strains were compared to the parental strain 3D7. Reaction conditions are given in Table 19.

Table 19 Genotyping PCR conditions.

Reaction mixture	
Component	Volume (µl)
ddH_2O	41.5
10x ThermoPol Buffer	5
10 mM dNTPs	1
100 µM forward primer	0.5
100 µM reverse primer	0.5
Genomic DNA	1
Taq DNA Polymerase	0.5
Final volume	50

Thermocycling conditions		
Temperature (°C)	Time (s)	
95	30	
95	30	
45	30	X 35 cycles
68	100	
68	300	
4	hold	

2.5.11 Saponin lysis of *P. falciparum* infected red blood cells

To enrich malaria parasites for western blots or fluorescence measurements, red blood cells were removed by saponin lysis (Benting et al. 1994). Usually a synchronized 14 ml culture containing trophozoites was centrifuged at 300 x g for 5 min. The cell pellet was resuspended in 14 ml ice-cold PBS containing 0.03% saponin and incubated on ice for 10 min. Parasites

were separated from lysed red blood cells by centrifugation at 1800 x g for 10 min at 4°C. The cell pellet was washed with 10 ml ice-cold PBS. For fluorescence measurements the pellet was resuspended in 150 µl PBS and analyzed using the ClarioStar. For western blot analysis the cell pellet was immediately frozen in liquid nitrogen for further use.

PBS 1.84 mM KH_2PO_4, 10 mM Na_2HPO_4, 137 mM NaCl, 2.7 mM KCl, pH = 7.4

2.5.12 Growth curve determination

To analyze the impact of GlcN on the growth of the His_8-*PFKELCH-glmS* and His_8-*PFKELCH-M9* strain, asynchronous cultures were set to a parasitemia of 0.1% and split into four. Each culture was treated with GlcN resulting in the final concentrations of 0, 0.3, 1, and 2 mM GlcN. The medium containing the appropriate GlcN concentration was renewed every day. Giemsa-stained blood smears were prepared daily. At least 2000 red blood cells were counted and the parasitemia was calculated. Three independent experiments were performed.

2.5.13 EC_{50} determination with SYBR Green I

To determine the sensitivity of *P. falciparum* towards drugs the growth at different drug concentrations was quantified. Since red blood cells (RBCs) do not contain DNA and the DNA amount in infected RBCs directly correlate with the parasite growth (Smilkstein et al. 2004), DNA quantification was directly used as a readout for growth. The assay was already successfully used in determining the sensitivity of different *P. falciparum* strain towards redox-active compounds (Wezena et al. 2017). Cultures were synchronized with sorbitol twice. Early ring stage parasites were diluted in 10 ml RPMI 1640 containing 200 µM hypoxanthine, 5 µg/ml gentamicin and 0.9% AlbuMAX. The hematocrit and parasitemia were adjusted to 3% and 0.3%, respectively. As a control, uninfected RBCs were used. Into each well 50 µl RPMI containing 200 µM hypoxanthine and 5 µg/ml gentamicin were pipetted. For a 1 to 3 dilution 25 µl of the stock solution (Table 20) were added to wells A1-A3 and B2-G2. A serial dilution was prepared by pipetting the same volume into the next wells. All measurements were performed in triplicates. For easier understanding, Fig. 10 shows the pipetting scheme. Wells B11-G11 does not contain any drug and serve as the references for

maximal parasite growth (infected RBCs: iRBCs). Wells B1-G1 and H1-H3 serve as blanks for these references. After serial dilutions, 50 µl RBCs were pipetted into the outer wells, 50 µl iRBCs into the inner ones, yielding a final volume of 100 µl and a hematocrit of 1.5% per well.

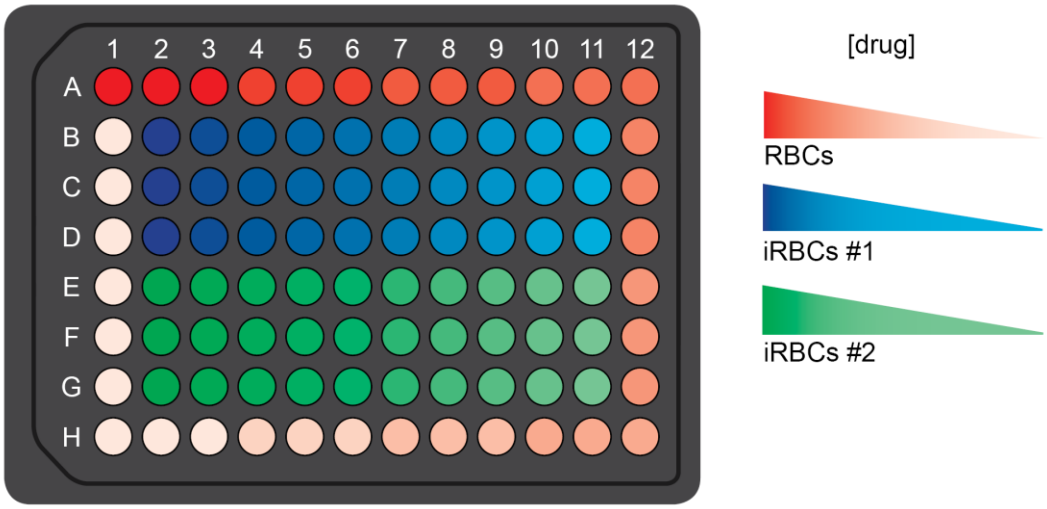

Fig. 10 Pipetting scheme of a 96-well plate for EC_{50} determination.

For information see text above. RBCs: red blood cells, iRBCs: infected red blood cells.

The plate was cultured under standard conditions for 140 h, and then stored at -80°C. The plate was thawed at RT for 1 h and placed into a ClarioStar. Afterwards, 100 µl EC_{50} lysis buffer containing 0.12 µl/ml SYBR Green were injected to each well. The plate was incubated in the dark for 1 h at RT. Fluorescence intensities were determined by measuring emission at 535 nm by an excitation at 485 nm. For this, the gain and optimal measuring height were internally adjusted to the highest expected intensities (here: well B11 and E11). Corresponding intensities of controls (RBCs + drug) were substracted from parasite treated ones. Resulted intensities were normalized to intensities from maximal growth of parasites (B11-D11 and E11-G11), plotted against the corresponding drug concentrations and fitted to a sigmoidal dose-response curve (four parameter Hill function) with SigmaPlot13.

EC_{50} lysis buffer	20 mM Tris, 5 mM EDTA, 0.08% (v/v) Triton X-100, 0.008% (w/v) saponin, pH = 7.5 (HCl)

Table 20 Tested drugs used for EC_{50} determination.

Stock solutions were freshly prepared in RPMI containing 200 µM hypoxanthine and 5 µg/ml gentamicin, and filter-sterilized.

Drug	Stock solution	Final concentration range
Artesunate (AS)	486 nM	0.01 – 81 nM
tBuOOH	38.88 mM	1 – 6480 µM
Diamide	48.6 mM	1.2 – 8100 µM
DTT	121.5 mM	3 – 20250 µM
DSM1	97.2 µM	2.5 – 16200 nM

2.5.14 Ring-stage survival assay (RSA)

Since 2013, the ring-stage survival assay has been the method of choice to determine artemisinin susceptibility *in vitro*. The assay takes up the short half-life of the drug in the human body, therefore making it comparable to the clearance time *in vivo*. In this work, the standard assay by Witkowski et al. 2013 was performed. To do so, parasites were highly synchronized by three consecutive sorbitol treatments with a time difference of 45 h. The synchronized culture was split in two and set to a parasitemia of 1% and a hematocrit of 2%. One culture was treated with 700 nM artesunate (AS), the other with the same DMSO concentration serving as a control. After exactly 6 h under standard culture conditions, the cultures were centrifuged (300 x g, 5 min) and washed four times with 5 ml supplemented RPMI medium. The culture was then resuspended in 14 ml supplemented RPMI medium and cultured for further 66 h to reach a total culturing time of 72 h. Giemsa-stained blood smear were prepared and parasitemia was determined by counting. If the DMSO treated cells reached a parasitemia of more than 3%, the survival rate was calculated as follows:

$$\text{Survival rate } (\%) = \frac{\text{Parasitemia (AS treated)}}{\text{Parasitemia (DMSO treated)}} \times 100\%$$

2.6 Protein biochemical methods

2.6.1 Expression screen of *Pf*Kelch13 variants in *E.coli*

To produce *Pf*Kelch13 in *E. coli*, different constructs were generated and produced under various expression conditions (section 3.1.1). Plasmids listed in Table 23 were transformed in different *E. coli* strains and selected on LB agar plates supplemented with the appropriate

antibiotics. Cells were grown at 37°C overnight except for T7 SHuffle Express cells. These cells were grown at 30°C. For each construct, 20 ml LB medium containing the appropriate antibiotics were inoculated with a single colony. The cultures were grown in an Innova 44R shaker at 170 rpm at 37°C (or 30°C for T7 SHuffle Express) overnight. With this pre-culture, 1 l LB medium containing the appropriate antibiotics were inoculated with the pre-culture to an OD_{600} of 0.05 and further cultured. Production of protein variants were induced at different OD_{600} and temperatures with different IPTG concentrations and grown for different times indicated in Table 23. When auto induction was carried out, 20 ml of the pre-culture was used to inoculate 400 ml auto induction medium (Table 21) containing the appropriate antibiotics. Production was carried out in 2 l baffled flasks in an Innova 44R shaker at 220 rpm at 30°C overnight. After the indicated production times, cells were transferred to centrifugation buckets and incubated in an ice-water bath for 10 min. The cultures were centrifuged at 4000 x g for 15 min at 4°C. The cell pellets were resuspended in 10 ml ice-cold purification buffer and stored at -20°C until purification.

The cell suspensions were thawed, supplemented with 10 mg lysozyme and a spatula tip DNase and stirred on ice for 1 h. For efficient cell lyses, cells were sonicated on ice by 5 cycles for 10 s each with 10 s breaks in between (60% power). The lysate was cleared by centrifugation at 10000 x g for 30 min at 4°C. During centrifugation, 250 µl Ni-NTA resin were loaded into a Poly-Prep chromatography column connected to a peristaltic pump and equilibrated with 5 ml purification buffer at a flow rate of ~2 ml/min. The supernatant of the cleared *E. coli* cell lysate was loaded onto the resin and passed through. The resin was washed with 5 ml ice-cold purification buffer. Finally, the protein was eluted with 500 µl ice-cold elution buffer by gravity and stored on ice. Proteins frations were analyzed by SDS-PAGE.

Table 21 Auto induction medium components.

Stock	Components	Concentration
ZY	peptone from casein	1% (w/v)
	yeast extract	0.5% (w/v)
$MgSO_4$	$MgSO_4$	1 mM
5052	D-(+)-Glycerol	0.5% (w/v)
	D-(+)-Glucose	0.05% (w/v)
	D-(+)-Galactose	0.1% (w/v)
NPS	$(NH_4)_2SO_4$	25 mM
	KH_2PO_4	50 mM

	Na_2HPO_4	50 mM
Trace metals	$FeCl_3 \bullet 6H_2O$	50 µM
	$CaCl_2$	20 µM
	$MnCl_2 \bullet 4H_2O$	10 µM
	$ZnSO_4 \bullet 7H_2O$	10 µM
	$CoCl_2 \bullet 6H_2O$	2 µM
	$CuCl_2 \bullet 2H_2O$	2 µM
	$NiCl_2$	2 µM
	$Na_2MoO_4 \bullet 2H_2O$	2 µM
	H_3BO_3	2 µM
	Na_2SeO_3	2 µM

Purification buffer	50 mM $Na_xH_yPO_4$, 300 mM NaCl, 20 mM imidazol, pH = 8.0
Elution buffer	50 mM $Na_xH_yPO_4$, 300 mM NaCl, 200 mM imidazol, pH = 8.0

2.6.2 Production and purification of *Pf*AOP and *Pf*Grx from *E. coli*

*Pf*AOP^{wt}, *Pf*AOP^{C117S}, *Pf*AOP^{C143S} and *Pf*Grx$^{C32/88S}$ were produced and purified as previously described (Djuika et al. 2013). The plasmids were transformed into XL1-Blue cells. Cells were selected on LB agar plates containing ampicillin at 37°C overnight. For each construct 20 ml LB medium containing ampicillin were inoculated with a single colony. The cultures were grown in an Innova 44R shaker at 170 rpm at 37°C overnight. With this pre-culture, 1 l LB medium containing ampicillin were inoculated with the pre-culture to an OD_{600} of 0.05 and further cultured. When the OD_{600} reached a value of ~0.5, production of the proteins was induced by the addition of 500 µM IPTG. After 4 h, cells were transferred to centrifugation buckets an incubated in an ice-water bath for 10 min. The culture was centrifuged at 4000 x g for 15 min at 4°C. The cell pellet was resuspended in 10 ml ice-cold purification buffer and stored at -20°C until purification. The cell suspension was thawed, supplemented with 10 mg lysozyme and a spatula tip DNase and stirred on ice for 1 h. For efficient cell lyses, cells were sonicated on ice by 5 cycles for 10 s each with 10 s breaks in between (60% power). The lysate was cleared by centrifugation at 10000 x g for 30 min at 4°C. During centrifugation, 500 µl Ni-NTA resin were loaded into a Poly-Prep chromatography column connected to a peristaltic pump and equilibrated with 10 ml purification buffer at a flow rate of ~2 ml/min. The supernatant of the cleared *E. coli* cell lysate was loaded onto the resin and passed through.

The resin was washed with 10 ml ice-cold purification buffer. Finally, the protein was eluted with 1 ml ice-cold elution buffer by gravity and stored on ice. The purified proteins were immediately used for downstream assays.

Purification buffer 50 mM $Na_xH_yPO_4$, 300 mM NaCl, 20 mM imidazol, pH = 8.0

Elution buffer 50 mM $Na_xH_yPO_4$, 300 mM NaCl, 200 mM imidazol, pH = 8.0

2.6.3 Stopped-flow kinetic measurements

Freshly purified *Pf*AOP was incubated with 5 mM DTT on ice for 30 min to obtain fully reduced protein. Excess DTT and imidazol were removed by using a PD-10 desalting column pre-equilibrated with ice-cold assay buffer. The protein was eluted with 3.5 ml ice-cold assay buffer. Protein concentration was calculated by measuring the absorbance at 280 nm using the molar extinction coefficient ε_{280} = 21.43 $mM^{-1}cm^{-1}$. Usually the protein concentration was about 200 µM. The protein was diluted in assay buffer to a concentration of 2 µM containing 1 equivalent tBuOOH and incubated on ice for 30 min. Oxidized *Pf*AOP was mixed in a thermostatted SX-20 stopped-flow spectrofluorometer with different concentrations of GSH in an ration of 1 to 1 resulting in a final concentration of 1 µM *Pf*AOP. The fluorescence was measured as the total emission at an excitation wavelength of 295 nm with a slit width of 2 mm. The fluorescence was recorded over a time range of 10 s. The values of three consecutive measurements were averaged and fitted by single exponential regression using the Pro-data SX software (Applied Photophysics).

Assay buffer 100 mM $Na_xH_yPO_4$, 0.1 mM DTPA, pH = 7.4

2.6.4 Production and purification of *Pf*Kelch13$^{337-726}$ expressed in Sf21 cells

One litre of Sf21 cells with a density of 10^6 cells/ml were infected with 5 ml V_1 encoding for His_8-*Pf*Kelch13$^{337-726}$. Cells were cultured under standard culturing conditions. After 72 h cells were harvested at 650 x g for 10 min. The supernatant was discarded and the cell pellet stored at -20°C. The cell pellet was resuspended in 30 ml ice-cold lysis buffer and divided into four 50 ml tubes, each containing a volume of ~10 ml. Cells were disrupted by three freeze-

thaw cycles using liquid nitrogen. The suspension was centrifuged at 10000 x g for 30 min at 4°C. During centrifugation, 800 µl Ni-NTA resin were loaded into a Poly-Prep chromatography column connected to a peristaltic pump and equilibrated with 10 ml equilibration buffer at a flow rate of ~2 ml/min. The supernatant of the cleared Sf21 cell lysate was loaded onto the resin and passed through. The resin was washed with 10 ml ice-cold washing buffer. Finally, the protein was eluted with 4 ml ice-cold elution buffer by gravity and stored on ice. The purified protein was immediately used for downstream assays.

Lysis buffer (30 ml)	10 mM $MgCl_2$, 1 spatula tip DNase, 1 tablet cOmplete EDTA-free (Roche), 50 mM $Na_xH_yPO_4$, 300 mM NaCl, 20 mM imidazol, pH = 8.0
Equilibration buffer	50 mM $Na_xH_yPO_4$, 300 mM NaCl, 20 mM imidazol, pH = 8.0
Washing buffer	50 mM $Na_xH_yPO_4$, 300 mM NaCl, 50 mM imidazol, pH = 8.0
Elution buffer	50 mM $Na_xH_yPO_4$, 300 mM NaCl, 250 mM imidazol, pH = 8.0

2.6.5 Antigen preparation for an *Pf*Kelch13 antibody

For the generation of an antibody detecting *Pf*Kelch13, *Pf*Kelch13$^{337\text{-}726}$ was extracted from inclusion bodies produced in *E. coli* cells. The plasmid pET45b-*PFKELCH13*$^{337\text{-}726}$ was transformed into T7 SHuffle express cells. Cells were selected on LB agar plates containing ampicillin at 30°C overnight. 20 ml LB medium containing ampicillin were inoculated with a single colony. The culture was grown at 170 rpm at 30°C overnight. 1 l LB medium containing ampicillin were inoculated with the pre-culture to an OD_{600} of 0.05 and further cultured. When the OD_{600} reached a value of ~0.5, production of *Pf*Kelch13$^{337\text{-}726}$ was induced by the addition of 500 µM IPTG. After 4 h cells were transferred to centrifugation buckets an incubated in an ice-water bath for 10 min. The culture was centrifuged at 4000 x g for 15 min at 4°C. The cell pellet was resuspended in 10 ml ice-cold purification buffer and stored at -20°C until purification.

The cell suspension was thawed, supplemented with 10 mg lysozyme and a spatula tip DNase and stirred on ice for 1 h. For efficient cell lyses cells were sonicated on ice by 5 cycles for 10 s each with 10 s breaks in between (60% power). The lysate was cleared by centrifugation at 10000 x g for 30 min at 4°C. The remaining pellet containing the inclusion bodies was washed

twice with 10 ml washing buffer at RT. After washing, the pellet was solubilized in 10 ml solubilization buffer by sonication. Excess SDS was precipitated by incubation at 4°C overnight. After centrifugation at 10000 x g for 30 min at 4°C *Pf*Kelch13$^{337-726}$ was concentrated to 60 µM using a spin concentrating column. The solubilized protein was fully reduced by the addition of 40 mM DTT and heating at 95°C for 10 min. The protein was used as an antigen to immunize rabbits by the company Pineda-Antikörper Service (Berlin).

Purification buffer	50 mM $Na_xH_yPO_4$, 300 mM NaCl, pH = 8.0
Washing buffer	50 mM Tris, 300 mM NaCl, 2% (w/v) Triton X-100, 2 M urea, pH = 8.0 (HCl)
Solubilization buffer	50 mM Tris, 300 mM NaCl, 2% (w/v) SDS, 8 M urea, pH = 8.0 (HCl)

2.6.6 Purification of an *Pf*Kelch13 antibody

To purify *Pf*Kelch13 antibodies from serum, the SDS-solubilized *Pf*Kelch13$^{337-726}$ antigen was first coupled to CNBr-activated sepharose. The buffer of the antigen was replaced with ice-cold coupling buffer by using a spin concentrating column. The antigen was concentrated to a concentration of 60 µM by using the molar extinction coefficient of ε = 59.82 $mM^{-1}cm^{-1}$.
330 mg of dry CNBr-activated sepharose were swollen in 10 ml ice-cold activation buffer for 2 h at 4°C on a rocking platform. The resin was centrifuged at 500 x g for 5 min at 4°C and 2.5 ml of the antigen was added. Coupling was performed at 4°C overnight on a rocking platform. The resin was centrifuged at 500 x g for 5 min at 4°C. Efficient coupling was checked by measuring the OD_{280} of the supernatant resulting in a calculated coupling efficiency of more than 85%. 5 ml coupling buffer were added to the resin and incubated on a nutator mixer for 30 min at RT. After centrifugation at 500 x g for 5 min, non-reacted CNBr groups were blocked by the addition of 5 ml quenching buffer and an incubation time of 1 h. The resin was washed 3 times with 10 ml of alternate washing with high pH wash buffer and low pH wash buffer. Then, the resin was washed twice with 10 ml PBS buffer. 3.5 ml PBS buffer and 1.5 ml serum were added to the resin and incubated at 4°C overnight on a rocking platform. The suspension was packed into a Poly-Prep chromatography column (Bio-Rad). The solution passed through the resin by gravity. The resin was washed twice with 5 ml PBS buffer.

The antibody was eluted with elution buffer in 10x 1 ml fractions. Immediately after elution, 30 µl Tris buffer and 20 µl salt solution were added to each fraction. Antibody fractions were stored at 4°C and probed for western blots or coupled to CNBr-activated sepharose used for pull-down experiments.

Activation buffer	1 mM HCl
Coupling buffer	100 mM $NaHCO_3$, 500 mM NaCl, pH = 8.3 (HCl)
Quenching buffer	100 mM Tris, pH = 8.0 (HCl)
High pH wash buffer	100 mM Tris, 500 mM NaCl, pH = 8.0 (HCl)
Low pH wash buffer	100 mM NaOAc, 500 mM NaCl, pH = 4.0 (HCl)
PBS buffer	1.84 mM KH_2PO_4, 10 mM Na_2HPO_4, 137 mM NaCl, 2.7 mM KCl, pH = 7.3 (HCl)
Elution buffer	100 mM glycine, pH = 2.4 (HCl)
Tris buffer	3 M Tris, pH = 8.8 (HCl)
Salt solution	5 M NaCl

2.6.7 Coupling of the *Pf*Kelch13 antibody to CNBr-activated Sepharose

For pull-down experiments the purified *Pf*Kelch13 antibody was coupled to CNBr-activated sepharose using a standard protocol (Kavran and Leahy 2014). The buffer of the *Pf*Kelch13 antibody was replaced with ice-cold coupling buffer by using a spin concentrating column. The antibody was concentrated to a concentration of 1 mg/ml by assuming an OD_{280} of 1.4. 250 mg of dry CNBr-activated sepharose were swollen in 5 ml ice-cold activation buffer for 2 h at 4°C on a rocking platform. The resin was centrifuged at 1000 x g for 5 min at 4°C and 2 ml of the antibody was added. Coupling was performed at 4°C overnight on a rocking platform. The resin was centrifuged at 1000 x g for 5 min at 4°C. Efficient coupling was checked by measuring the OD_{280} of the supernatant showing absorbance values below 0.1. 5 ml coupling buffer were added to the resin and incubated on a nutator mixer for 30 min at RT. After centrifugation at 1000 x g for 5 min, non-reacted CNBr groups were blocked by the addition of 5 ml quenching buffer and an incubation time of 3 h. The resin was washed 3 times with 10 ml of alternate washing with high pH wash buffer and low pH wash buffer. Finally, the resin was washed with 5 ml PBS buffer and stored in 1 ml PBS at 4°C for further use.

Activation buffer	1 mM HCl
Coupling buffer	100 mM $NaHCO_3$, 500 mM NaCl, pH = 8.3 (HCl)
Quenching buffer	100 mM Tris, pH = 8 (HCl)
High pH wash buffer	100 mM Tris, 500 mM NaCl, pH = 8 (HCl)
Low pH wash buffer	100 mM NaOAc, 500 mM NaCl, pH = 4 (HCl)
PBS buffer	1.84 mM KH_2PO_4, 10 mM Na_2HPO_4, 137 mM NaCl, 2.7 mM KCl, pH = 7.3 (HCl)

2.6.8 Immunoprecipitation of *Pf*Kelch13

For denaturing immunoprecipitation of *Pf*Kelch13, 56 ml (4x 14 ml cultures) parasite culture with a parasitemia of ~10% trophozoites were harvested by centrifugation at 300 x g for 5 min. Red blood cells were saponin-lysed. The remaining parasite cell pellet was resuspended in 250 µl lysis buffer containing cOmplete EDTA-free protease inhibitor (Roche) and frozen in liquid nitrogen. After thawing, the lysate was cleared by centrifugation at 16000 x g for 10 min at RT. The supernatant was diluted 1 to 20 with dilution buffer resulting in a total volume of 5 ml. After the addition of 100 µl *Pf*Kelch13 antibody coupled to CNBr sepharose, the suspension was incubated at 4°C overnight rotating end over end. The sepharose was centrifuged at 500 x g for 5 min at 4°C and washed three times with 1 ml dilution buffer. Bound proteins were eluted by adding 100 µl 2x laemmli buffer and heating at 95°C for 5 min. Samples were subjected to SDS-PAGE and western blot analysis.

Lysis buffer	10 mM Tris, 150 mM NaCl, 2% (w/v) SDS, 1% Triton X-100, pH = 7.5
Dilution buffer	10 mM Tris, 150 mM NaCl, pH = 7.5

2.6.9 Sodium dodecyl sulfate polyacrylamide gel electrophoresis (SDS-PAGE)

Proteins were separated by discontinuous sodium dodecyl sulfate gel electrophoresis (Laemmli 1970) using the Mini-PROTEAN system (BioRad). Gels with a thickness of 1 mm were used and prepared according to the manufacturer's instructions. Depending on the expected size of the proteins, different percentages of acrylamide were used. The separating gel was

poured between the glasses and overlaid with 100% isopropanol. After polymerization, the alcohol was removed. The stacking gel was poured on top of the separating gel and the comb was placed between the glasses. After polymerization, gels were stored at 4°C up to 2 weeks. Protein samples were mixed with laemmli buffer and boiled. When reducing conditions were used, 15% (v/v) β-mercaptoethanol was added. Gels were placed in the electrophoresis tank filled with SDS running buffer and ran at 15 A/gel until the dye front ran out of the gel. Proteins were then either stained with Coomassie or blotted on PVDF membranes.

Table 22 Recipes for SDS-gels.

	Separating gel			**Stacking gel**
	10%	**12%**	**15%**	**4%**
30% Acrylamide/bisacrylamide	3.3 ml	4.0 ml	5 ml	0.33 ml
1.5 M Tris-HCl, pH = 6.8	-	-		0.25 ml
1 M Tris-HCl, pH = 8.8	2.5 ml	2.5 ml	2.5 ml	-
10% SDS	100 µl	100 µl	100 µl	20 µl
10% APS	100 µl	100 µl	100 µl	20 µl
TEMED	4 µl	4 µl	4 µl	4 µl
ddH_2O	ad 10 ml	ad 10 ml	ad 10 ml	ad 2 ml

SDS running buffer 25 mM Tris, 250 mM glycine, 0.1% (w/v) SDS, pH = 8.3

2x Laemmli buffer 125 mM Tris, 20% (v/v) glycerol, 4% (w/v) SDS, 0.04% (w/v) bromophenol blue, pH = 6.8 (HCl)

5x Laemmli buffer 250 mM Tris, 25% (v/v) glycerol, 10% (w/v) SDS, 0.1% (w/v) bromophenol blue, pH = 6.8 (HCl)

2.6.10 In-gel protein staining by Coomassie Brilliant Blue

To visualize proteins in a SDS gel, the gel was carefully transferred into a box containing a Coomassie Blue solution. Proteins were staining for at least 1 h. The staining solution was removed and destaining solution was added. After 1 h the solution was replaced with ddH_2O, and further destained over night.

Staining solution 25% (v/v) isopropanol, 10% (v/v) acetic acid, 0.05% (w/v) Coomassie Blue G250

Destaining solution 25% (v/v) isopropanol, 10% (v/v) acetic acid

2.6.11 Protein concentration determination

For a purified protein the molar extinction coefficient at 280 nm was used to calculate the protein concentration. The coefficient was calculated using the web-server EXPASy ProtParam. When the concentration in a more complex sample was quantified, e.g. a whole cell lysate, the protein concentration was estimated according to the Bradford method (Bradford 1976). First a standard curve was generated by preparing eight cuvettes containing 0, 2, 4, 6, 8, 10, 12, 14 µg BSA in 800 µl ddH_2O. Into each cuvette 200 µl 5x Bradford reagent was added and mixed thoroughly. After an incubation time of 15 min, the absorbance at 595 nm was measured. Absorbance values were plotted against the corresponding BSA concentration. Data points were fitted to a hyperbolic curve. To estimate the protein concentration in the optimal curve window, different volumes of protein samples were diluted in 800 µl ddH_2O and Bradford reagent was added as previously described. When a used volume was in the dynamic range of the standard curve, the protein concentration was calculated. All measurements were performed in duplicates.

2.6.12 Circular Dichroism (CD) spectroscopy

To test proper folding of *Pf*Kelch13$^{337-726}$ produced in Sf21 cells, secondary structure elements were determined by CD spectroscopy. Freshly purified *Pf*Kelch13$^{337-726}$ was concentrated in CD buffer by using an Amicon spin concentrating column. CD spectra were recorded in the AG Keller (TU Kaiserslautern) with a thermostatted Chirascan CD spectrometer (Applied Photophysics).

CD buffer 50 mM $Na_xH_yPO_4$, 100 mM NaF, pH = 7.4

2.6.13 Determination of free thiols using DTNB

To determine the number of accessible cysteines in *Pf*Kelch13$^{337-726}$, the Ellman's reagent was used (Ellman 1958). Freshly purified *Pf*Kelch13$^{337-726}$ produced in Sf21 cells was reduced with 5 mM DTT for 30 min on ice. Excess DTT was removed by using a PD-10 desalting column and native buffer. The protein was diluted with native buffer to a concentration of ~10 µM and ~30 µM in a final volume of 400 µl by using the molar extinction coefficient of $\varepsilon = 59.82\ mM^{-1}cm^{-1}$. To determine the number of free thiols in *Pf*Kelch13$^{337-726}$, a standard curve was generated with DTT: 400 µl of native buffer containing 0, 10, 30, 40, 50, 60, 70, and 80 µl DTT were transferred to cuvettes. Two solutions of 1.2 mM DTNB were prepared: one in native buffer for determination under native conditions, the other in denaturing buffer for the determination under denaturing conditions. For this, 400 µl of each DTNB solution were mixed with the DTT standards and incubated for 5 min at RT. The absorbance at 412 nm was measured and plotted against the corresponding DTT concentration. The data points were fitted with a linear regression. Analogous to the standard curve, 400 µl of ~30 µM and ~10 µM *Pf*Kelch13$^{337-726}$ were mixed with the same volume native buffer and denaturing buffer containing DTNB respectively and incubated for 5 min at RT. After incubation, the absorbance at 412 nm was measured. Using the linear regression formula, the corresponding DTT concentration was calculated. Since DTT contains two thiols, the corresponding DTT concentration was multiplied by two. Dividing by the exact protein concentration led to the number of accessible thiols in *Pf*Kelch13$^{337-726}$ under native and denaturing conditions. The number of accessible thiols under both conditions was determined in three independent experiments.

Native buffer	50 mM Na_xH_yPO4, 300 mM NaCl, pH = 8.0
Denaturing buffer	50 mM Na_xH_yPO4, 300 mM NaCl, 2% (w/v) SDS, pH = 8.0

2.6.14 Immunodetection of proteins by western blotting

Gel-resolved proteins were blotted on PVDF membranes and probed with different antibodies. All blots in this thesis were performed using the Mini-PROTEAN wet blotting system (Bio-Rad). PVDF membranes were activated for 30 s in 100% ethanol and equilibrated together with SDS gels in ice-cold blotting buffer for 10 min. Gels, membranes and Whatman

papers were placed in blotting cassettes according to manufacturer's instructions. Proteins were transferred at 4°C at 15 V/gel overnight. Efficiency of transfer was checked by incubating the membrane in Ponceau S solution for 2 min and subsequently destained with ddH_2O. Membranes were completely destained by washing with TBS buffer several times until no red bands could be detected. Unoccupied positions on the membrane were blocked with TBS containing 5% milk powder for 1 h at RT. Then, the membranes were incubated with specific primary antibodies at 4°C overnight on a rocking platform. After incubation, membranes were subsequently washed five times with TBS-T buffer. Thereafter, membranes were incubated with HRP-coupled secondary antibodies for 1 h at RT, followed by five washing steps with TBS-T for 10 min each. Chemiluminescent signals were induced by Roti-Lumin plus (ROTH) and immediately recorded with a CDD camera documenting system (Vilber). After documentation membranes were washed with ddH_2O and dried or stripped for reprobing with other antibodies.

Blotting buffer	20 mM Tris, 150 mM glycine, 20% (v/v) methanol
Ponceau S solution	0.1% (w/v) Ponceau S, 1% (v/v) acetic acid
TBS buffer	10 mM Tris, 0.9% (w/v) NaCl, pH = 7.4 (HCl)
TBS-T buffer	10 mM Tris, 0.9% (w/v) NaCl, 0.05% Tween20, pH = 7.4 (HCl)

2.6.15 Stripping and reprobing of western blots

To detect an antigen on an already stained membrane, antibodies were stripped from the membranes by incubating membranes in an acidic buffer. First, membranes were washed twice with TBS buffer for 10 min each. Then, antibodies were stripped by incubating with stripping buffer three times for 10 min each. After three neutralization steps with TBS buffer for 10 min each, membranes were incubated in TBS containing 5% milk powder and probed with primary antibodies.

TBS buffer	10 mM Tris, 0.9% (w/v) NaCl, pH = 7.4 (HCl)
Stripping buffer	200 mM glycine, 0.1% (w/v) SDS, 1% (v/v) Tween20, pH = 2.2

3 Results

3.1 Recombinant production of *Pf*Kelch13

3.1.1 Screening expression conditions in *E. coli* did not result in soluble *Pf*Kelch13

To characterize *Pf*Kelch13 *in vitro*, we first tried to produce full length protein as well as *Pf*Kelch13$^{337\text{-}726}$ comprising the BTB/kelch propeller domain recombinantly in *E. coli*. For this numerous conditions were tested (Table 23). We tried commonly used strategies to produce soluble proteins such as decreasing the temperature, lowering the inducer concentration, alternative N-terminal His_6-, GST- or MBP-tags, as well as the use of a weaker promoter and different expression strains. To test the impact of cysteine residues on the solubility, single serine mutants of all cysteines were generated and tried to produce. None of the tested conditions resulted in the production of soluble protein indicating an intrinsic folding problem in *E. coli*. We further tried to produce His_8-tagged *Pf*Kelch13 and *Pf*Kelch13$^{337\text{-}726}$ in *Pichia pastoris* cells (GS115) and *Leishmania tarentolae* cells (LEXSY system; Jena Bioscience). In both eukaryotic systems no overexpression of the heterologous genes was detected and no soluble recombinant protein could be purified.

Table 23 Tested conditions to produce recombinant *Pf*Kelch13 and *Pf*Kelch13$^{337\text{-}726}$ in *E. coli*.

Plasmid	Strain	Temperature	OD_{600} at induction	[IPTG]	Time of expression	Modified expression
pET45b-*PFKELCH13*	T7 SHuffle Express	30°C	0.5	0.5 mM	4 h	
		16°C	0.5	0.2 mM	o/n	
		30°C			24 h	Auto induction
	Rosetta-gamiB(DE)pLysS	37°C	0.5	0.5 mM	4 h	
		16°C	0.5	0.2 mM	o/n	
	BL21pLysS	37°C	0.5	0.5 mM	4 h	
		16°C	0.5	0.2 mM	o/n	
pET45b-*PFKELCH13*$^{337\text{-}726}$	T7 SHuffle Express	30°C	0.5	0.5 mM	4 h	
						pGroEL/S
		16°C	0.5	0.2 mM	o/n	
						pGroEL/S
	Rosetta-gamiB(DE)pLysS	37°C	0.5	0.5 mM	4 h	
		16°C	0.5	0.2 mM	o/n	
	BL21pLysS	37°C	0.5	0.5 mM	4 h	
		16°C	0.5	0.2 mM	o/n	

pET45b-*PFKELCH13*$^{337\text{-}726/C447S}$	T7 SHuffle Express	16°C	0.5	0.2 mM	o/n	
pET45b-*PFKELCH13*$^{337\text{-}726/C469S}$	T7 SHuffle Express	16°C	0.5	0.2 mM	o/n	
pET45b-*PFKELCH13*$^{337\text{-}726/C473S}$	T7 SHuffle Express	16°C	0.5	0.2 mM	o/n	
pET45b-*PFKELCH13*$^{337\text{-}726/C532S}$	T7 SHuffle Express	16°C	0.5	0.2 mM	o/n	
pET45b-*PFKELCH13*$^{337\text{-}726/C542S}$	T7 SHuffle Express	16°C	0.5	0.2 mM	o/n	
pET45b-*PFKELCH13*$^{337\text{-}726/C580S}$	T7 SHuffle Express	16°C	0.5	0.2 mM	o/n	
pET45b-*PFKELCH13*$^{337\text{-}726/C580Y}$	T7 SHuffle Express	16°C	0.5	0.2 mM	o/n	
pET45b-*PFKELCH13*$^{337\text{-}726/C696S}$	T7 SHuffle Express	16°C	0.5	0.2 mM	o/n	
pQE30-*PFKELCH13*	T7 SHuffle Express	30°C	0.5	0.5 mM	4 h	
			1.5			
		16°C	0.5	0.1 mM	o/n	
			0.1			
			0.1			3% ethanol
pQE30-*PFKELCH13*$^{337\text{-}726}$	T7 SHuffle Express	30°C	0.5	0.5 mM	4 h	
			1.5			
		16°C	0.5	0.1 mM	o/n	
			0.1			
			0.1			3% ethanol
pGEX-4T-1-*PFKELCH13*	T7 SHuffle Express	30°C	0.5	0.5 mM	4 h	
		16°C	0.5	0.2 mM	o/n	
	XL1-Blue	37°C	0.5	0.5 mM	4 h	
		16°C	0.5	0.2 mM	o/n	
pGEX-4T-1-*PFKELCH13*$^{337\text{-}726}$	T7 SHuffle Express	30°C	0.5	0.5 mM	4 h	
		16°C	0.5	0.2 mM	o/n	
	XL1-Blue	37°C	0.5	0.5 mM	4 h	
		16°C	0.5	0.2 mM	o/n	
pMAL-c5x-TEV-*PFKELCH13*	T7 SHuffle Express	30°C	0.5	0.5 mM	4 h	
		16°C	0.5	0.2 mM	o/n	
	XL1-Blue	37°C	0.5	0.5 mM	4 h	
		16°C	0.5	0.2 mM	o/n	
pMAL-c5x-TEV-*PFKELCH13*$^{337\text{-}726}$	T7 SHuffle Express	30°C	0.5	0.5 mM	4 h	
						pGroEL/S
		16°C	0.5	0.2 mM	o/n	
	XL1-Blue	37°C	0.5	0.5 mM	4 h	
		16°C	0.5	0.2 mM	o/n	

3.1.2 An antibody raised against denatured recombinant *Pf*Kelch13$^{337-726}$ allows specific detection of *Pf*Kelch13 in *P. falciparum* lysates

Although it was not possible to produce correctly folded *Pf*Kelch13 in *E. coli*, an antibody was raised against the BTB/kelch propeller domain of *Pf*Kelch13. Since this truncated protein was not soluble in all conditions tested (Table 23), detergents were tested to solubilize *Pf*Kelch13$^{337-726}$. Only 2% SDS resulted in efficient solubilization of *Pf*Kelch13$^{337-726}$ compared to 2% DOC and 2% Triton X-100 (Fig**.** 11a). To purify this solubilized protein, a purification protocol was developed consisting of the pre-isolation of insoluble compartments of the cell (containing *Pf*Kelch13$^{337-726}$), the solubilization and the purification of *Pf*Kelch13$^{337-726}$ by Ni-NTA affinity chromatography. Since SDS is not recommended by Qiagen (The QIAexpressionist), and we also had the impression that SDS decreases protein binding, excess SDS was precipitated on ice following solubilization. Although a lot of the protein coprecipitated, a high amount of bound and finally purified protein was achieved (Fig**.** 11b). Using this purified protein as the antigen, two rabbits were immunized by Pineda Antikörper-Service (Berlin). Sera were taken post 120 d and tested for reactivity with the antigen. High levels of immunity were detected (data not shown). From these sera, antibodies were purified using *Pf*Kelch13$^{337-726}$ coupled to CNBr-activated sepharose. All eluted fractions showed reactivity with the antigen in western blots. The fraction with the strongest signal in western blots was used to detect *Pf*Kelch13 in *P. falciparum* lysates (Fig**.** 11c). Probing with the purified antibody (AB) resulted in the specific detection of a protein with a size of ~90 kDa indicating the correct detection of *Pf*Kelch13. We further asked, if the generated antibody can be used for pull-down experiments. Indeed, probing the antibody in 3D7 lysates under denaturing conditions resulted in a strong enrichment of *Pf*Kelch13 (Fig. 11d, left). To test the specificity, we also tested the antibody for strain His_8-*PFKELCH13* (section 3.5.2). Using an anti His_6 antibody resulted in the detection of *Pf*Kelch13 in the elute fraction (Fig. 11d, right), clearly showing an enrichment of *Pf*Kelch13 and high specificity of the antibody towards *Pf*Kelch13. Therefore, it can be concluded that this antibody can be used to determine interactoms of *Pf*Kelch13 in *P. falciparum* lysates as previously reported (Gnädig et al. 2020).

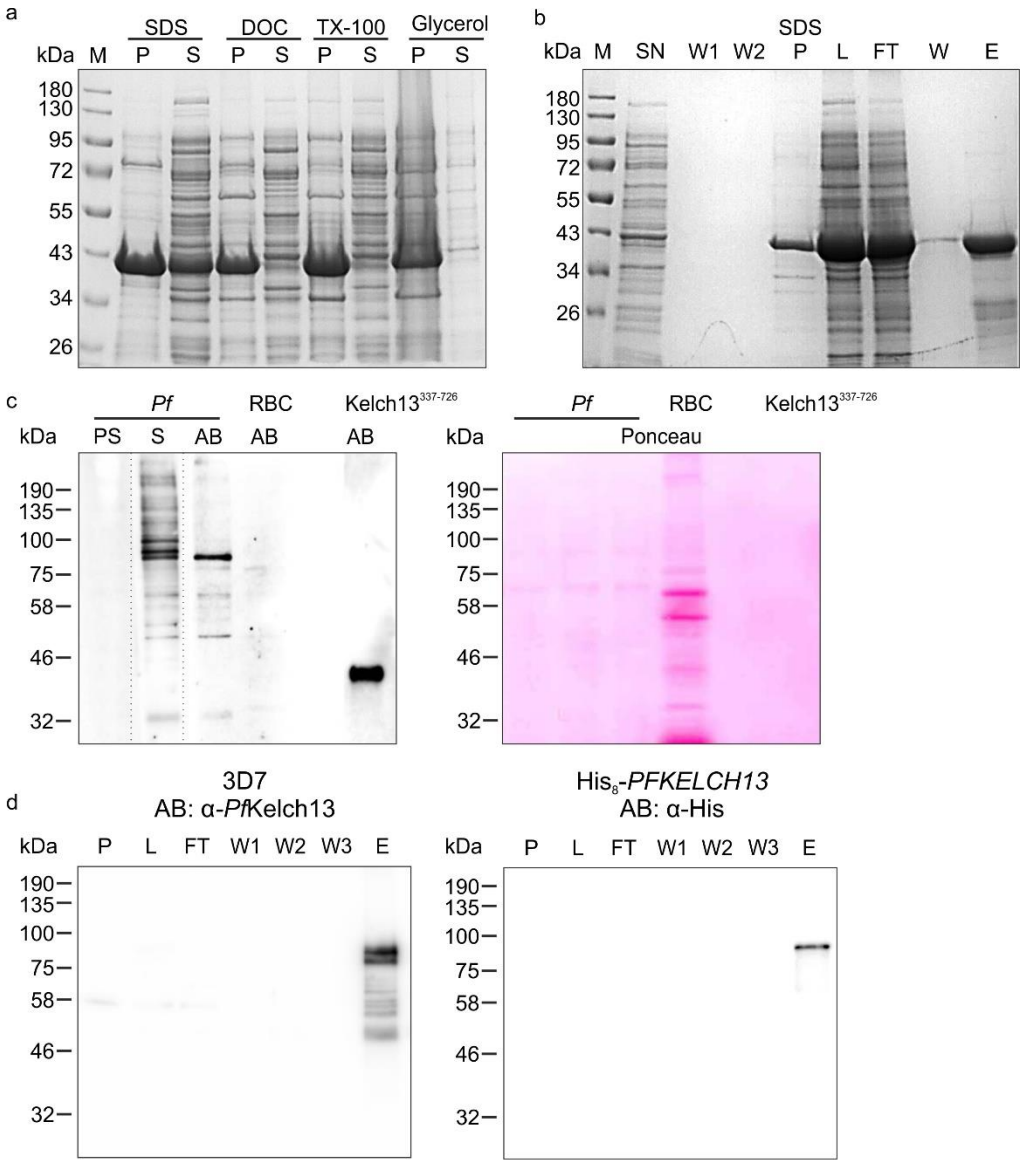

Fig. 11 Generation of an antibody detecting *Pf*Kelch13 in *P. falciparum* lysates.

(a) Solubilization screen of recombinant *Pf*Kelch13$^{337-726}$. High levels of *Pf*Kelch13$^{337-726}$ could be solubilized with 2% SDS, whereas 2% DOC, 2% Triton X-100 (TX-100) and 50% glycerol did not show a solubilization effect. P: pellet, S: supernatant. **(b)** Purification of SDS-solubilzed *Pf*Kelch13$^{337-726}$. Cells were lysed by sonication. After centrifugation, the soluble fraction (SN) was discarded. Inclusion bodies containing *Pf*Kelch13$^{337-726}$ were washed twice (W1, W2) and solubilized with 2% SDS. Excess SDS was precipitated on ice (SDS P). The supernatant (L) was loaded on a Ni-NTA agarose column. After washing of unbound material (W), the protein was eluted with 200 mM imidazole (E). FT: flow through. **(c)** Probing of the *Pf*Kelch13 antibody. Left: Serum (S) as well as purified *Pf*Kelch13 antibody (AB) detects a protein with a molecular mass of ~90 kDa corresponding to *Pf*Kelch13 in a parasite lysate. The detection was specific to parasites. No signal was detected in uninfected red blood cells (RBCs). When using the preserum (PS), no protein was detected. Recombinant *Pf*Kelch13$^{337-726}$ served as a positive control. 3 x 10^7 of purified trophozoites, 3 x 10^7 uninfected RBC and 10 ng *Pf*Kelch13$^{337-726}$ were loaded. Right: Ponceau S staining of the membrane served as a loading control. **(d)** Pull-down experiments using the purified *Pf*Kelch13 antibody. The *Pf*Kelch13 antibody was coupled to CNBr-activated sepharose and used for pull-down experiments. *Pf*Kelch13 could be efficiently enriched from a denatured parasite lysate from 6 x 10^9 purified trophozoites using either a 3D7 wild-type strain (left) or a SLI-derived 3D7 strain with chromosomally encoded His_8-*Pf*Kelch13 (right). 0.2% of the load (L) and 6.7% of the elute (E) were loaded. The purified proteins were either detected using our *Pf*Kelch13 rabbit antibody or a commecial anti-His_6 mouse antibody.

3.1.3 Recombinant production of *Pf*Kelch13$^{337-726}$ in Sf21 cells yields soluble protein of high purity

Although a crystal structure of the BTB/kelch propeller domain of *Pf*Kelch13 is available (PDB: 4YY8), no protocol for the production of this construct has been published yet. Here, we demonstrate the successful production of a similar construct in Sf21 cells, that could be purified via Ni-NTA affinity chromatography. The construct contains an N-terminal His_8 tag followed by amino acid residues 337-726 of *Pf*Kelch13 (Fig. 12a). After purification, around 6 mg of highly pure protein per liter of culture were obtained (Fig. 12b). The protein ran at a size of ~43 kDa in a SDS gel, which is in accordance with the calculated mass of 46 kDa. To further confirm that the purified protein is the expected product, we excised the band from the gel and analyzed it by mass spectrometry (MS). High intensity signals of peptides corresponding to *Pf*Kelch13$^{337-726}$ were detected. MS revealed a high sequence coverage of the protein around 74%. Covered amino acids are indicated in Fig. 12b. To address the folding of *Pf*Kelch13$^{337-726}$, CD spectra were measured, clearly indicating a high percentage of ordered secondary structure elements (Fig. 12c). Calculation of the proportions of secondary structure elements using the K2D2 software (Perez-Iratxeta and Andrade-Navarro 2008) resulted in 23% α-helix and 24% β-sheet content. Using the webserver 2StrucCompare we calculated the content of these elements from the crystal structure (PDB: 4YY8) yielding 10% α-helix and 34% β-sheet structures. We therefore recognized a higher percentage of α-helices and a lower one of β-sheets suggesting some flexibility of the secondary structure elements when comparing the protein in solution and in a crystal. Interestingly, the structurally similar protein KEAP1 also shows a higher content of α-helix in CD spectra compared to its crystal structure (Gao et al. 2007). Moreover, we asked for thermal stability of the secondary structure elements. At around 50°C the ellipticity at characteristic wavelengths started to change (Fig. 12d). A further increase of the temperature resulted in the approximation of the ellipticity to zero in accordance with the observed precipitation of the protein. We could not observe a stepwise unfolding but more a direct precipitation of the protein recognized by temperatures greater than 50°C.

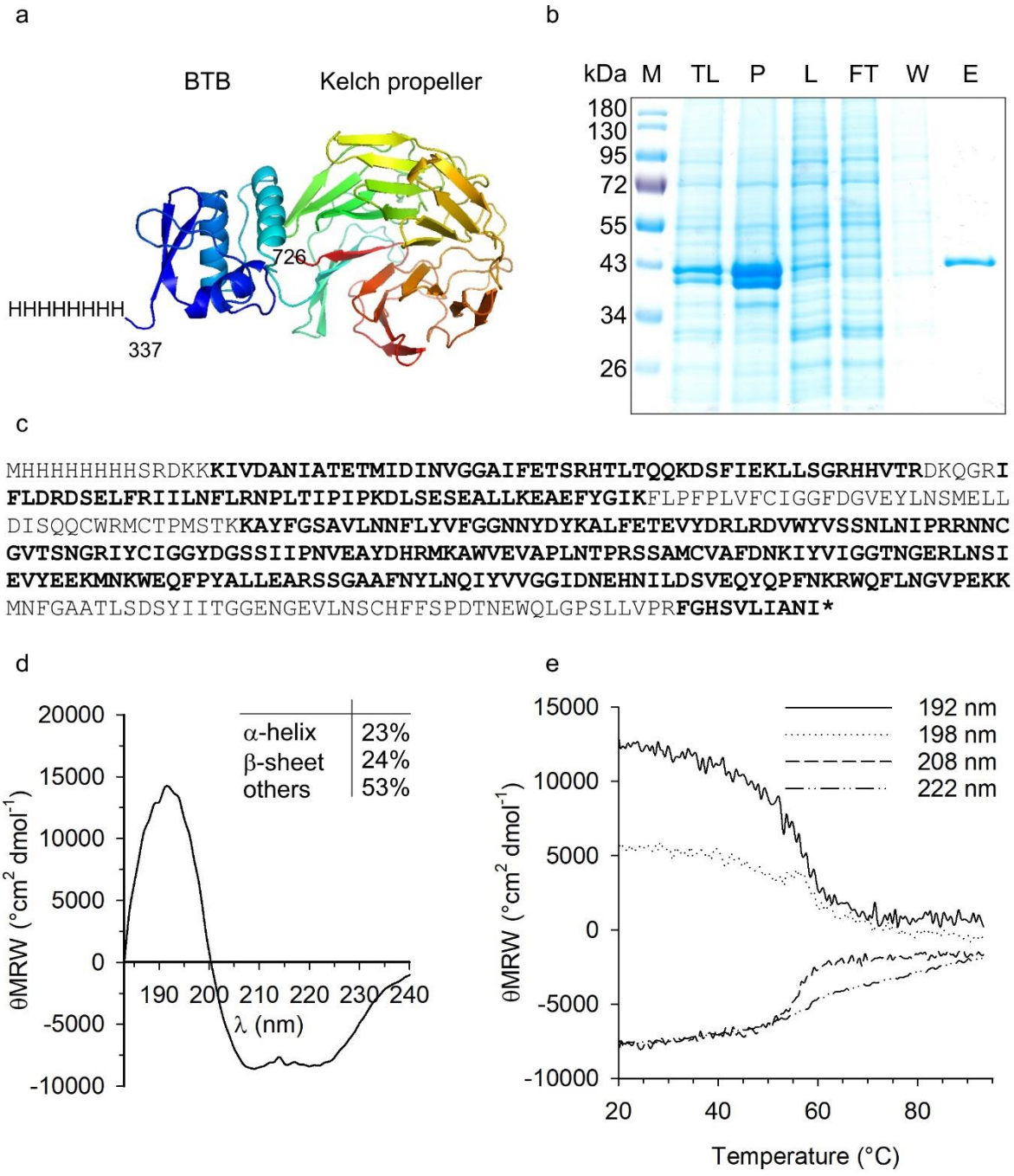

Fig. 12 High yield and purity of folded *Pf*Kelch13$^{337-726}$ expressed in Sf21 cells.

(a) Designed construct for the production in Sf21 cells based on the released unpublished crystal structure (PDB: 4YY8). The construct contains an N-terminal His_8 tag and the amino acid residues 337-726. **(b)** Purification of *Pf*Kelch13$^{337-726}$. Sf21 cells producing *Pf*Kelch13$^{337-726}$ were lysed by three freeze-thaw cycles (TL). After separation of the insoluble compartments (P), the supernatant (L) was loaded on a Ni-NTA agarose column. Unbound material (FT) was discarded. The resin was washed (W) and the bound protein eluted (E) with 250 mM imidazol. **(c)** Sequence coverage of purified *Pf*Kelch13$^{337-726}$ by mass spectrometry. Detected amino acid residues are highlighted (bold). **(d)** CD spectrum of *Pf*Kelch13$^{337-726}$ in 50 mM $Na_xH_yPO_4$, 100 mM NaF, pH 7.4 at 20°C. Proportions of secondary structure elements were calculated using the K2D2 software. **(e)** Thermal stability of *Pf*Kelch13$^{337-726}$ in the same buffer. Ellipticity at characteristic wavelengths approximates to zero with increasing temperature beginning at around 50°C. At this temperature the protein started to precipitate.

3.1.4 Recombinant *Pf*Kelch13$^{337-726}$ coexists as homotetramers, -dimers and monomer and has two accessible cysteines

Since the BTB/kelch propeller domain crystallizes as a dimer (PDB: 4YY8), we asked how this truncated version of *Pf*Kelch13 behaves in solution. Therefore, freshly purified *Pf*Kelch13$^{337-726}$ was loaded on a Superdex 200 Increase 10/300 GL column which was ran with 50 mM $Na_xH_yPO_4$ (pH = 8) containing 300 or 0 mM NaCl at 10°C. Two independent purifications and runs showed different elution patterns of the protein (Fig. 13a). According to the calibration curve of proteins with known molecular sizes, prominent peaks in the elution profile are monomeric, dimeric, as well as tetrameric species of *Pf*Kelch13$^{337-726}$. We cannot explain the different profiles of the two runs yet. However, such a behavior may indicate a dynamic equilibrium between these three species. What we clearly observed was a loss of oligomeric species when the running buffer did not contain NaCl (Fig. 13b).

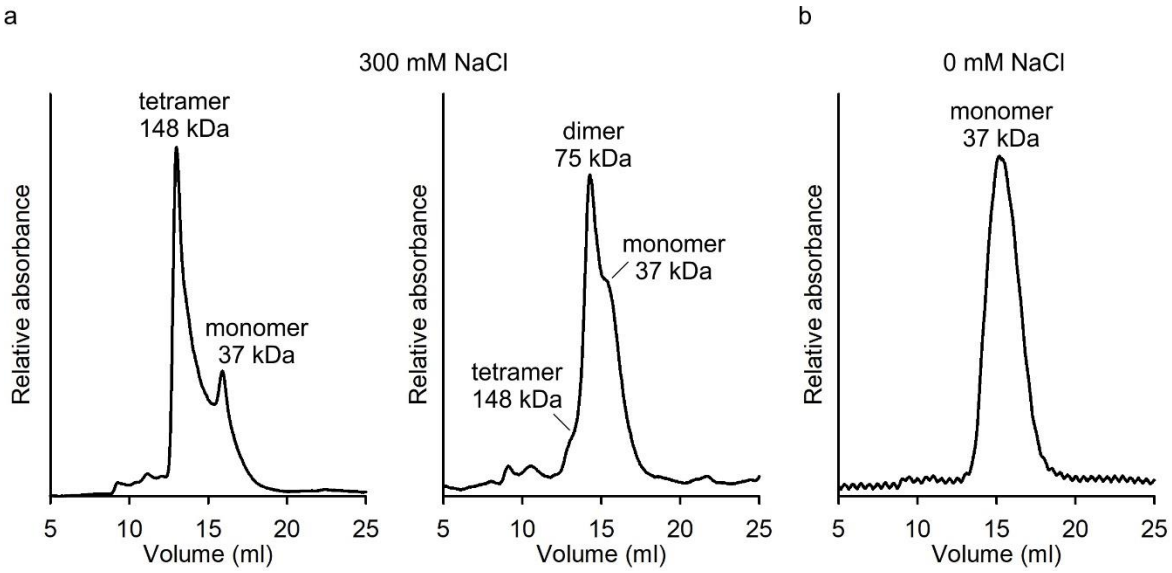

Fig. 13 *Pf*Kelch13$^{337-726}$ shows different oligomeric states.

Freshly purified *Pf*Kelch13$^{337-726}$ was loaded on a Superdex 200 Increase 10/300 GL column with 50 mM $Na_xH_yPO_4$ (pH = 8) containing **(a)** 300 or **(b)** 0 mM NaCl as running buffer at 10°C. In the presence of sodium chloride three peaks were observed corresponding to monomeric, dimeric and tetrameric species. The apparent masses are indicated. When no sodium chloride was present in the running buffer, the protein eluted as a monomer.

Using Ellman's reagent we determined the number of free thiols in reduced *Pf*Kelch13$^{337-726}$ under native and denaturing conditions. Under native and denaturing conditions values of 1.81 ± 0.16 and 6.84 ± 0.42 thiols per protein were calculated, respectively. *Pf*Kelch13$^{337-726}$ contains 7 cysteines in total, which is in very good agreement with the calculated value under

denaturing conditions. A value of around 2 under native conditions indicates that two cysteines are accessible to DTNB in the folded protein. It is likely that these two cysteines are the most surface exposed ones, which are, according to the crystal structure (PDB: 4YY8), residues C469 and C473.

3.2 A mobility shift between endogenous and recombinant *Pf*Kelch13 suggests a non-identified post-translational modification

We were able to generate and produce N-terminal His-tagged full length *Pf*Kelch13 in *P. falciparum* strain His_8-*PFKELCH13* (section 3.4), Sf21 and *E. coli*, even though the recombinant protein from Sf21 and *E. coli* was insoluble. By probing with an anti His antibody, we recognized a different mobility of the protein as detected by SDS-PAGE (Fig. 14a). When *Pf*Kelch13 was produced in *P. falciparum* it ran slower, which might indicate a post-translational modification that was absent in Sf21 and *E. coli*. Since pull-down experiments worked well with the generated anti *Pf*Kelch13 antibody (Fig**.** 11d), we excised the band corresponding to *Pf*Kelch13 and analyzed it by mass spectrometry. As expected, the highest intensity of signals corresponded to peptides of *Pf*Kelch13. However, neither proteins nor post-translational modifications that could explain the different running behavior were detected and a putative translational read-through until the next stop codon would have increased the mass by just 1.8 kDa. The N-terminus of all three constructs had to be intact based on the detectability using the anti His antibody. The C-terminus is buried in the crystal structure and was also detected by mass spectrometry for recombinant *Pf*Kelch13$^{337\text{-}726}$ (Fig. 12c). Hence, absent degradation patterns in both Sf21 and *E. coli* rather contradict a C-terminal truncation. The following residues did not seem to be modified based on the identified residues (Fig. 14b). Hence, the mass shift could be due to a modification within the remaining sequence.

a

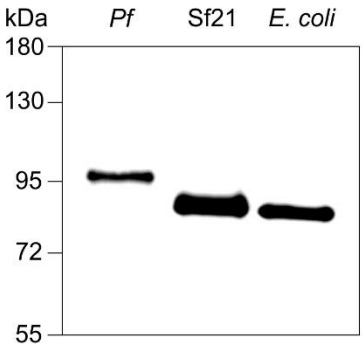

	Size (Da)	N-terminus	
Pf	85232	PASMH$_8$VD-	*PFKELCH13*$^{2-726}$
Sf21	85005	MH$_8$SR-	
E. coli	84947	MAH$_6$VGTM-	

b

PASMHHHHHHHHVDEGEKVK**TKANSISNFSMTYDR**ESGGNSNSDDKSGSSSENDSNSFMNLTSDKNEK**TENN**
SFLLNNSSYGNVKDSLLESIDMSVLDSNFDSKKDFLPSNLSRTFNNMSKDNIGNKYLNKLLNKKKDTITNEN
NNINHNNNNNNLTANNITNNLINNNMNSPSIMNTNK**KENFLDAANLINDDSGLNNLKKFSTVNNVNDTYEKK**
IIETELSDASDFENMVGDLRITFINWLKKTQMNFIREKDKLFK**DKKELEMER**VR**LYKELENRKNIEEQKLHD**
ERKKLDIDISNGYKQIKKEKEEHRK**RFDEERLRFLQEIDKIKLVLYLEKEKYYQEYKNFENDK**KKIVDANIA
TETMIDINVGGAIFETSR**HTLTQQKDSFIEK**LLSGRHHVTRDKQGR**IFLDRDSELFRIILNFLRNPLTIPIP**
KDLSESEALLKEAEFYGIKFLPFPLVFCIGGFDGVEYLNSMELLDISQQCWRMCTPMSTKKAYFGSAVLNNF
LYVFGGNNYDYK**ALFETEVYDRLRDVWYVSSNLNIPR**RNNCGVTSNGRIYCIGGYDGSSIIPNVEAYDHR**MK**
AWVEVAPLNTPRSSAMCVAFDNK**IYVIGGTNGERLNSIEVYEEKMNKWEQFPYALLEAR**SSGAAFNYLNQIY
VVGGIDNEHNILDSVEQYQPFNKR**WQFLNGVPEKK**MNFGAATLSDSYIITGGENGEVLNSCHFFSPDTNEWQ
LGPSLLVPR**FGHSVLIANI***

Fig. 14 Different running behavior of endogenous and recombinant His-tagged full-length *Pf*Kelch13.

(a) N-terminally His-tagged *Pf*Kelch13 was produced in *P. falciparum*, Sf21, and *E. coli* cells. Crude lysates were probed with an anti His antibody. Expected molecular sizes and differences of the tagged N-terminus are indicated. The His-tagged *Pf*Kelch13 in *P. falciparum* starts with the amino acids PAS because of the N-terminal 2A self-cleaving peptide (see Fig. 24). **(b)** Sequence coverage of encoded His-tagged *Pf*Kelch13 in *P. falciparum* following affinity chromatography according to Fig. 11d. Detected amino acid residues by mass spectrometry are highlighted (bold).

3.3 Folding properties of recombinant *Pf*Kelch13$^{333-726}$ mutants correlates with artemisinin susceptibility in the field

Specific mutations in *Pf*Kelch13, especially in the propeller domain, are associated with an increased parasite survival upon artemisinin treatment that can be tested in ring stage survival assays (RSAs). The most prevalent mutation in South East Asia (SEA) is a cysteine to tyrosine mutation at position 580 with survival rates of around 2-15% depending on the genetic background (Straimer et al. 2015). Other mutations showing even stronger decreases in artemisinin susceptibility are R539T and I543T (Straimer et al. 2015). These mutations are indicated in the crystal structure of the BTB/kelch propeller domain of *Pf*Kelch13 (Fig. 15a).

Here, we asked if these three prominent mutations alter the stability of the protein as speculated in the literature (Coppée et al. 2019). Indeed, production of *Pf*Kelch13$^{337-727}$ in Sf21 cells carrying one of the mentioned mutations resulted in completely insoluble protein

(Fig. 15c) indicating an influence of these mutations on protein folding. Interestingly, neither the substitution of C580 nor of C532 to a serine showed the detected insolubility of C580Y and C580F.

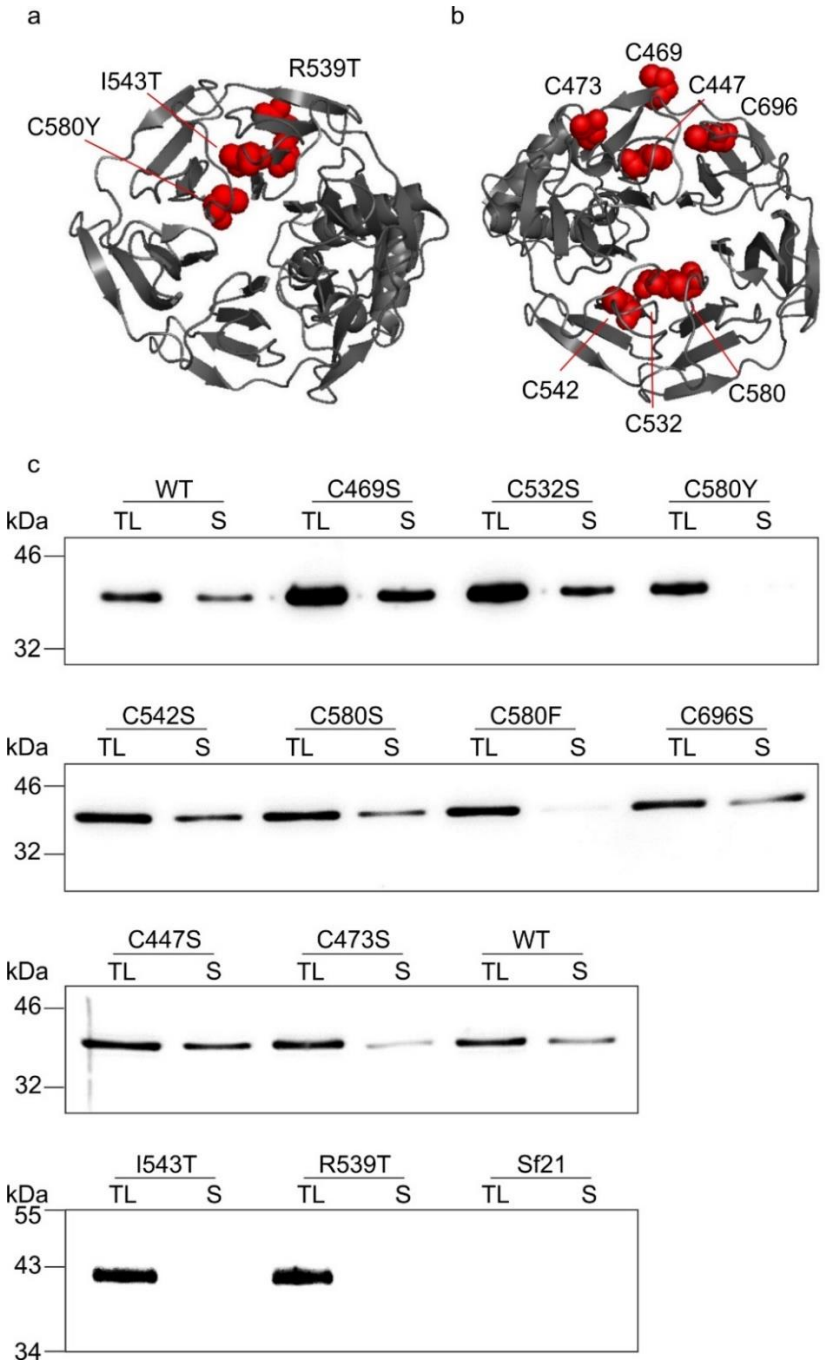

Fig. 15 Solubility of *Pf*Kelch13 mutants expressed in Sf21 cells correlates with artemisinin resistant field muations.

(a) Crystal structure of *Pf*Kelch13 BTB/kelch propeller domain with highlighted mutations that are prevalent in *P. falciparum* field isolates and lead to decreased artemisinin susceptibility. **(b)** Crystal structure of *Pf*Kelch13 BTB/Kelch propeller domain showing the positions of all cysteines within the protein. **(c)** Solubility screen of *Pf*Kelch13$^{337\text{-}726}$ mutants. Cells were harvested 72 h after infection with virus 1. Cells were lysed by 3 freeze-thaw cycles. Equal amounts of total lysate (TL) and the soluble fraction (S) were loaded on a SDS gel, blotted on PVDF membrane and probed with an anti His antibody. Mutants existing in the field and showing increased survival rates in RSAs (C580Y, I543T, R539T) show nearly complete insolubility indicating a link between *Pf*Kelch13 solubility and artemisinin resistance.

According to the crystal structure of *Pf*Kelch13, C580 and C532 are able to form a disulfide bond (Fig. 16a) which was speculated to stabilize the structure of the protein (Coppée et al. 2019). Purification of recombinant *Pf*Kelch13$^{337\text{-}726}$ carrying either the C532S or C580S mutation resulted in soluble proteins, whereas mutations of C580 to Y or F did not (Fig. 16b). This result strongly indicates that improper folding of *Pf*Kelch13 is not caused by the impossibility to form a disulfide bond but rather that a specific amino acid substitution at position 580, here tyrosine or phenylalanine, is responsible for the insolubility.

To address a possible role of *Pf*Kelch13 in redox signaling, we mutated all cysteines to serines (Fig. 15b). All recombinant single cysteine-to-serine mutants were soluble. However, *Pf*Kelch13^{C473S} resulted in a relatively weak signal in the soluble fraction indicating some folding problems in this mutant. According to the crystal structure, C473 is one out of two cysteines that are exposed to the surface of *Pf*Kelch13 (Fig. 17a). If *Pf*Kelch13 is involved in redox signaling processes, it is likely that these two accessible cysteines could be involved. To analyze the recognized weaker signal of C473S in western blots (Fig. 15c), we purified this mutant resulting in less protein in the eluate fraction compared to all other cysteine-to-serine mutants tested (Fig. 16b, 17b).

In summary, truncated *Pf*Kelch13$^{337\text{-}726}$ mutants represent the following detected solubility: field isolates ≤ C580Y/F < C473S < all other cysteine-to-serine mutants, suggesting a redox-independent and protein folding-dependent correlation between artemisinin resistance and protein solubility.

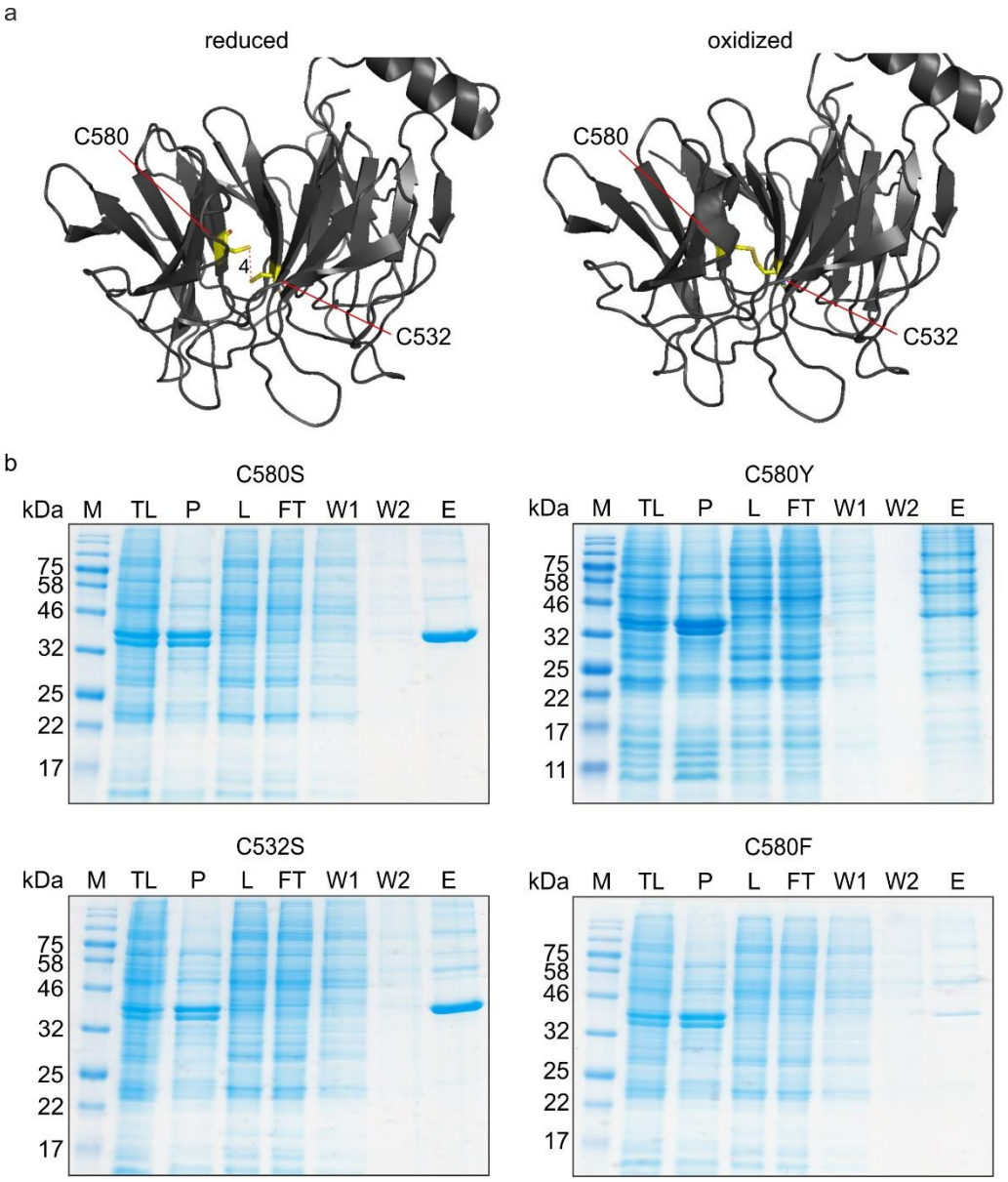

Fig. 16 The disulfide bond between C532 and C580 is not necessary for proper folding of *Pf*Kelch13$^{337-726}$.

(a) The crystal structure of *Pf*Kelch13 shows that C532 and C580 can form a reversible disulfide bond (left: reduced, PDB: 4YY8; right: oxidized, PDB: 4ZGC). The distance between the two cysteine sulfur atoms in the reduced protein is 4 Å. **(b)** Purification of C532S and C580S/Y/F from 25 ml cultures. Sf21 cells expressing *Pf*Kelch13$^{337-726}$ mutants were lysed by three freeze-thaw cycles (TL). After separation of the insoluble compartments (P), the supernatant (L) was loaded on a Ni-NTA agrose column. Non-bound material (FT) was discarded. The resin was washed (W) and the bound protein eluted (E) with 250 mM imidazol. Serine mutants could be purified whereas the tyrosine and phenylalanine mutant were both insoluble.

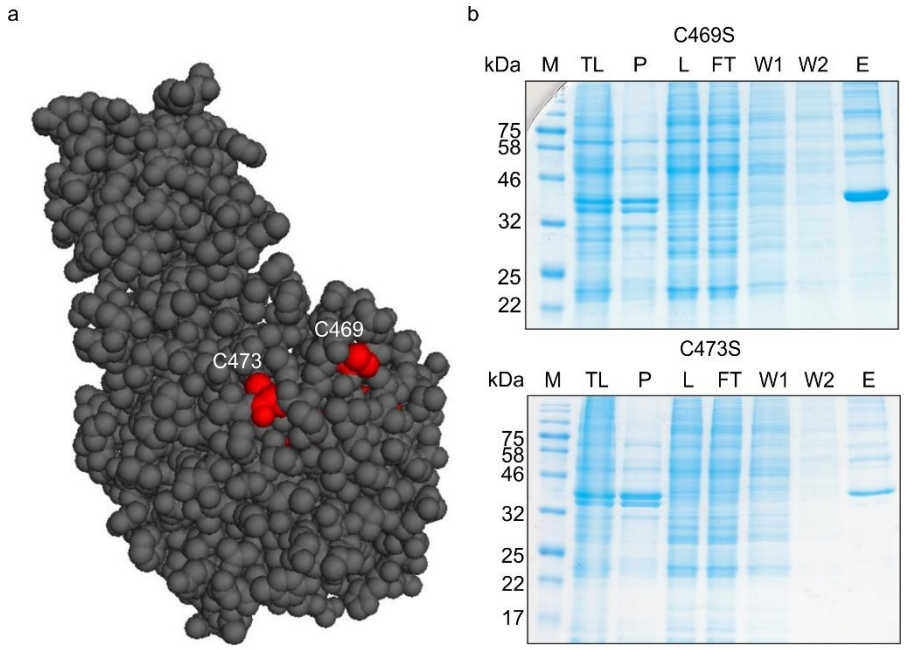

Fig. 17 Mutants of the two surface-exposed cysteines of *Pf*Kelch13 show different folding properties.

(a) The crystal structure of *Pf*Kelch13 shows that C469 and C473 are exposed at the surface (PDB: 4YY8). **(b)** Purification of recombinant C469S and C473S mutants from 25 ml cultures. Sf21 cells expressing *Pf*Kelch13$^{337-726}$ mutants were lysed by three freeze-thaw cycles (TL). After separation of the insoluble compartments (P), the supernatant (L) was loaded on a Ni-NTA agarose column. Non-bound material (FT) was discarded. The resin was washed (W) and the bound protein eluted (E) with 250 mM imidazol. Compared to C469S, C473S showed a lower yield and purity.

3.4 Knock-down of *PFKELCH*13 decreases artemisinin susceptibility

It was shown that disruption of *PFKELCH* results in a complete growth inhibition of *P. falciparum* parasites arguing for an essential function of this gene (Birnbaum et al. 2017). Inducible mislocalization led to increased survival rates in RSAs (Yang et al. 2019). Stronger mislocation led to growth arrest in the ring stage (Birnbaum et al. 2017). Instead of mislocalizing the protein from its site of action, we wanted to test another strategy starting at the mRNA level. Here, we generated and analyzed a *Pf*Kelch13 knock-down using the *glmS* riboswitch.

3.4.1 Generation and validation of chromosomal *PFKELCH13-glmS*

To test a possible impact of *Pf*Kelch13 protein levels on artemisinin susceptibility, a knock-down strain was generated using the SLI method (Birnbaum et al. 2017). We designed a plasmid leading to the disruption of the endogenous *PFKELCH13* gene and replacing it with His_8-*PFKELCH13-glmS*. We transfected the designed plasmid (Fig. 18a) into the 3D7 wild-type

strain. After successful selection of the plasmid, integration events were selected with DSM1. Successful integration was confirmed by genotyping the strains (Fig. 18b). We checked integration by choosing different primer pairs confirming the integration of the construct from the 5' and the 3' end. The absence of the endogenous *PFKELCH13* gene elsewhere in the genome was also checked by choosing a primer pair that binds up- and downstream of the homology region but inside the *PFKELCH13* gene. No wild-type locus amplicon was detected. As a control for downstream experiments, the fusion of *PFKELCH13* to an inactive riboswitch was also used, here referred as *M9*.

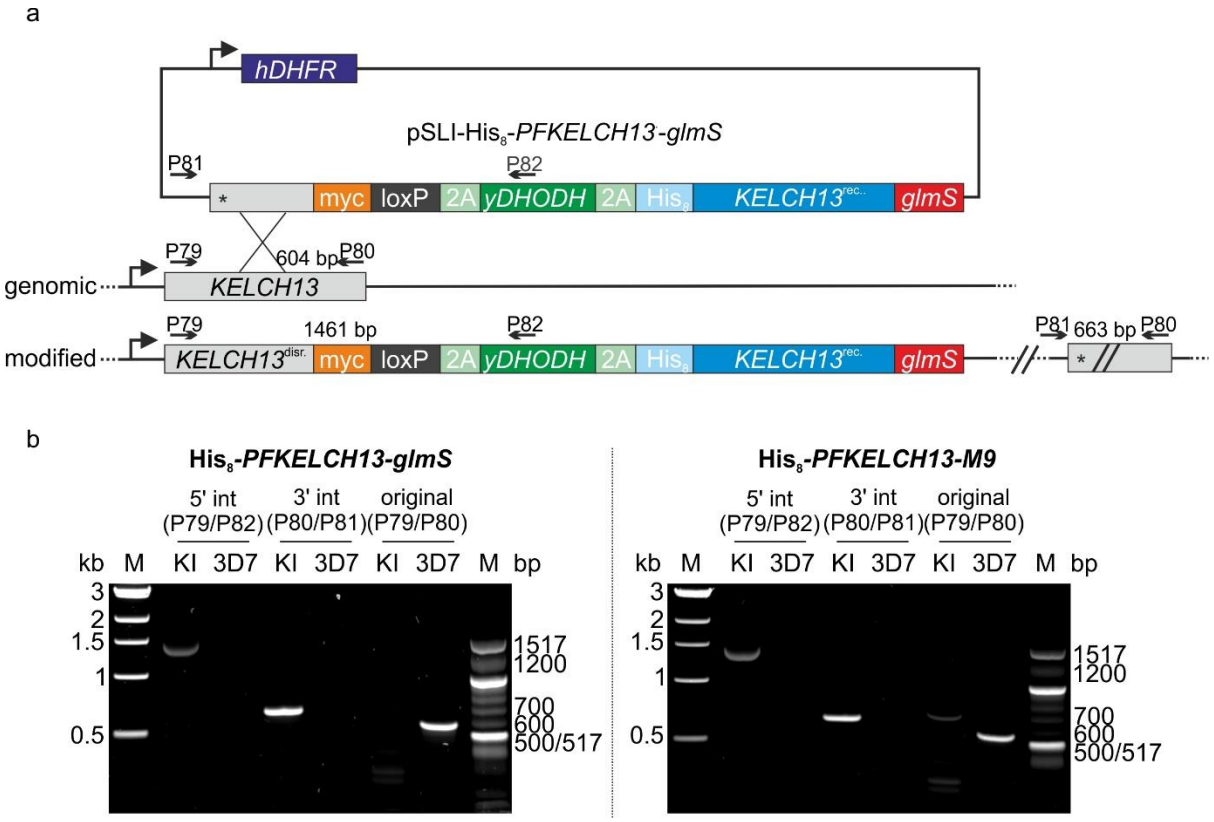

Fig. 18 Confirmation of His$_8$-*PFKELCH13-glmS* strains.

(a) Schematic representation of pSLI-His$_8$-*PFKELCH13-glmS* and the SLI strategy. The plasmid is integrated by homologues recombination into the *PFKELCH13* locus. The original *PFKELCH13* gene is disrupted. The cassette containing the selection marker *yDHODH* that is linked to His$_8$-*PFKELCH13-glmS* by a skip peptide 2A-encoding sequence is only expressed under the control of the endogenous *PFKELCH13* promoter. Resistance towards DSM1 indicates successful integration. **(b)** Genotyping of His$_8$-*PFKELCH13-glmS* and His$_8$-*PFKELCH13-M9*. Correct integration was confirmed by genotyping PCRs. Annealing sites as well as expected PCR product sizes are indicated in (a). KI: knock-in refers to the genetically modified strain after successful integration. 5' int and 3' int stand for the site integration of the cassette into the *PFKELCH13* that was tested.

3.4.2 Decreased levels of *Pf*Kelch13 phenocopy reduced artemisinin susceptibility in the field

After successful generation of strain His_8-*PFKELCH13-glmS* and its inactive variant His_8-*PFKELCH13-M9*, we tested the impact of GlcN treatment on the growth of both strains. To directly compare the effect of the GlcN concentration in the respective strain, an asynchronous parasite culture split into four cultures with a parasitemia of 0.1%. The cultures were treated with 0, 0.3, 1, and 2 mM GlcN. Giemsa-stained blood smears were prepared daily showing an inhibitory growth effect at 1 and 2 mM GlcN in the His_8-*PFKELCH13-glmS* strain. After five days, treatment with 1 mM and 2 mM GlcN resulted in growth inhibitions around 25% and more than 50% respectively, whereas in the presence of 0.3 mM GlcN cells grew normal (Fig. 19). To exclude a growth inhibitory effect of GlcN, we treated His_8-*PFKELCH13-M9* cells with the same GlcN concentrations. In the presence of 0.3 and 1 mM GlcN no altered growth phenotype was detected. When treated with 2 mM GlcN cells grew significantly slower. After five days treatment with 2 mM GlcN, cells showed a growth inhibition around 30% indicating an effect of GlcN itself on parasite growth independent of a *Pf*Kelch13 down-regulation. We also tested higher concentrations of GlcN (5 and 10 mM) in both strains resulting in complete growth arrest, further supporting the toxicity of GlcN at concentrations higher than 1 mM. Although the treatment with GlcN did not result in a complete growth arrest because of a *Pf*Kelch13 knock-down, up to 2 mM GlcN can be used to study biological characteristics of the His_8-*PFKELCH13-glmS*.

In summary, knock-down of *Pf*Kelch13 in the His_8-*PFKELCH13-glmS* strain at ≤ 1mM GlcN resulted in a gene-specific growth defect.

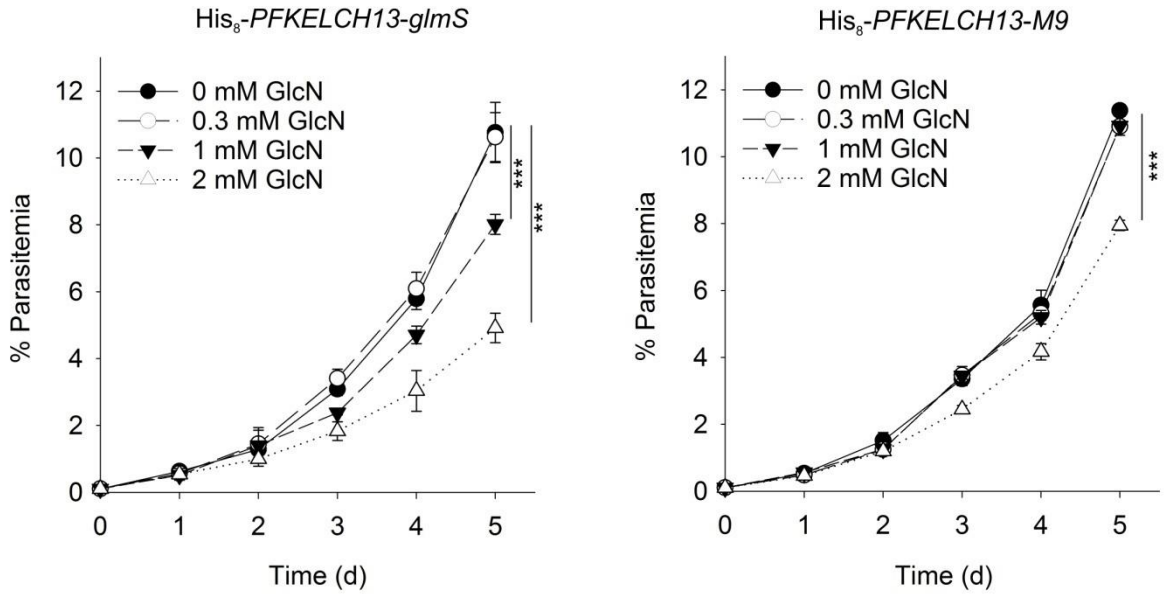

Fig. 19 Knock-down of *Pf*Kelch13 decreases parasite growth.

Asynchronous standard cultures of the strains His$_8$-*PFKELCH13-glmS* and His$_8$-*PFKELCH13-M9* were set to a parasitemia of 0.1%. Cells were treated with different concentrations of GlcN and the parasitemia was determined daily showing a dose-dependent growth inhibition in the His$_8$-*PFKELCH13-glmS* strain. For the His$_8$-*PFKELCH13-M9* strain a growth inhibition around 30% was detected in the presence of 2 mM GlcN indicating a toxicity effect of the compound itself. Higher concentrations of GlcN led to complete growth arrest in both strains (data not shown). All data points represent the mean ± standard deviation of three biological replicates. Statistical significance was tested using the one-way ANOVA method.

Since the resistance marker *y*DHODH was fused to His$_8$-*Pf*Kelch13 via a skip-peptide, both proteins are encoded on the same mRNA transcript (Fig. 18a). We asked if in the presence of GlcN also *yDHODH* mRNA is degraded. As a readout we quantified the growth of the His$_8$-*PFKELCH13-glmS* and *–M9* strain in the presence of different DSM1 concentrations. As a sensitive strain towards DSM1 we used the parental strain 3D7. In the presence of GlcN, the His$_8$-*PFKELCH13-glmS* strain showed a dose-dependent loss of resistance towards DSM1 (whereas the His$_8$-*PFKELCH13-M9* strain showed even in the presence of 2 mM GlcN high resistance towards DSM1 (Fig. 20). Thus, the efficient wild-type *glmS*-dependent knock-down of the fusion construct was confirmed by the loss of resistance towards DSM1.

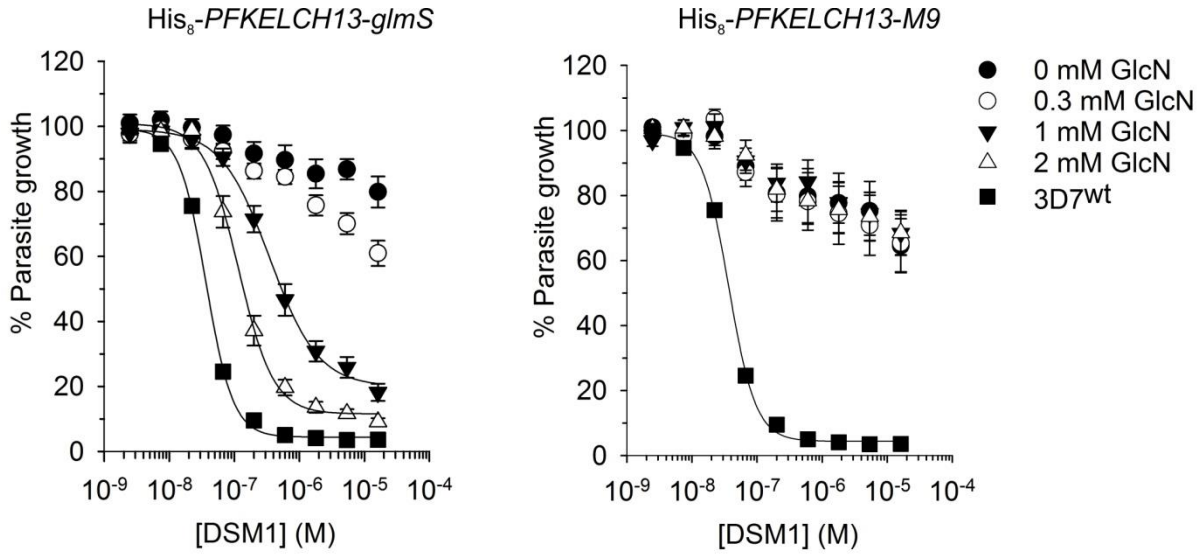

Fig. 20 In the presence of GlcN the His$_8$-*PFKELCH13-glmS* strain becomes sensitive towards DSM1 demonstrating a *glmS*-dependent *Pf*Kelch13 down-regulation.

The strains His$_8$-*PFKELCH13-glmS* and His$_8$-*PFKELCH13-M9* were selected with DSM1. The selection marker *y*DHODH was fused via a skip-peptide to *Pf*Kelch13. In the presence of GlcN the His$_8$-*PFKELCH13-glmS* strain showed a dose-dependent loss of DSM1 resistance whereas the His$_8$-*PFKELCH13-M9* strain did not show any alteration in sensitivity towards DSM1. The loss of DSM1 resistance directly shows the knock-down of yDHODH and/or *Pf*Kelch13. Strain 3D7 served as a sensitive positive control. All data points represent the mean ± SEM of four biological replicates.

We further addressed the efficiency of the riboswitch on *Pf*Kelch13 protein levels by western blot analysis with an anti His antibody (Fig. 21c). Four independent biologically experiments showed a strong decrease in the detected levels of *Pf*Kelch13 following GlcN treatment. Since the antibody detected two bands in parasite lysates, we quantified the intensity as the sum of both bands. As a housekeeping protein we used an anti aldolase antibody and normalized the intensities to this protein. In the presence of GlcN, *Pf*Kelch13 protein levels decreased in a dose-dependent manner reaching a down-regulation of more than 90% upon treatment with 2 mM GlcN (Fig. 21b). Treatment of the His$_8$-*PFKELCH13-M9* strain with the same GlcN amounts did not show significantly lower protein levels. Thus, *Pf*Kelch13 protein levels were *glms*- and GlcN- dependently down-regulated.

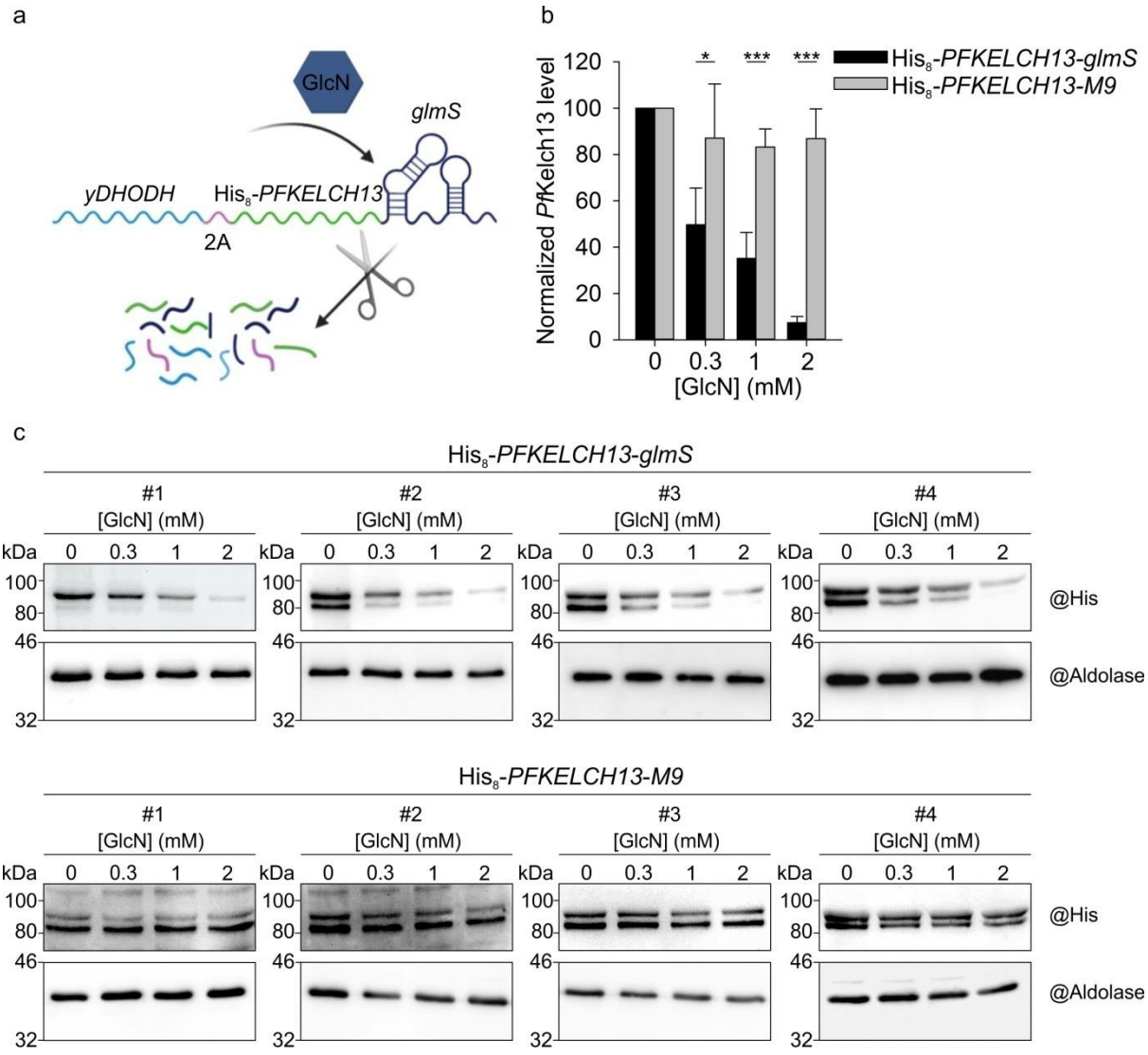

Fig. 21 Efficient down-regulation of *Pf*Kelch13 protein levels in His$_8$-*PFKELCH13-glmS* upon GlcN treatment.

(a) Scheme of *Pf*Kelch13 down-regulation. *PfKELCH13* is linked to the *glmS* riboswitch and via a skip peptide 2A-encoding sequence to the selection marker *yDHODH*. In the presence of GlcN, the riboswitch is activated resulting in the degradation of the mRNA. **(b)** Relative normalized *Pf*Kelch13 levels in the presence of GlcN. Quantification of signal intensities from (c). *Pf*Kelch13 levels were significantly down-regulated in the His$_8$-*PFKELCH13-glmS* strain. The His$_8$-*PFKELCH13-M9* strain served as a negative control (inactive riboswitch) showing no significant down-regulation in the presence of GlcN. All data points represent the mean ± standard deviation of four biological replicates. Statistical significance was tested using the one-way ANOVA method. **(c)** Western blots probed with anti His antibody in His$_8$-*PFKELCH13-glmS* and His$_8$-*PFKELCH13-M9* strains cultured for two cycles in the presence of the indicated [GlcN]. Decoration with an anti aldolase antibody was used as a loading control for normalization.

Next, following the confirmation of a GlcN dose-dependent knock-down of *Pf*Kelch13 by western blots and EC_{50} measurements, we asked if reduced levels of *Pf*Kelch13 can phenocopy a reduced artemisinin susceptibility comparable to *Pf*Kelch13 mutants. Indeed, pretreatment with 1 mM GlcN for two cycles resulted in ring stage survival rates of more than 35% in a classical RSA (Fig. 22). Further increase of the GlcN concentration to 2 mM did not

raise the survival rate drastically, indicating a saturation of this value of around 40%. This value was more than twice as high as the one for NF54K13^{C580Y} around 14%. The negative control His$_8$-*PFKELCH13-M9* did not show any significant higher survival rates in the presence of GlcN. Hence, reduced *Pf*Kelch13 protein levels led to a decreased artemisinin susceptibility with a maximum survival rate of around 40%.

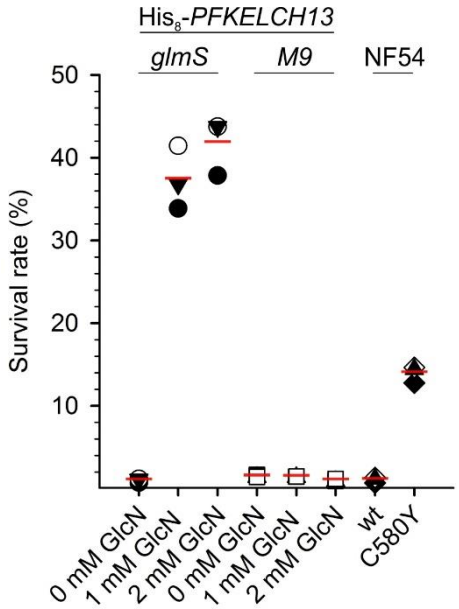

Fig. 22 Knock-down of *Pf*Kelch13 increases the survival rate in ring stage survival assays.

In the presence of 1 and 2 mM GlcN His$_8$-*PFKELCH13-glms* parasites showed survival rates around 40%. The inactive riboswitch *M9* did not show an increase of the survival rate in the presence of GlcN and served as a negative control. The resistant strain NF54K13^{C580Y} and wild-type NF54 served as positive and negative controls, respectively. Each symbol resprents one of three biological replicates.

3.5 Influence of cysteines residues C580 and C532 of *Pf*Kelch13 on the sensitivity towards redox agents and artemisinin

3.5.1 *Pf*Kelch13^{C580Y} mutant does not alter the EC$_{50}$ upon treatment with redox agents and artesunate

Next, we addressed if the mutation C580Y in *Pf*Kelch13 has an effect on the sensitivity of blood-stage parasites towards redox agents. We determined the EC$_{50}$ of the oxidants diamide and tBuOOH, the reductant DTT, and the antimalarial drug artesunate (Fig. 23) in NF54K13^{C580Y} and its corresponding wild-type strain NF54 (Ghorbal et al. 2014). We achieved

EC_{50} values comparable to already published values (Wezena et al. 2017). No significant differences were observed between both strains (Table 24).

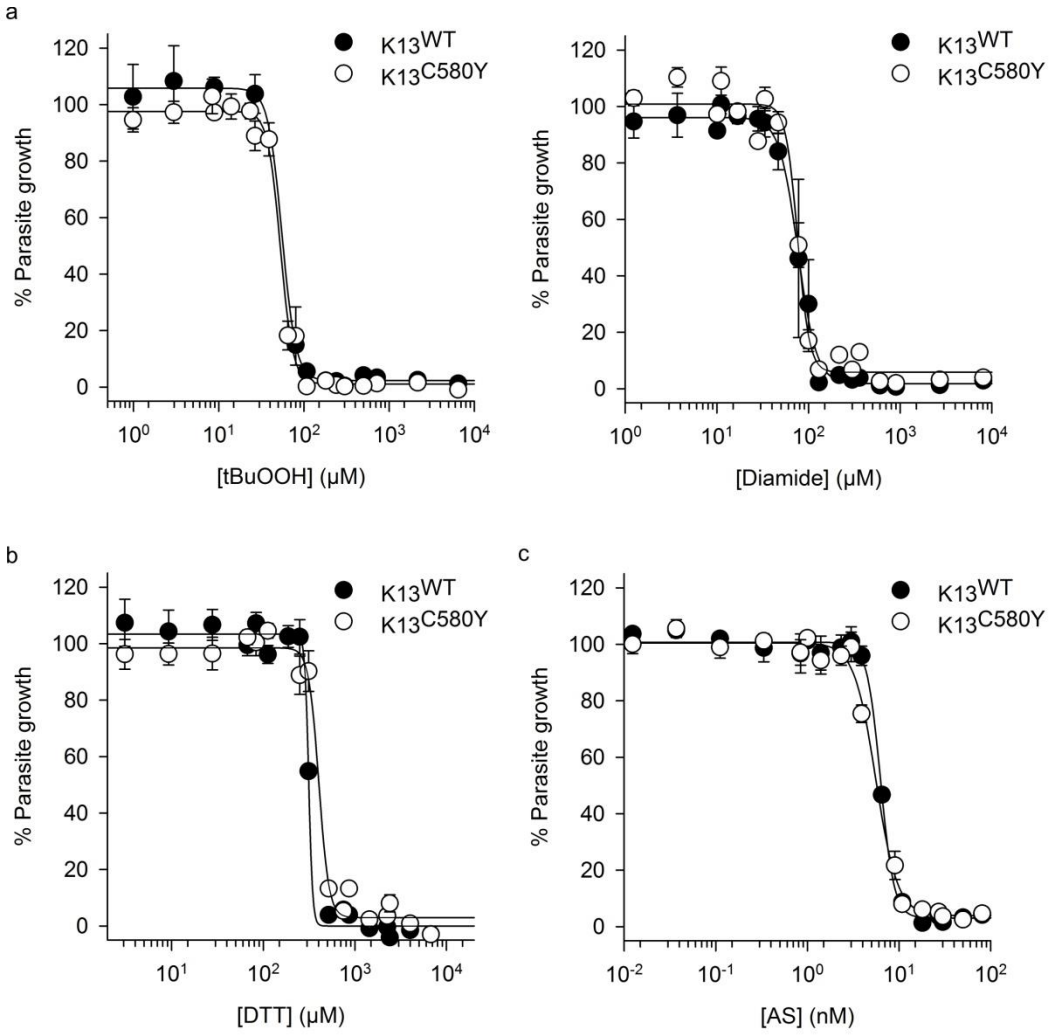

Fig. 23 Substitution of C580 to tyrosine does not change the EC_{50} towards redox agents and artesunate.

Parasite growth in response to bolus treatments of ring-stage parasites with different doses of the oxidants **(a)** tBuOOH and **(b)** diamide, the reductant **(c)** DTT and the antimalarial drug **(d)** artesunate (AS). Values are given in Table 24. Each curve represents the mean ± standard deviation of three biological replicates. Statistical significance was tested using the one-way ANOVA method.

Table 24 EC_{50} values for redox agents and artesunate in NF54K13^{wt} and NF54K13^{C580Y}.

EC_{50} values were calculated from curves in Fig. 23.

	Artesunate (AS)	Diamide	tBuOOH	DTT
K13^{wt}	6.4 ± 0.2 nM	76 ± 4 µM	53 ± 3 µM	314 ± 5 µM
K13^{C580Y}	5.7 ± 0.5 nM	77 ± 5 µM	57 ± 4 µM	405 ± 28 µM

3.5.2 Chromosomally encoded *Pf*Kelch13^{C532S} and *Pf*Kelch13^{C580S} do not alter the artemisinin susceptibility

Since the substitution of C580 to tyrosine showed increased survival rates in ring stage survival assays, we wondered if this decrease in sensitivity is caused by the non-formation of an intramolecular disulfide bond between C532 and C580. We mutated both residues to serines and integrated the constructs using the SLI method (Birnbaum et al. 2017). The designed plasmids carrying the desired mutation (Fig. 24a) were transfected into the 3D7 strain, first selected for the plasmid using *hDHFR* and afterwards for integration using *yDHODH*. We validated successful integration by choosing different primer pairs showing correct integration of the construct from the 5' and the 3' end. The absence of the endogenous *PFKELCH13* gene elsewhere in the genome was also tested by choosing a primer pair that binds up- and downstream of the homology region but inside the *PFKELCH13* gene (Fig. 24a). After validation of correct integration by genotyping PCRs (Fig. 24b), ring stage survival assays were performed.

We were not able to integrate the gene encoding a His-tagged C580Y or C473S mutant in three independent experiments, one of which was performed in parallel with the successful experiments for the other mutants. Hence, His-tagging in combination with the mutations of either C580Y or C473S appear to be lethal. Because of this, we used an already validated strain carrying the C580Y mutation raised with the CRISPR/Cas method (Ghorbal et al. 2014). The mutant and its corresponding parental wild-type strain were kindly provided by Jose-Juan Lopez-Rubio (Montpellier, France).

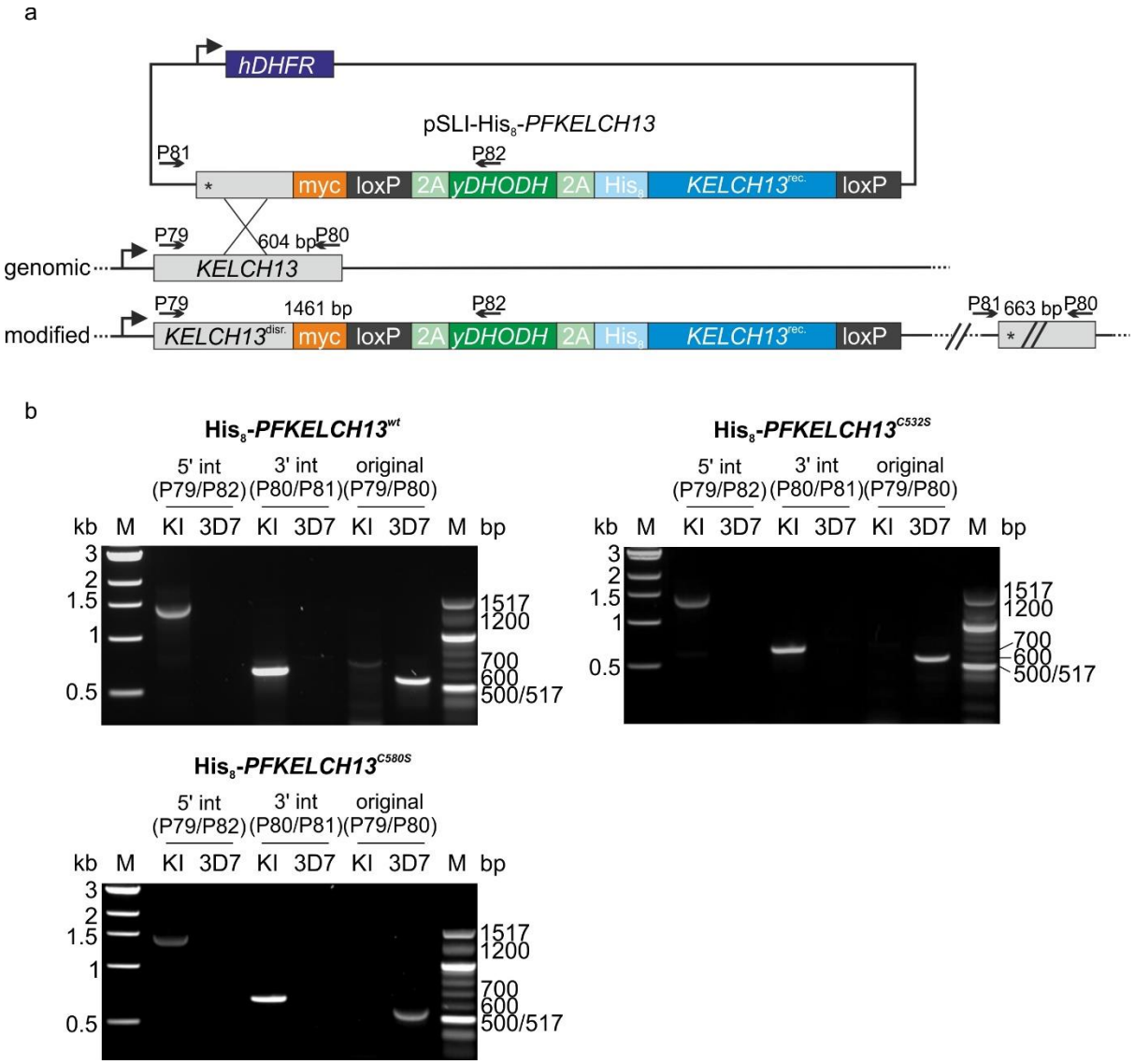

Fig. 24 Confirmation of His$_8$-*PFKELCH13*^{wt}, His$_8$-*PFKELCH13*^{C532S} and His$_8$-*PFKELCH13*^{C580S} strains.

(a) Schematic representation of pSLI-His$_8$-*PFKELCH13* and the SLI strategy. The plasmid is integrated by homologues recombination into the *PFKELCH13* locus. The original *PFKELCH13* gene is disrupted. The cassette containing the selection marker *yDHODH* and His$_8$-*PFKELCH13* is expressed under the control of the endogenous *PFKELCH13* promoter. Resistance towards DSM1 indicates successful integration. **(b)** Genotyping of His$_8$-*PFKELCH13*^{wt}, His$_8$-*PFKELCH13*^{C532S} and His$_8$-*PFKELCH13*^{C580S}. Correct integration was confirmed by genotyping PCRs. Annealing sites as well as expected PCR product sizes are indicated in (a).

We performed ring stage survival assays for both strains which resulted in the expected resistance of the C580Y strain with a survival rate of around 14% and the expected sensitivity in the wild-type strain with a survival rate around 1%. When performing this assay with the C532S and C580S mutant, no increase in the survival rates were observed compared to the corresponding control containing His-tagged wild-type *Pf*Kelch13 in a 3D7 background (Fig. 25). Thus, the redox state of neither C532 nor C580 is responsible for a decrease in artemisinin

susceptibility supporting a structural and not a redox-dependent involvement of residue C580.

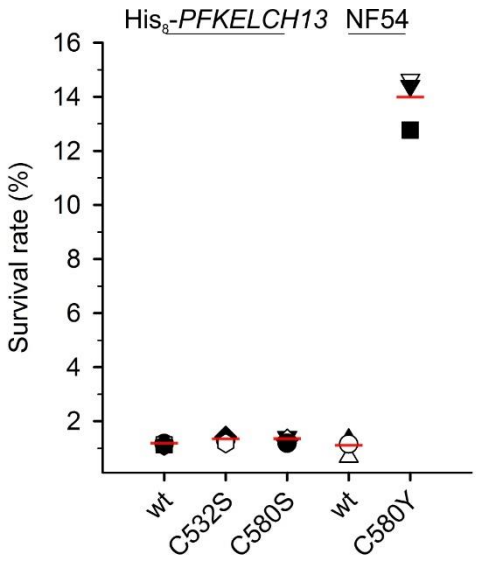

Fig. 25 The intramolecular disulfide bond C532-C580 in *Pf*Kelch13 is not involved in artemisinin susceptibility.

His$_8$-*PFKELCH13*^{C532S} and His$_8$-*PFKELCH13*^{C580S} showed survival rates like the corresponding wild-type strain His$_8$-*PFKELCH13*^{wt}. The strain NF54K13^{C580Y} served as a positive control for the correct performance of the assay. Each symbol represents one of three biological replicates.

3.5.3 A rescue plasmid to test non-viable *Pf*Kelch13 cysteine mutants

Recombinant *Pf*Kelch13^{C473S} was partially insoluble *in vitro* (section 3.3). Whether this mutation also results in a decreased artemisinin susceptibility in cell culture could not be tested, since we were not able to introduce His-tagged *Pf*Kelch13^{C473S} and *Pf*Kelch13^{C580Y} into the 3D7 wild-type strain using the SLI method. To analyze the protein level of endogenous His-tagged *Pf*Kelch13^{C473S}, we generated a rescue plasmid for the blasticidin concentration-dependent overexpression of GFP-*Pf*Kelch13 as a control. We showed that GFP-*Pf*Kelch13 was produced in the wild-type His$_8$-*PFKELCH13* strain (Fig. 26b) and localizes to defined foci (Fig. 26a). Thus, N-terminal GFP-tagging did not result in mislocalized *Pf*Kelch13. We also demonstrated overexpression of GFP-*Pf*Kelch13 from plasmid pHBIRH-*GFP-PFKELCH13* in the plasmid-containing strains pSLI-His$_8$-*PFKELCH13*^{C473S} and pSLI-His$_8$-*PFKELCH13*^{C580Y} (Fig. 26c). Both strains are now ready for the analysis of the protein levels of GFP-*Pf*Kelch13 and His-tagged *Pf*Kelch13^{C473S} or *Pf*Kelch13^{C580Y} following selection-linked integration at different concentrations of blasticidin.

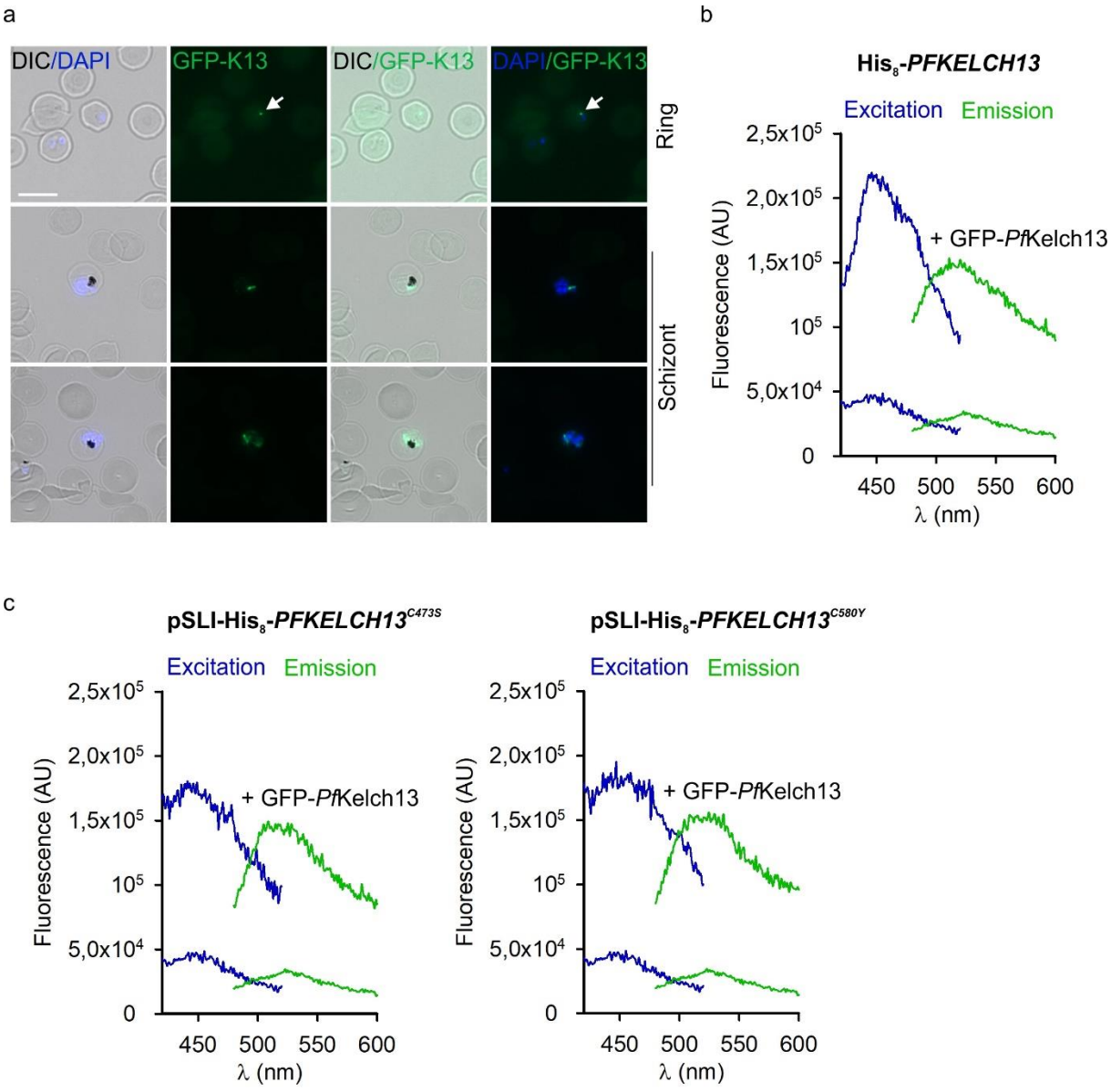

Fig. 26 Overexpression of GFP-*Pf*Kelch13 in different parasite strains.

(a) Microscopy showing correct localization of GFP-*Pf*Kelch13 (green). Nuclei were stained with DAPI (blue). Scale bar: 10 µm. **(b)** Fluorescence spectra of His$_8$-*PFKELCH13* parasites episomally expressing GFP-*Pf*Kelch13 from plasmid pHBIRH in the presence of 2 µg/ml blasticidin. **(c)** Fluorescence spectra of pSLI-His$_8$-*PFKELCH13*^{C473S} and pSLI-His$_8$-*PFKELCH13*^{C580Y} parasites episomally expressing GFP-*Pf*Kelch13 from plasmid pHBIRH in the presence of 2 µg/ml blasticidin. Spectra were recorded in a Clariostar plate reader using isolated parasites in PBS that were liberated by saponin treatment.

3.6 Characterization of the reductive half-reaction of *Pf*AOP

3.6.1 Oxidized *Pf*AOP is glutathionylated by GSH and reduced by *Pf*Grx

The kinetic parameters for the reduction of hydroperoxides by recombinant *Pf*AOP were determined by stopped-flow measurements (Staudacher et al. 2018). Moreover, steady-state kinetics revealed that *Pf*Grx and GSH are true substrates for the reduction of *Pf*AOP (Djuika et al. 2013). From these results three different models of *Pf*AOP catalysis were drawn. Subsequent steady-state measurements for recombinant wild-type and mutant *Pf*AOP suggested a preference for GSH as the first and *Pf*Grx as the second reducing agent (Staudacher et al. 2015). However, qualitative western blot analysis (Djuika et al. 2013) were not fully conclusive and the second order rate constant for the isolated reductive half-reaction remained to be determined.

Incubation of tBuOOH-oxidized *Pf*AOP with one equivalent GSH for 30 min on ice resulted in a strong signal when probing with an anti glutathione antibody (Fig. 27). Hence, the sulfenic acid was efficiently glutathionylated by GSH. Incubation of reduced *Pf*AOP with 60 equivalents GSSG also resulted in the glutathionylation of *Pf*AOP. However, much lower signal intensities were detected, indicating a much lower efficiency for the GSSG-dependent glutathionylation reaction. This might suggest that the reduced cysteine residue is not accessible to GSSG, whereas the sulfenic acid is accessible to GSH.

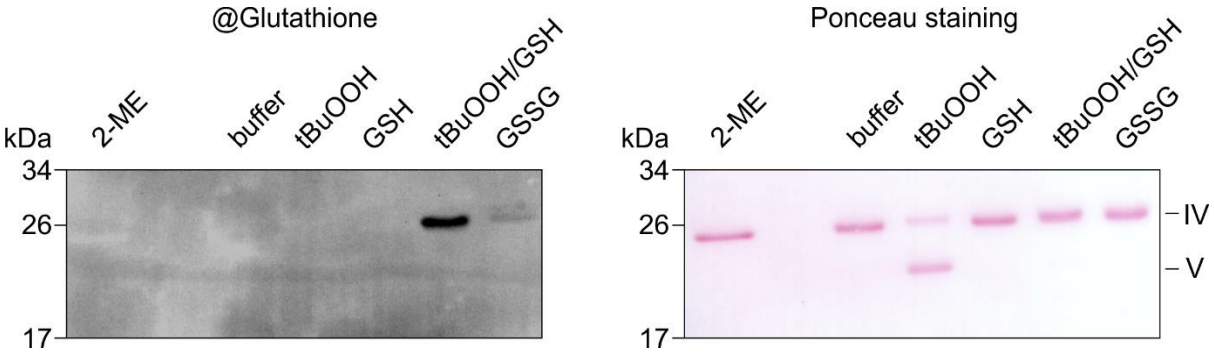

Fig. 27 GSH glutathionylates oxidized *Pf*AOP.

Left: Western blot demonstrating that the sequential treatment of 20 µM *Pf*AOP with 1 equivalent tBuOOH and 1 equivalent GSH resulted in the glutathionylation of the protein. A weak signal was also detected following treatment of 20 µM reduced *Pf*AOP with 60 equivalents GSSG. Subsequent redox reactions were blocked by the addition of 20 mM iodoacetamide in the Laemmli buffer. Right: Ponceau staining served as a loading control. The calculated mass of *Pf*AOP is 22.6 kDa. Refer to bands IV and V from Djuika et al. 2013.

We further showed that glutathionylated *Pf*AOP is reduced by a single cysteine variant of *Pf*Grx (Fig. 28). Incubation for 30 min on ice resulted in the loss of the signal of glutathionylated *Pf*AOP in a dose-dependent relationship to *Pf*Grx$^{C32/88S}$.

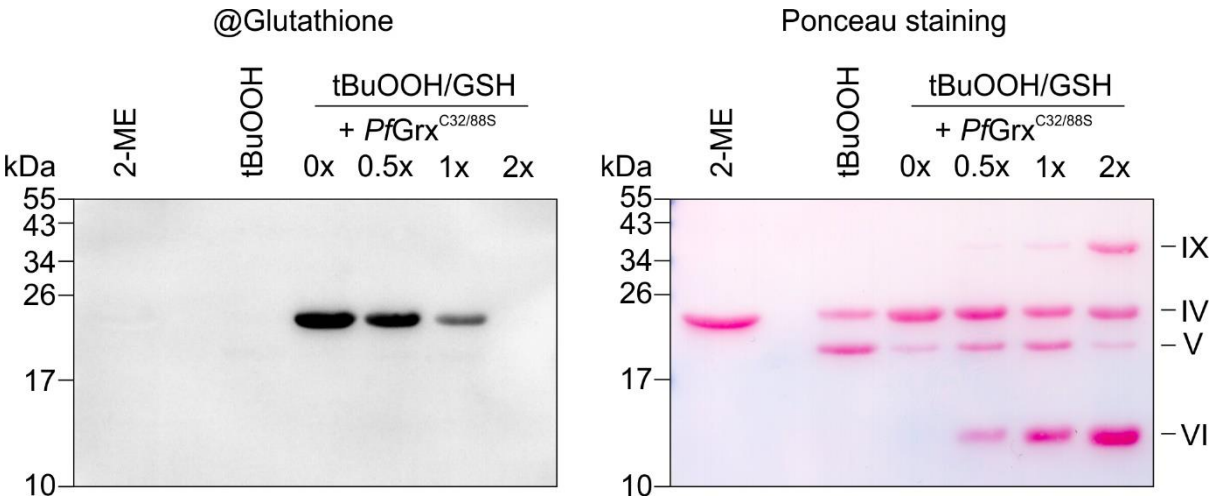

Fig. 28 *Pf*Grx reduces glutathionylated *Pf*AOP.

Left: Western blot demonstrating that the sequential treatment of 20 µM glutathionylated *Pf*AOP with the indicated equivalents of *Pf*Grx resulted in a dose-dependent deglutahionylation of *Pf*AOP. Subsequent redox reactions were blocked by the addition of 20 mM iodoacetamide in the Laemmli buffer. Right: Ponceau staining served as a loading control. The calculated masses of *Pf*AOP and PfGrx$^{C32/88S}$ are 22.6 kDa and 13.7 kDa, repectively. Refer to bands IV, V, VI and IX from Djuika et al. 2013.

To analyze which of the two cysteine residues in oxidized *Pf*AOP is glutathionylated, we tested both serine mutants (Fig. 29). Substitution of C143 to serine showed glutathionylation of the oxidized species and deglutathionylation via *Pf*Grx, whereas active-site mutant C117S did not result in a glutathione signal in western blots. This result indicates that oxidized C117 is responsible for the reaction with GSH.

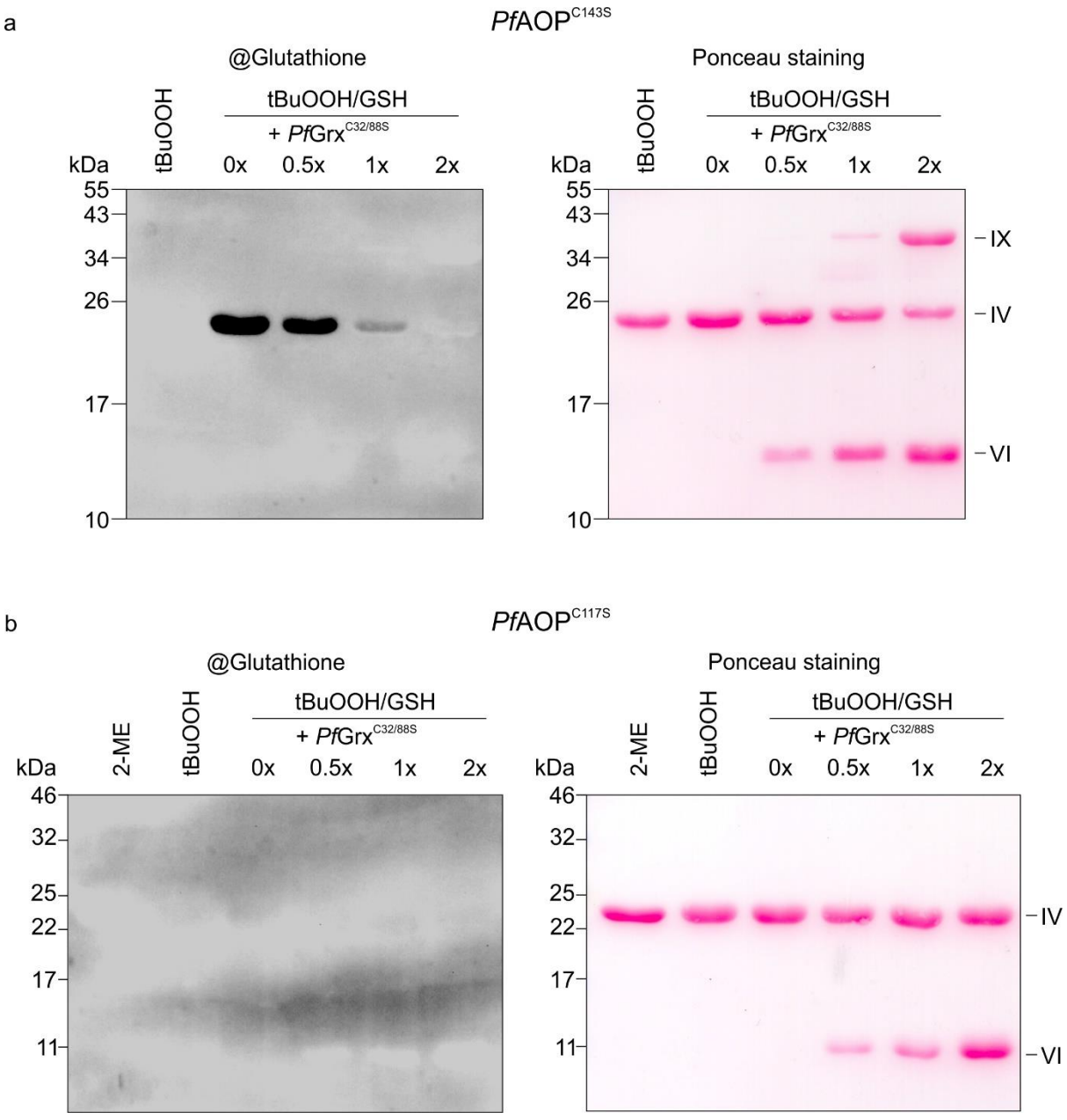

Fig. 29 GSH glutathionylates C117 but not C143 in peroxide-treated *Pf*AOP.

(a) Left: Western blot demonstrating that the sequential treatment of 20 µM *Pf*AOP^{C143S} with 1 equivalent tBuOOH and 1 equivalent GSH resulted in the glutathionylation of C117. Treatment of glutathionylated *Pf*AOP^{C143S} with *Pf*Grx resulted in a dose-dependent deglutathionylation of *Pf*AOP^{C143S}. Right: Ponceau staining served as loading control. **(b)** Left: Western blot showing that the sequential treatment of *Pf*AOP^{C117S} with tBuOOH and GSH does not result in a glutathionylation signal. Left: Ponceau staining serves as loading control. Subsequent redox reactions were blocked by the addition of 20 mM iodoacetamide in the Laemmli buffer. The calculated masses of *Pf*AOP and PfGrx$^{C32/88S}$ are 22.6 kDa and 13.7 kDa, repectively. Refer to bands IV, VI and IX from Djuika et al. 2013.

We expected a transfer of glutathione from *Pf*AOP to *Pf*Grx. We were not able to detect glutathionylated *Pf*Grx (Fig. 28, Fig. 29). Since just 1 equivalent GSH was used, it is rather unlikely that after the transfer of glutathione to *Pf*Grx the glutaredoxin is completely reduced

by GSH. To show the transfer of glutathione from *Pf*AOP to *Pf*Grx, we therefore performed mobility shift assays using the alkylation agent mmPEG (Fig. 30). Treatment of reduced *Pf*AOP and *Pf*Grx with mmPEG resulted in a shift to higher molecular weights demonstrating the alkylation of the free thiols in both proteins. Sequential treatment of glutathionylated *Pf*AOP with *Pf*Grx and mmPEG resulted in the loss of the alkylated *Pf*Grx species indicating that the thiol group of *Pf*Grx was blocked by the transferred glutathione moiety. Taken together, here we showed that oxidized *Pf*AOP can be glutathionylated by GSH and that the transfer of glutathione from *Pf*AOP to *Pf*Grx completely reduces *Pf*AOP.

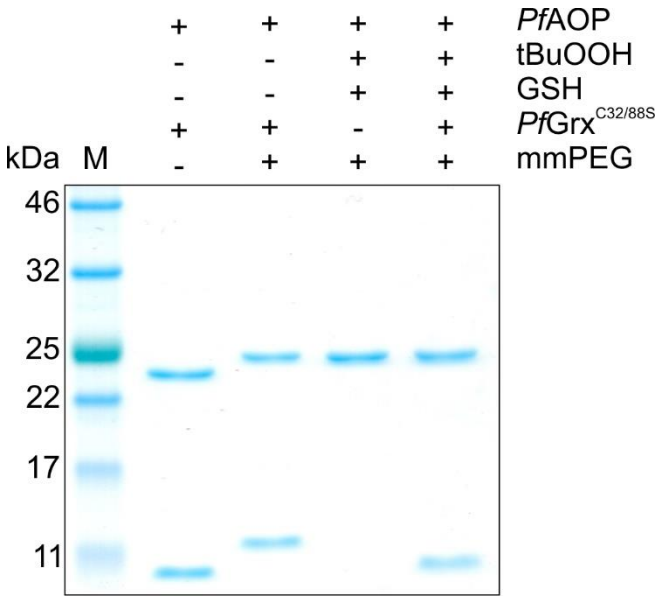

Fig. 30 Glutathione is transferred from *Pf*AOP to *Pf*Grx$^{C32/88S}$.

Treatment of reduced 20 µM *Pf*AOP and 20 M *Pf*Grx$^{C32/88S}$ with mmPEG results in a shift to higher molecular weights (lane 2 vs lane 1). Sequential incubation of *Pf*Grx with glutathionylated *Pf*AOP and mmPEG did prevented the mobility shift for *Pf*Grx$^{C32/88S}$ indicating its glutathionylation.

3.6.2 Determination of the reaction kinetics for the reductive half-reaction of *Pf*AOP with GSH

To quantify the kinetic parameters for the glutathionylation of oxidized *Pf*AOP, stopped-flow measurements were performed. Mixing tBuOOH-oxidized *Pf*AOP with different concentrations of GSH resulted in a fast increase in fluorescence (Fig. 31). No change in fluorescence was observed for *Pf*AOP^{C117S} demonstrating that the reaction depends on active site residue C117.

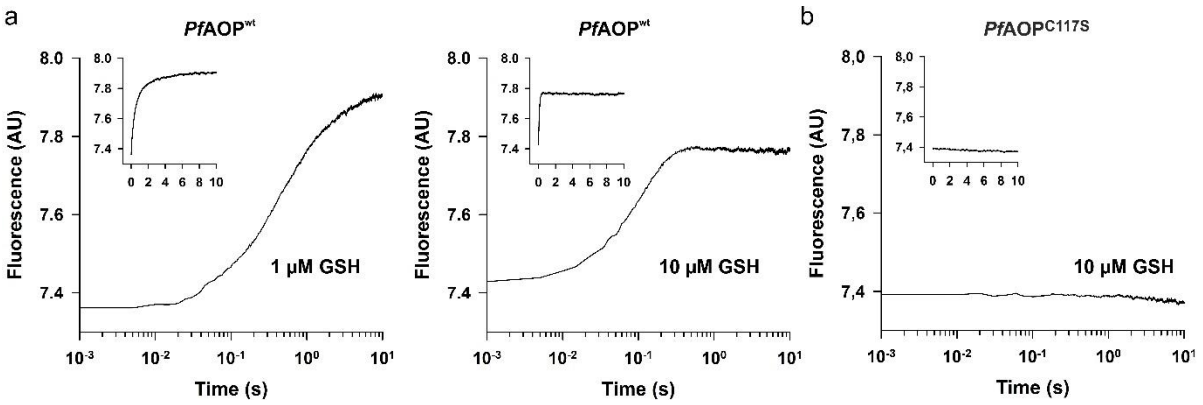

Fig. 31 Stopped-flow kinetics of the glutathionylation of tBuOOH-oxidized *PfAOP*.

(a) Representative stopped-flow kinetics of 1 µM tBuOOH-oxidized *Pf*AOP upon mixing with GSH. **(b)** The active-site mutant *Pf*AOP^{C117S} served as a negative control.

All measured kinetics were fitted by single exponential regression. The k_{obs} values were plotted against the corresponding GSH concentration and fitted by linear regression resulting in the second order rate constants *k* as the slope of the curve (Fig. 32). We performed these measurements at 5 different temperatures (5, 10, 15, 20, 25°C) resulting in rate constants ranging from 1.82 x 10^5 to 6.07 x 10^5 $M^{-1}s^{-1}$ (Table 25).

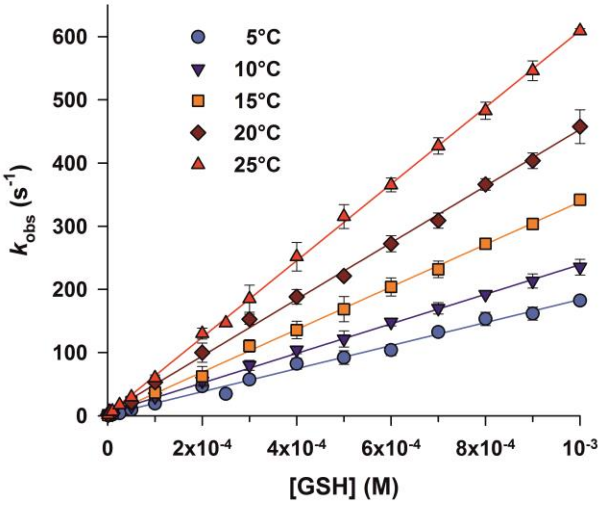

Fig. 32 Temperature dependency of the k_{obs} values for the glutathionylation of oxidized *Pf*AOP.

Data sets at the indicated temperatures were fitted by linear regression. The slopes yielded the second order rate constants *k* that are listed in Table 25. Data were obtained from three or four independent biological replicates.

Table 25 Rate constants of the glutathionylation of *Pf*AOP at different temperatures.

Rate constants represent the slopes of the curves in Fig. 32.

Temperature	k (x 10^5 $M^{-1}s^{-1}$)
5°C	1.82 ± 0.03
10°C	2.34 ± 0.03
15°C	3.37 ± 0.04
20°C	4.49 ± 0.05
25°C	6.07 ± 0.05

Since measurements at different temperatures were performed, we calculated the activation energy E_a and the pre-exponential factor A as well as the activation enthalpy $\Delta H^{\ddagger}$ and entropy $\Delta S^{\ddagger}$ according to the Arrhenius equation and Eyring equation, respectively (Fig. 33). The activation energy was 41.1 kJ/mol with a pre-exponential factor of 1.43 x 10^{13} $M^{-1}s^{-1}$. The enthalpy of activation was calculated to be 39.8 kJ/mol and the entropy to be -0.79 J/mol. Please note that these estimates are based on macroscopic measurements in aqueous buffers with a postulated transmission coefficient κ and activity coefficients of 1 and therefore have to be interpreted with care. Since the entropy of activation was close to zero, the Gibbs free energy of activation $\Delta G^{\ddagger}$ was rather temperature-independent.

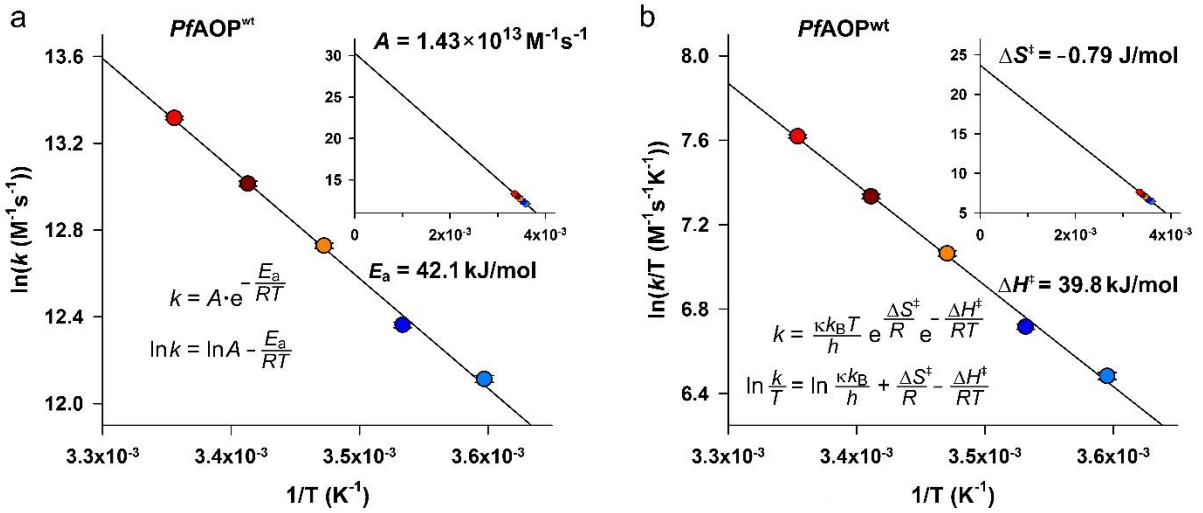

Fig. 33 Energetic values for the reaction between oxidized *Pf*AOP and GSH.

(a) The temperature-dependent rate constants (Table 25) were plotted according to the Arrhenius equation. Following linear regression analysis, the pre-exponential factor A and the activation energy E_a were determined from the y-axis intercept and the slope, respectively. **(b)** The temperature-dependent rate constants (Table 25) were plotted according to the Eyring equation. Following linear regression analysis, the enthalpy $\Delta H^{\ddagger}$ and entropy $\Delta S^{\ddagger}$ were determined.

4 Discussion

4.1 *Pf*Kelch13 and its role in artemisinin susceptibility

Since 2014, mutations in the kelch propeller domain of *Pf*Kelch13 are used as a marker for decreased artemisinin susceptibility (Ariey et al. 2014). Especially the substitution C580Y spread intensively in South East Asia (World Health Organization 2020). To understand the correlation between *Pf*Kelch13 mutations and artemisinin susceptibility much research was conducted to understand the function of this protein in the recent years. Based on a crystal structre (PDB: 4YY8) that shows the BTB and kelch propeller domain of *Pf*Kelch13, it was speculated that the protein functions as a substrate adaptor in ubiquitination processes (Tilley et al. 2016). Recently published studies suggest a direct link between *Pf*Kelch13 protein levels, hemoglobin uptake and artemisinin resistance (Birnbaum et al. 2020, Yang et al. 2019). Hence, two aspects of *Pf*Kelch13 seem to influence artemisinin susceptibility: 1. *Pf*Kelch13 protein stability and 2. Redox-dependent function of *Pf*Kelch13 in ubiquitination processes. However, to which degree these two factors contribute to artemisinin susceptibility remains still to be answered.

4.1.1 *Pf*Kelch13 protein stability

High resolution imaging demonstrated that *Pf*Kelch13 localizes close to the plasma membrane in cytostome-like structures and is involved in hemoglobin uptake (Yang et al. 2019). The idea of that *Pf*Kelch13 is involved in endocytosis was supported by the detection of an Eps15-like protein in close proximity of *Pf*Kelch13 (Birnbaum et al. 2020). Eps15 was shown to have an essential function in endocytosis in mammalian cell cultures (Carbone et al. 1997). Hence, a *Pf*Kelch13-defined endocytosis pathways was proposed for *Plasmodium falciparum* (Birnbaum et al. 2020). Substitution of C580 to tyrosine resulted in a decreased hemoglobin uptake arguing for a direct link to the observed decreased artemisinin susceptibility (Birnbaum et al. 2020, Yang et al. 2019). Less heme would result in less activation of artemisinin and therefore a decrease in artemisinin susceptibility (Fig. 7c). Interestingly, episomal overexpression of the mutant restored sensitivity towards artemisinin (Birnbaum et al. 2020). Therefore, it was speculated that the mutation destabilizes *Pf*Kelch13

resulting in less protein levels. An early study that showed the interaction of *Pf*Kelch13 with the phosphaditylinositol-3-kinase (*Pf*PI3K) did not find a significant difference in the protein level of the mutant compared to the corresponding wild-type strain (Mbengue et al. 2015). However, more recently published studies showed significant lower *Pf*Kelch13 protein levels in the *Pf*Kelch13^{C580Y} strain of up to 50% (Birnbaum et al. 2020; Gnädig et al. 2020). Further evidence for a correlation between *PFKELCH13* expression and artemisinin susceptibility *in vivo* was demonstrated by the study of Silva et al. 2019. This study revealed a positive correlation between *PFKELCH13* expression and the clearance time upon an artemisinin treatment. Mislocalization studies of *Pf*Kelch13 to the nucleus resulted in a decreased artemisinin susceptibility (Yang et al. 2019). Therefore, a direct link between *Pf*Kelch13 protein level and artemisinin susceptibility was demonstrated. However, since *Pf*Kelch13 is still present in the cell, such an experiment can not exclude metabolic site effects that resulted from this mislocalization.

An alternative method to study the function of essential proteins is to knock them down using the *glmS* riboswitch. This system was already successfully used in *P. falciparum* (Prommana et al. 2013). In the presence of glucoseamine-6-phosphate (GlcN6P) or glucosamine (GlcN) the transcript is self-cleaved whereby less mRNA is translated (Collins et al. 2007). To test the system for a *PFKELCH13* knock-down, we generated a construct by linking the *glmS* sequence downstream of the *PFKELCH13* gene. With western blots we confirmed the knock-down of *Pf*Kelch13 in a GlcN concentration-dependent manner with a maximum knock-down efficiency of more than 90% (Fig. 21). This result was strengthened by EC_{50} measurements towards DSM1, an inhibitor of *y*DHODH which was fused to *Pf*Kelch13 via a skip peptide (2A). In the presence of GlcN, parasites became sensitive towards the drug (Fig. 20).

Since *Pf*Kelch13 is essential (Birnbaum et al. 2017), we asked if a knock-down will decrease the growth rate of the parasites. In the presence of 1 and 2 mM GlcN parasites grew significantly slower. However, complete growth arrest could not be achieved at 2 mM GlcN. Although it has been reported that concentrations of GlcN could be used up to 10 mM without altering the growth in a 3D7 wild-type strain (Cobb et al. 2017), we recognized a complete growth arrest starting at 5 mM GlcN in an inactive *glms* strain (*M9*). We already measured a toxic affect of GlcN at a concentration of 2 mM. Nevertheless, it seems that a maximum of 10% compared to the basal level of *Pf*Kelch13 is still enough for the essential function of the protein. Interestingly, mislocalization of *Pf*Kelch13 from its site of action of more than 90%

did not change parasite growth at all (Birnbaum et al. 2017) but decreases artemisinin susceptibility drastically (Yang et al. 2019). Our ring stage survival assays confirmed this observation. In the presence of 1 mM and 2 mM GlcN, the survival rates were around 35%, and 40%, respectively. Hence, it is likely that there is a negative correlation between *Pf*Kelch13 protein levels and the survival rate (Fig. 34). Interestingly, it seems that the maximal survival rate is around 40%. Such a high survival rate was detected in a Cambodian strain carrying the R539T mutation in *Pf*Kelch13 (Straimer et al. 2015) and might indicate the maximal possible survival rate.

We further provide hints that *Pf*Kelch13 field mutants with a decreased artemisinin susceptibility are destabilized resulting in a lower protein abundance by analyzing the solubility of recombinant *Pf*Kelch13$^{337\text{-}726}$ mutants. Following the establishment of a protocol for the production of recombinant *Pf*Kelch13$^{337\text{-}726}$, we showed that the mutations C580Y, I543T or R539T resulted in insoluble recombinant protein (Fig. 15).

Indicating a correlation between artemisinin resistance and *Pf*Kelch13 protein levels the following question could be addressed: Why is there no spreading of a *Pf*Kelch13 mutation in the field resulting in much lower protein levels?

As indicated in our growth measurements, a down-regulation of *Pf*Kelch13 resulted in a decreased growth rate (Fig. 19). The slower growth rate can be explained by less hemoglobin uptake, that will lead to less amino acids which can be used for biosynthesis processes. Interestingly, Cambodian artemisinin resistant strains showed a fitness loss under amino acid starvation (Bunditvorapoom et al. 2018), which could be explained by a decreased basal hemoglobin uptake rate. Moreover, artemisinin resistant strains showed a prolonged ring stage (Siddiqui et al. 2020). In collaboration with the AG Ganter (Heidelberg) we are currently studying the stage length for our *glmS Pf*Kelch13 knock-down strains to address whether *Pf*Kelch13 protein levels alter the stage lengths leading to an altered artemisinin susceptibility.

In general, a strain with a slower growth rate will not outcompete a strain with a higher fitness in an *in vitro* experiment. However, other intrinsic features of the parasite influence its distribution in the field, including the degree of gametocytosis or the resistance towards the human immune system. Interestingly, the genetic background of the C580Y mutant seems to play an essential role. Introducing the C580Y mutation in a Cambodian strain (CamWT) did not alter the growth rate whereas in a Vietnamese strain (V1/S) it does (Straimer et al. 2017).

It was shown that Cambodian strains carrying the C580Y substitution also have mutations in genes encoding for proteins involved in DNA repair (Xiong et al. 2020). It was speculated that these mutations are responsible for the compensation of possible fitness costs in *Pf*Kelch13 mutants. Recently, the C580Y mutation was found in Guyana and emerged independently from South East Asia (Mathieu et al. 2020). Parasites in Guyana carrying this mutation revealed a fitness cost, which likely explains why this mutation does not spread more frequently. Moreover, in the rodent malaria model *P. berghei* ortholog *Pf*Kelch13 mutations leading to a decreased artemisinin susceptibility also showed decreased growth rates (Simwela et al. 2020). Several attempts to introduce the C580Y mutation in *P. berghei* failed indicating that this mutant is not viable. We also failed to introduce a His-tagged *Pf*Kelch13^{C580Y} mutant in the 3D7 wild-type strain. Since the untagged mutant was already generated in this background (Ghorbal et al. 2014) it is likely that the His-tag together with the mutation is not viable. In general it can be stated, that there is a fine-tuning between fitness costs and artemisinin resistance that is strongly influenced by structural changes in *Pf*Kelch13 and the genetic background of malaria parasites.

4.1.2 Redox function of *Pf*Kelch13

Because of its high structural similary to mammalian Keap1, it was speculated that *Pf*Kelch13 functions as a redox-regulated substrate adaptor in ubiquitination processes (Tilley et al. 2016). Keap1 works as a redox sensor in the cell. Under normal conditions it binds the transcriptional factor Nrf2 that is ubiquitinated and subsequently degraded (Zhang et al. 2005). Oxidation of Keap1 leads to the formation of an intramolecular disulfide bond and the release of Nrf2. The transcriptional factor can enter the nucleus and activate stress response genes (Suzuki et al. 2019). An interaction of *Pf*Kelch13 with a transcriptional factor was not found yet. However, it was shown that the wild-type protein interacts with the phosphatidylinositol 3-kinase (PI3K) whereas the mutation C580Y does not (Mbengue et al. 2015). It was proposed that the decrease in PI3P levels decreases artemisinin susceptibility. Recently published pull-downs using an anti *Pf*Kelch13 antibody (Gnädig et al. 2020) or proximity labeling of *Pf*Kelch13 (Birnbaum et al. 2020) raises doubts of this previous finding since no PI3K was detected. Moreover, the two independent interactomes did not detect

typical proteins that are involved in ubiquitination processes such as ubiquitine ligases (E3) or cullins. Hence, the function of *Pf*Kelch13 as a substrate adaptor in ubiquitination processes seems unlikely. But can a redox regulation of *Pf*Kelch13 be excluded?

It was shown, that artemisinin-resistant *Pf*Kelch13 mutants have higher glutathione levels (Siddiqui et al. 2017). Glutathione has diverse functions within a cell (Deponte 2017). One of its main functions is to remove hydroperoxides. Therefore, it was proposed that artemisinin resistant parasites are also more resistant to oxidative stress (Tilley et al. 2016). We induced oxidative stress in *P. falciparum* with the two oxidants diamide and tBuOOH. Our EC_{50} determinations did not show significant differences between the C580Y mutant and the wild-type (Fig. 23). In addition, the EC_{50} towards artesunate was also not different comparing both strains. This result is in line with observations of other groups (e.g., Siddiqui et al. 2020). The difference between the EC_{50} measurement and a ring stage survival assay could be explained by the duration of drug pressure. Whereas in an EC_{50} measurement the drug is present the whole time of the assay, in a ring stage survival assay, parasites are exposed to the drug with a short pulse. Therefore, it might be possible that C580Y mutant parasites are able to manage oxidant challenges better than the wild-type strain for short but not for long drug exposures (similar to the observed effect for artemisinin for ring stage survival assays in contrast to EC_{50} measurements). In the future it would be interesting to test the toxic effect of oxidants on a shorter time scale in a RSA.

Since C532 and C580 can form a disulfide bond according to the crystal structure (PDB: 4YY8), we wondered whether the redox state of the cysteine residues might explain the decreased artemisinin susceptibility in the C580Y mutant.

We generated the corresponding serine mutations. Both serine mutants showed survival rates similar to the wild-type strain. This result strongly indicates that the redox state of neither C532 nor C580 is responsible for the decreased artemisinin susceptibility. We also found that the serine mutants do not show a decreased solubility when recombinantly expressed in insect cells (Fig. 15). Therefore, it is likely that both mutations do not result in a destabilization of the protein. In the future, growth curves and western blots will clarify if the fitness of the parasites and the protein levels of our mutant *Pf*Kelch13 variants are altered in the parasites. So far, evidence is given that the specific tyrosine substitution at amino acid residue 580 causes a decreased artemisinin susceptibility, maybe through a destabilization of the protein by sterically unfavorable contacts (Singh 2016). The idea that the alteration of

artemisinin susceptibility is linked to specific amino acid substitutions via a general protein destabilization is supported by the spatial distribution of mutations (Chhibber-Goel and Sharma 2019). Unfortunately, we were not able to generate the His-tagged C580Y mutation. Since this mutation was already generated in the same genetic background we used (Ghorbal et al. 2014), it is likely that the introduced N-terminal His-tag has an influence on protein stability.

Although solely the protein level of *Pf*Kelch13 can be responsible for an alteration of artemisinin susceptibility (Fig. 22), specific functions of single amino acid substitutions can not be excluded. In this context we found that – according to the crystal structure - two cysteines of *Pf*Kelch13 are exposed to the surface (C469 and C473), which could have a regulatory function for the protein depending on their redox state. In a DTNB assay we confirmed that two of the seven cysteines are accessible which is in accordance with the crystal structure. Interestingly, a substitution of C469 to tyrosine was found in the field and confirmed to have a decreased artemisinin susceptibility (Siddiqui et al. 2020). We generated the corresponding serine mutation and confirmed it by genotyping PCRs (data not shown). In the future, the performance of a ring stage survival assay will show if the redox state of this cysteine residue has an impact on artemisinin susceptibility. An increased survival rate will hint to a redox involvement whereas an unaltered survival rate will point to a destabilization effect due to the tyrosine substitution (analogous to the mutants C580S and C580Y). Interestingly, we were not able to generate the C473S mutant, which might point to an essential redox-dependent function. To my knowledge mutations of cysteine residue C473 were not detected in the field yet giving at least little evidence that C473 could be essential. To test a possible function of this amino acid residue, I designed a plasmid encoding for GFP-*Pf*Kelch13 to rescue the not viable C473S mutation. The plasmid was also transfected into the His_8-*PFKELCH13* strain to check correct localization of the protein. Microscopy showed defined foci of GFP signals in the periphery of the parasite comparable to the known *Pf*Kelch13 localization (Yang et al. 2019). We checked the overall expression of GFP-*Pf*Kelch13 by measuring the fluorescence of GFP. The strain is ready to select for integration. After successful integration, localization and quantification measurements of His_8-*Pf*Kelch13^{C473S} should be performed in the presence of GFP-*Pf*Kelch13. A decreased His_8-*Pf*Kelch13^{C473S} level would support a destabilization of His_8-*Pf*Kelch13 whereas an unaltered level would support an essential function of the thiol group of C473.

Overall, we provide strong hints that the protein level of *Pf*Kelch13 is directly linked to the artemisinin susceptibility. We propose that specific amino acid substitutions in the propeller domain of *Pf*Kelch13 destabilize the protein resulting in a lower protein level (Fig. 34). The decreased protein level will lead to less hemoglobin uptake which results in less activation of artemisinin. As a consequence parasites will show a decreased growth rate and artemisinin susceptibility. Since the fitness of the parasites is linked to artemisinin susceptibility we propose a maximal survival rate upon an artemisinin treatment of around 40%. Furthermore, we showed that the thiol group of C580 is irrelevant for artemisinin susceptibility, whereas the thiol group of C473 might be essential for the physiological function of *Pf*Kelch13.

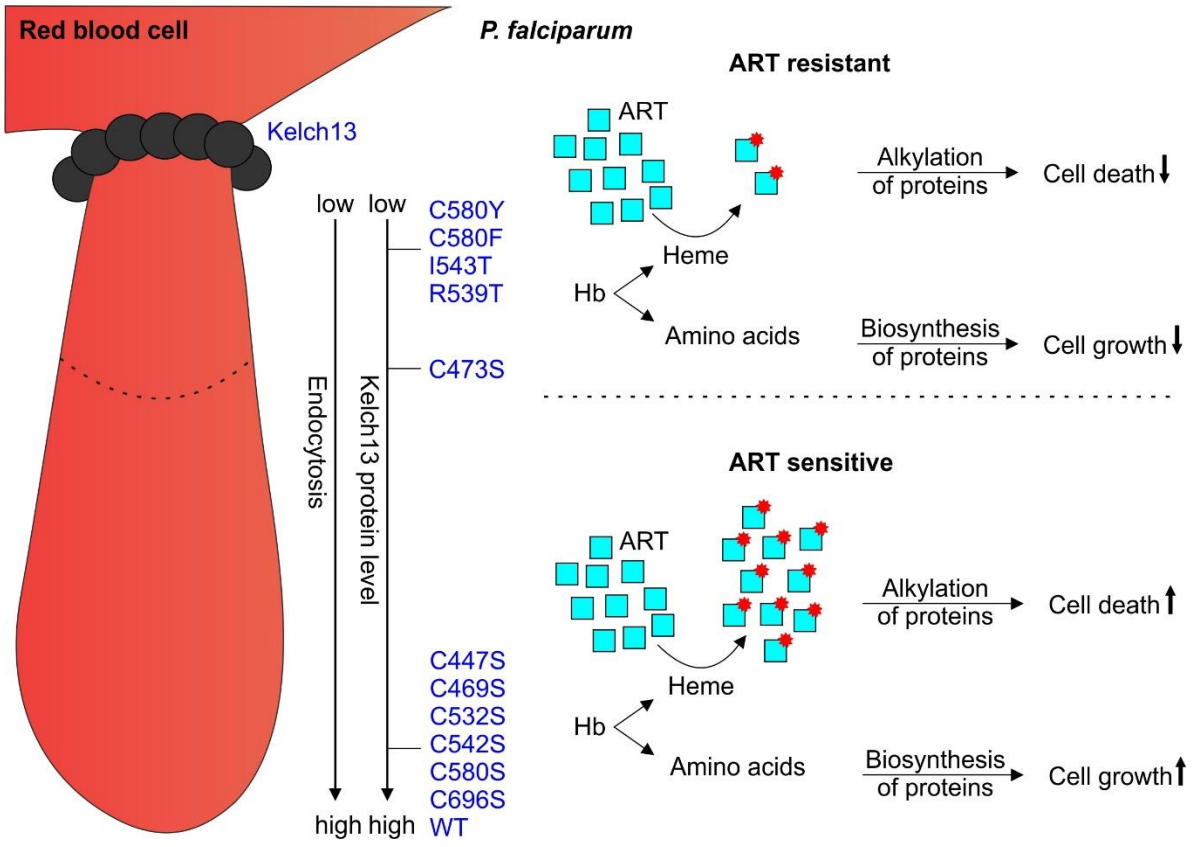

Fig. 34 Proposed model how *Pf*Kelch13 influences the artemisinin susceptibility.

*Pf*Kelch13 is essential for the formation of cytostomes and thereby regulating the uptake of hemoglobin (Hb). The amount of the Hb uptake correlates with the protein level of *Pf*Kelch13. Specific mutations in the propeller domain of the protein destabilize the protein resulting in lower protein levels and a reduced Hb uptake. Upon Hb digestion heme and amino acids are liberated. Amino acids are used for the biosynthesis of proteins guaranteeing normal growth. Heme activates artemisinin (ART) which is thought to result in alkylation processes or to prevent hemozoin formation and parasite death. Parasites with a decreased *Pf*Kelch13 protein level tested with solubility studies in insect cells (indicated mutations in blue) have a decreased artemisinin susceptibility and a decreased growth rate.

4.1.3 The catalytic cycle of *Pf*AOP

*Pf*AOP is one out of five known peroxiredoxins (Prxs) of *P. falciparum*. Mechanistically it belongs to the 1-Cys Prxs and couples to the GSH/Grx system (Djuika et al. 2013). After oxidation of C117 to the sulfenic acid, the surrounding of the peroxidatic cysteine locally unfolds. The exposed sulfenic acid is then either glutathionylated or forms a disulfide intermediate with *Pf*Grx. Indirect evidence was given for a first glutathionylation (Staudacher et al. 2018). We qualitatively tested if oxidized *Pf*AOP can be glutathionylated. Western blots showed that this reaction is possible, and that glutathione can be transferred to *Pf*Grx$^{C32/88S}$.
What could be the advantage of this glutathionylation compared to a mixed disulfide with *Pf*Grx? One advantage could be the availability of high amounts of GSH in the cell, which would guarantee efficient glutathionylation. Although the GSH concentration was not determined in the apicoplast yet, the total concentration in the cell is around 1 mM (Müller 2015). Moreover, it was shown that the redox potential of the apicoplast is -267 mV indicating a high GSH to GSSG ratio (Mohring et al. 2017).
Another advantage could be an effective protection against hyperoxidation. Rate constants for the oxidation of the sulfenic acid in monothiol Prxs are typically in the range of 10^4 $M^{-1}s^{-1}$ (Feld et al. 2019; Staudacher et al. 2018). The here determined rate constants for the glutathionylation of oxidized *Pf*AOP were in the range of 10^5 $M^{-1}s^{-1}$ (Table 25) with an activation energy of ~40 kJ/mol corresponding to the energy of two to three hydrogen bonds. We also recognized a low entropic factor assuming that the glutathionylation of *Pf*AOP is highly enthalpically driven and temperature independent. Such a high rate constant with a low activation energy reflects efficient protection against hyperoxidation. A similar protection against hyperoxidation by glutathionylation was suggested for the typical 2-Cys Prx2 (Peskin et al. 2016). However, the rate constant was much lower, with a value of 500 $M^{-1}s^{-1}$.
The here determined rate constants are around one magnitude higher than the calculated k_{cat}/K_m value determined in an earlier study (Djuika et al. 2013). This difference might indicate a GSH concentration-dependent conformational change that does not result in a change in tryptophan fluorescence which we used as a readout for the here determined rate constant. Whether this conformational change (e.g., local unfolding of the sulfenic acid species) occurs before or after the reaction with GSH remains unclear. In other words, does GSH react with the fully folded protein resulting in a rate-limiting glutathione-induced local unfolding, or does

GSH induce a local unfolding before it reacts with the sulfenic acid (Fig. 35b). In the future, CD measurements could answer if, and at which step, a conformational change in the glutathionylation process is involved. Furthermore, determination of the kinetic values for the glutathionylation of *Pf*AOP^{L109M} will also give hints for a conformational change in this reaction since this mutant is thought to promote local unfolding.

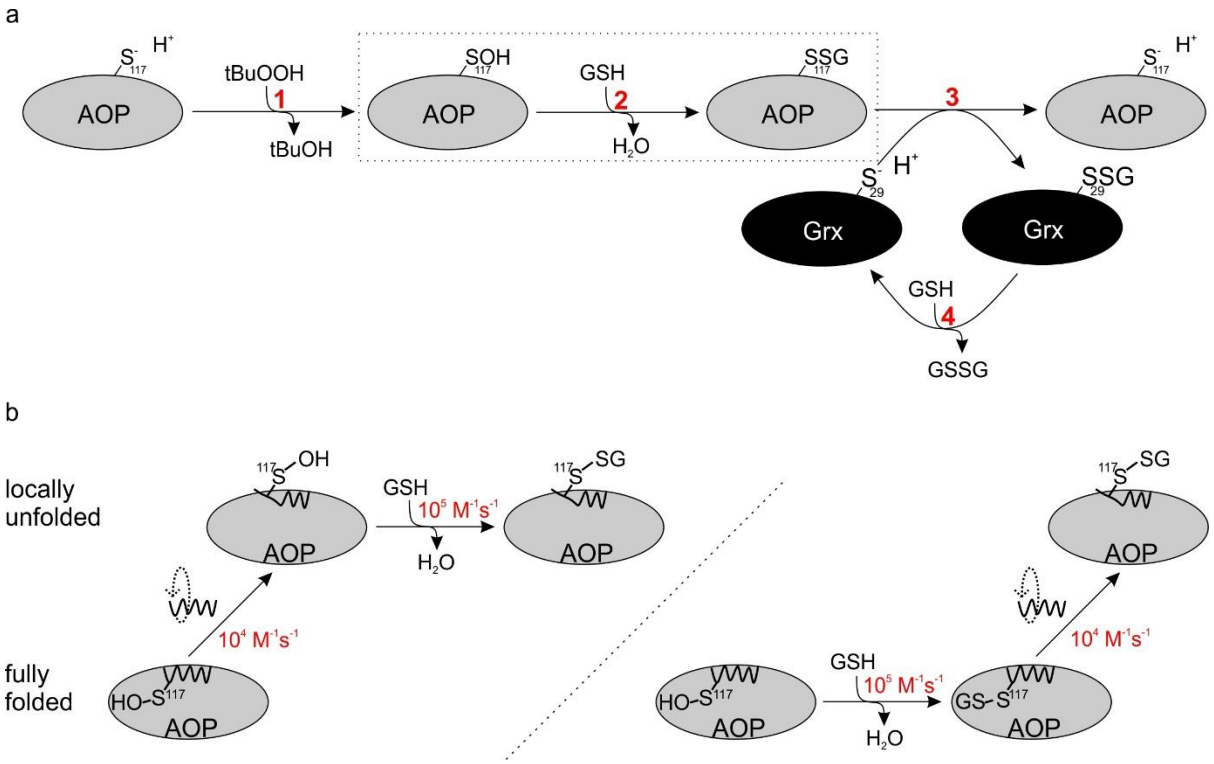

Fig. 35 Model of *Pf*AOP catalysis.

(a) (1) The peroxidatic cysteine C117 of *Pf*AOP is oxidized by a hydroperoxide (here: tBuOOH) to the sulfenic acid whereas the hydroperoxide is reduced to the corresponding alcohol (here: tBuOH). (2) Then, the sulfenic acid is glutathionylated by GSH by the dissociation of a water molecule. (3) The glutathione is transferred from *Pf*AOP to *Pf*Grx reducing *Pf*AOP completely, which can reduce hyroperoxides anew. (4) Glutathionylated *Pf*Grx is reduced by another molecule GSH generating GSSG. **(b)** Reaction steps of the glutathionylation of oxidized *Pf*AOP. By assuming that a local unfolding is the rate-limiting step, two sequential steps of the glutahionylation are possible. Oxidized *Pf*AOP is locally unfolded and then glutathionylated (left) or oxidized *Pf*AOP is first glutahionylated and then locally unfolds (right).

5 References

Abshire JR, Rowlands CJ, Ganesan SM, So PTC, Niles JC (2017) Quantification of labile heme in live malaria parasites using a genetically encoded biosensor. Proc Natl Acad Sci U S A 114:E2068-E2076. https://doi.org/10.1073/pnas.1615195114

Abu Bakar N, Klonis N, Hanssen E, Chan C, Tilley L (2010) Digestive-vacuole genesis and endocytic processes in the early intraerythrocytic stages of Plasmodium falciparum. J Cell Sci 123:441–450. https://doi.org/10.1242/jcs.061499

Achan J (2011) Quinine, an old anti-malarial drug in a modern world: role in the treatment of malaria. Malar J 10:1–12. https://doi.org/10.1186/1475-2875-10-144

Aly ASI, Vaughan AM, Kappe SHI (2009) Malaria parasite development in the mosquito and infection of the mammalian host. Annu Rev Microbiol 63:195–221. https://doi.org/10.1146/annurev.micro.091208.073403

Ariey F, Witkowski B, Amaratunga C, Beghain J, Langlois A-C, Khim N, Kim S, Duru V, Bouchier C, Ma L, Lim P, Leang R, Duong S, Sreng S, Suon S, Chuor CM, Bout DM, Ménard S, Rogers WO, Genton B, Fandeur T, Miotto O, Ringwald P, Le Bras J, Berry A, Barale J-C, Fairhurst RM, Benoit-Vical F, Mercereau-Puijalon O, Ménard D (2014) A molecular marker of artemisinin-resistant Plasmodium falciparum malaria. Nature 505:50–55. https://doi.org/10.1038/nature12876

Baker MS, Gebicki JM (1984) The effect of pH on the conversion of superoxide to hydroxyl free radicals. Arch Biochem Biophys 234:258–264. https://doi.org/10.1016/0003-9861(84)90348-5

Bannister LH, Hopkins JM, Fowler RE, Krishna S, Mitchell GH (2000) A brief illustrated guide to the ultrastructure of Plasmodium falciparum asexual blood stages. Parasitol Today 16:427–433. https://doi.org/10.1016/s0169-4758(00)01755-5

Bartoloni A, Zammarchi L (2012) Clinical aspects of uncomplicated and severe malaria. Mediterr J Hematol Infect Dis 4:e2012026. https://doi.org/10.4084/MJHID.2012.026

Becker K, Rahlfs S, Nickel C, Schirmer RH (2003) Glutathione--functions and metabolism in the malarial parasite Plasmodium falciparum. Biol Chem 384:551–566. https://doi.org/10.1515/BC.2003.063

Bécuwe P, Gratepanche S, Fourmaux MN, van Beeumen J, Samyn B, Mercereau-Puijalon O, Touzel JP, Slomianny C, Camus D, Dive D (1996) Characterization of iron-dependent endogenous superoxide dismutase of Plasmodium falciparum. Mol Biochem Parasitol 76:125–134. https://doi.org/10.1016/0166-6851(95)02552-9

Benting J, Mattei D, Lingelbach K (1994) Brefeldin A inhibits transport of the glycophorin-binding protein from Plasmodium falciparum into the host erythrocyte. Biochem J 300 (Pt 3):821–826. https://doi.org/10.1042/bj3000821

Bhattacharjee S, Coppens I, Mbengue A, Suresh N, Ghorbal M, Slouka Z, Safeukui I, Tang H-Y, Speicher DW, Stahelin RV, Mohandas N, Haldar K (2018) Remodeling of the malaria parasite and host human red cell by vesicle amplification that induces artemisinin resistance. Blood 131:1234–1247. https://doi.org/10.1182/blood-2017-11-814665

Billker O, Shaw MK, Margos G, Sinden RE (1997) The roles of temperature, pH and mosquito factors as triggers of male and female gametogenesis of Plasmodium berghei in vitro. Parasitology 115 (Pt 1):1–7. https://doi.org/10.1017/s0031182097008895

Billker O, Lindo V, Panico M, Etienne AE, Paxton T, Dell A, Rogers M, Sinden RE, Morris HR (1998) Identification of xanthurenic acid as the putative inducer of malaria development in the mosquito. Nature 392:289–292. https://doi.org/10.1038/32667

Billker O, Dechamps S, Tewari R, Wenig G, Franke-Fayard B, Brinkmann V (2004) Calcium and a calcium-dependent protein kinase regulate gamete formation and mosquito transmission in a malaria parasite. Cell 117:503–514. https://doi.org/10.1016/s0092-8674(04)00449-0

Birnbaum J, Flemming S, Reichard N, Soares AB, Mesén-Ramírez P, Jonscher E, Bergmann B, Spielmann T (2017) A genetic system to study Plasmodium falciparum protein function. Nat Methods 14:450–456. https://doi.org/10.1038/nmeth.4223

Birnbaum J, Scharf S, Schmidt S, Jonscher E, Hoeijmakers WAM, Flemming S, Toenhake CG, Schmitt M, Sabitzki R, Bergmann B, Fröhlke U, Mesén-Ramírez P, Blancke Soares A, Herrmann H, Bártfai R, Spielmann T (2020) A Kelch13-defined endocytosis pathway mediates artemisinin resistance in malaria parasites. Science 367:51–59. https://doi.org/10.1126/science.aax4735

Birnboim HC, Doly J (1979) A rapid alkaline extraction procedure for screening recombinant plasmid DNA. Nucleic Acids Res 7:1513–1523. https://doi.org/10.1093/nar/7.6.1513

Blackman MJ, Carruthers VB (2013) Recent insights into apicomplexan parasite egress provide new views to a kill. Curr Opin Microbiol 16:459–464. https://doi.org/10.1016/j.mib.2013.04.008

Bohme CC, Arscott LD, Becker K, Schirmer RH, Williams CH (2000) Kinetic characterization of glutathione reductase from the malarial parasite Plasmodium falciparum. Comparison with the human enzyme. J Biol Chem 275:37317–37323. https://doi.org/10.1074/jbc.M007695200

Boucher MJ, Ghosh S, Zhang L, Lal A, Jang SW, an Ju, Zhang S, Wang X, Ralph SA, Zou J, Elias JE, Yeh E (2018) Integrative proteomics and bioinformatic prediction enable a high-confidence apicoplast proteome in malaria parasites. PLoS Biol 16:e2005895. https://doi.org/10.1371/journal.pbio.2005895

Bradford MM (1976) A rapid and sensitive method for the quantitation of microgram quantities of protein utilizing the principle of protein-dye binding. Anal Biochem 72:248–254. https://doi.org/10.1006/abio.1976.9999

Brancucci NMB, Gerdt JP, Wang C, Niz M de, Philip N, Adapa SR, Zhang M, Hitz E, Niederwieser I, Boltryk SD, Laffitte M-C, Clark MA, Grüring C, Ravel D, Blancke Soares A, Demas A, Bopp S, Rubio-Ruiz B, Conejo-Garcia A, Wirth DF, Gendaszewska-Darmach E, Duraisingh MT, Adams JH, Voss TS, Waters AP, Jiang RHY, Clardy J, Marti M (2017) Lysophosphatidylcholine Regulates Sexual Stage Differentiation in the Human Malaria Parasite Plasmodium falciparum. Cell 171:1532-1544.e15. https://doi.org/10.1016/j.cell.2017.10.020

Bridgford JL (2018) Artemisinin kills malaria parasites by damaging proteins and inhibiting the proteasome. Nat Commun 9:1–9

Bunditvorapoom D, Kochakarn T, Kotanan N, Modchang C, Kümpornsin K, Loesbanluechai D, Krasae T, Cui L, Chotivanich K, White NJ, Wilairat P, Miotto O, Chookajorn T (2018) Fitness Loss under Amino Acid Starvation in Artemisinin-Resistant Plasmodium falciparum Isolates from Cambodia. Sci Rep 8:12622. https://doi.org/10.1038/s41598-018-30593-5

Carbone R, Fré S, Iannolo G, Belleudi F, Mancini P, Pelicci PG, Torrisi MR, Di Fiore PP (1997) eps15 and eps15R are essential components of the endocytic pathway. Cancer Res 57:5498–5504

Chakraborty A (2016) Understanding the biology of the Plasmodium falciparum apicoplast; an excellent target for antimalarial drug development. Life Sci 158:104–110. https://doi.org/10.1016/j.lfs.2016.06.030

Chhibber-Goel J, Sharma A (2019) Profiles of Kelch mutations in Plasmodium falciparum across South Asia and their implications for tracking drug resistance. Int J Parasitol Drugs Drug Resist 11:49–58. https://doi.org/10.1016/j.ijpddr.2019.10.001

Choi S (ed) (2018) Encyclopedia of Signaling Molecules, 2nd edn. Encyclopedia of Signaling Molecules. Springer International Publishing; Springer, Cham

Chugh M, Sundararaman V, Kumar S, Reddy VS, Siddiqui WA, Stuart KD, Malhotra P (2013) Protein complex directs hemoglobin-to-hemozoin formation in Plasmodium falciparum. Proc Natl Acad Sci U S A 110:5392–5397. https://doi.org/10.1073/pnas.1218412110

Cobb DW, Florentin A, Fierro MA, Krakowiak M, Moore JM, Muralidharan V (2017) The Exported Chaperone PfHsp70x Is Dispensable for the Plasmodium falciparum Intraerythrocytic Life Cycle. mSphere 2. https://doi.org/10.1128/mSphere.00363-17

Collins JA, Irnov I, Baker S, Winkler WC (2007) Mechanism of mRNA destabilization by the glmS ribozyme. Genes Dev 21:3356–3368. https://doi.org/10.1101/gad.1605307

Coppée R, Jeffares DC, Miteva MA, Sabbagh A, Clain J (2019) Comparative structural and evolutionary analyses predict functional sites in the artemisinin resistance malaria protein K13. Sci Rep 9:10675. https://doi.org/10.1038/s41598-019-47034-6

Cowman AF, Crabb BS (2006) Invasion of red blood cells by malaria parasites. Cell 124:755–766. https://doi.org/10.1016/j.cell.2006.02.006

Deitsch K, Driskill C, Wellems T (2001) Transformation of malaria parasites by the spontaneous uptake and expression of DNA from human erythrocytes. Nucleic Acids Res 29:850–853. https://doi.org/10.1093/nar/29.3.850

Deligianni E, Morgan RN, Bertuccini L, Kooij TWA, Laforge A, Nahar C, Poulakakis N, Schüler H, Louis C, Matuschewski K, Siden-Kiamos I (2011) Critical role for a stage-specific actin in male exflagellation of the malaria parasite. Cell Microbiol 13:1714–1730. https://doi.org/10.1111/j.1462-5822.2011.01652.x

Deponte M (2017) The Incomplete Glutathione Puzzle: Just Guessing at Numbers and Figures? Antioxid Redox Signal 27:1130–1161. https://doi.org/10.1089/ars.2017.7123

Djuika CF, Fiedler S, Schnölzer M, Sanchez C, Lanzer M, Deponte M (2013) Plasmodium falciparum antioxidant protein as a model enzyme for a special class of glutaredoxin/glutathione-dependent peroxiredoxins. Biochim Biophys Acta 1830:4073–4090. https://doi.org/10.1016/j.bbagen.2013.04.020

Djuika CF, Huerta-Cepas J, Przyborski JM, Deil S, Sanchez CP, Doerks T, Bork P, Lanzer M, Deponte M (2015) Prokaryotic ancestry and gene fusion of a dual localized peroxiredoxin in malaria parasites. Microb Cell 2:5–13. https://doi.org/10.15698/mic2015.01.182

Djuika CF, Staudacher V, Sanchez CP, Lanzer M, Deponte M (2017) Knockout of the peroxiredoxin 5 homologue PFAOP does not affect the artemisinin susceptibility of Plasmodium falciparum. Sci Rep 7. https://doi.org/10.1038/s41598-017-04277-5

Ellman GL (1958) A colorimetric method for determining low concentrations of mercaptans. Arch Biochem Biophys 74:443–450. https://doi.org/10.1016/0003-9861(58)90014-6

Epp C (2008) A regulatable transgene expression system for cultured Plasmodium falciparum parasites. Malar J 7:1–9. https://doi.org/10.1186/1475-2875-7-86

Fairfield AS, Meshnick SR, Eaton JW (1983) Malaria parasites adopt host cell superoxide dismutase. Science 221:764–766. https://doi.org/10.1126/science.6348944

Fast NM, Kissinger JC, Roos DS, Keeling PJ (2001) Nuclear-encoded, plastid-targeted genes suggest a single common origin for apicomplexan and dinoflagellate plastids. Mol Biol Evol 18:418–426. https://doi.org/10.1093/oxfordjournals.molbev.a003818

Feld K, Geissel F, Liedgens L, Schumann R, Specht S, Deponte M (2019) Tyrosine substitution of a conserved active-site histidine residue activates Plasmodium falciparum peroxiredoxin 6. Protein Sci 28:100–110. https://doi.org/10.1002/pro.3490

Florentin A, Cobb DW, Kudyba HM, Muralidharan V (2020) Directing traffic: Chaperone-mediated protein transport in malaria parasites. Cell Microbiol 22:e13215. https://doi.org/10.1111/cmi.13215

Foth BJ, Ralph SA, Tonkin CJ, Struck NS, Fraunholz M, Roos DS, Cowman AF, McFadden GI (2003) Dissecting apicoplast targeting in the malaria parasite Plasmodium falciparum. Science 299:705–708. https://doi.org/10.1126/science.1078599

Francis SE, Sullivan DJ, Goldberg DE (1997) Hemoglobin metabolism in the malaria parasite Plasmodium falciparum. Annu Rev Microbiol 51:97–123. https://doi.org/10.1146/annurev.micro.51.1.97

Gao L, Wang J, Sekhar KR, Yin H, Yared NF, Schneider SN, Sasi S, Dalton TP, Anderson ME, Chan JY, Morrow JD, Freeman ML (2007) Novel n-3 fatty acid oxidation products activate Nrf2 by destabilizing the association between Keap1 and Cullin3. J Biol Chem 282:2529–2537. https://doi.org/10.1074/jbc.M607622200

Garcia GE, Wirtz RA, Barr JR, Woolfitt A, Rosenberg R (1998) Xanthurenic acid induces gametogenesis in Plasmodium, the malaria parasite. J Biol Chem 273:12003–12005. https://doi.org/10.1074/jbc.273.20.12003

Gerald N, Mahajan B, Kumar S (2011) Mitosis in the human malaria parasite Plasmodium falciparum. Eukaryot Cell 10:474–482. https://doi.org/10.1128/EC.00314-10

Ghorbal M, Gorman M, Macpherson CR, Martins RM, Scherf A, Lopez-Rubio J-J (2014) Genome editing in the human malaria parasite Plasmodium falciparum using the CRISPR-Cas9 system. Nat Biotechnol 32:819–821. https://doi.org/10.1038/nbt.2925

Ginsburg H (1990) Some reflections concerning host erythrocyte-malarial parasite interrelationships. Blood Cells 16:225–235

Gisselberg JE, Dellibovi-Ragheb TA, Matthews KA, Bosch G, Prigge ST (2013) The suf iron-sulfur cluster synthesis pathway is required for apicoplast maintenance in malaria parasites. PLoS Pathog 9:e1003655. https://doi.org/10.1371/journal.ppat.1003655

Gnädig NF, Stokes BH, Edwards RL, Kalantarov GF, Heimsch KC, Kuderjavy M, Crane A, Lee MCS, Straimer J, Becker K, Trakht IN, Odom John AR, Mok S, Fidock DA (2020) Insights into the intracellular localization, protein associations and artemisinin resistance properties of Plasmodium falciparum K13. PLoS Pathog 16:e1008482. https://doi.org/10.1371/journal.ppat.1008482

Goldberg DE (2005) Hemoglobin degradation. Curr Top Microbiol Immunol 295:275–291. https://doi.org/10.1007/3-540-29088-5_11

Goldberg DE, Sigala PA (2017) Plasmodium heme biosynthesis: To be or not to be essential? PLoS Pathog 13:e1006511

Group WKG-PS (2019) Association of mutations in the Plasmodium falciparum Kelch13 gene (Pf3D7_1343700) with parasite clearance rates after artemisinin-based treatments—a WWARN individual patient data meta-analysis. BMC medicine 17:1–20. https://doi.org/10.1186/s12916-018-1207-3

Grüring C, Heiber A, Kruse F, Ungefehr J, Gilberger T-W, Spielmann T (2011) Development and host cell modifications of Plasmodium falciparum blood stages in four dimensions. Nat Commun 2:165. https://doi.org/10.1038/ncomms1169

Guggisberg AM, Amthor RE, Odom AR (2014) Isoprenoid biosynthesis in Plasmodium falciparum. Eukaryot Cell 13:1348–1359. https://doi.org/10.1128/EC.00160-14

Hall A, Nelson K, Poole LB, Karplus PA (2011) Structure-based insights into the catalytic power and conformational dexterity of peroxiredoxins. Antioxid Redox Signal 15:795–815. https://doi.org/10.1089/ars.2010.3624

Harding CR, Sidik SM, Petrova B, Gnädig NF, Okombo J, Herneisen AL, Ward KE, Markus BM, Boydston EA, Fidock DA, Lourido S (2020) Genetic screens reveal a central role for heme metabolism in artemisinin susceptibility. Nat Commun 11:4813. https://doi.org/10.1038/s41467-020-18624-0

Hempelmann E (2007) Hemozoin biocrystallization in Plasmodium falciparum and the antimalarial activity of crystallization inhibitors. Parasitol Res 100:671–676. https://doi.org/10.1007/s00436-006-0313-x

Herraiz T, Guillén H, González-Peña D, Arán VJ (2019) Antimalarial Quinoline Drugs Inhibit β-Hematin and Increase Free Hemin Catalyzing Peroxidative Reactions and Inhibition of Cysteine Proteases. Sci Rep 9:15398. https://doi.org/10.1038/s41598-019-51604-z

Huy NT, Shima Y, Maeda A, Men TT, Hirayama K, Hirase A, Miyazawa A, Kamei K (2013) Phospholipid membrane-mediated hemozoin formation: the effects of physical properties and evidence of membrane surrounding hemozoin. PLoS One 8:e70025. https://doi.org/10.1371/journal.pone.0070025

Ismail HM, Barton V, Phanchana M, Charoensutthivarakul S, Wong MHL, Hemingway J, Biagini GA, O'Neill PM, Ward SA (2016) Artemisinin activity-based probes identify multiple molecular targets within the asexual stage of the malaria parasites Plasmodium falciparum 3D7. Proc Natl Acad Sci U S A 113:2080–2085. https://doi.org/10.1073/pnas.1600459113

Jortzik E, Becker K (2012) Thioredoxin and glutathione systems in Plasmodium falciparum. Int J Med Microbiol 302:187–194. https://doi.org/10.1016/j.ijmm.2012.07.007

Kafsack BFC, Rovira-Graells N, Clark TG, Bancells C, Crowley VM, Campino SG, Williams AE, Drought LG, Kwiatkowski DP, Baker DA, Cortés A, Llinás M (2014) A transcriptional switch underlies commitment to sexual development in malaria parasites. Nature 507:248–252. https://doi.org/10.1038/nature12920

Kats LM, Black CG, Proellocks NI, Coppel RL (2006) Plasmodium rhoptries: how things went pear-shaped. Trends Parasitol 22:269–276. https://doi.org/10.1016/j.pt.2006.04.001

Kavran JM, Leahy DJ (2014) Coupling antibody to cyanogen bromide-activated sepharose. Methods Enzymol 541:27–34. https://doi.org/10.1016/B978-0-12-420119-4.00003-3

Ke H, Sigala PA, Miura K, Morrisey JM, Mather MW, Crowley JR, Henderson JP, Goldberg DE, Long CA, Vaidya AB (2014) The heme biosynthesis pathway is essential for Plasmodium falciparum development in mosquito stage but not in blood stages. J Biol Chem 289:34827–34837. https://doi.org/10.1074/jbc.M114.615831

Kehr S, Sturm N, Rahlfs S, Przyborski JM, Becker K (2010) Compartmentation of redox metabolism in malaria parasites. PLoS Pathog 6:e1001242. https://doi.org/10.1371/journal.ppat.1001242

Klonis N, Crespo-Ortiz MP, Bottova I, Abu-Bakar N, Kenny S, Rosenthal PJ, Tilley L (2011) Artemisinin activity against Plasmodium falciparum requires hemoglobin uptake and digestion. Proc Natl Acad Sci U S A 108:11405–11410. https://doi.org/10.1073/pnas.1104063108

Kobayashi A, Kang M-I, Watai Y, Tong KI, Shibata T, Uchida K, Yamamoto M (2006) Oxidative and electrophilic stresses activate Nrf2 through inhibition of ubiquitination activity of Keap1. Mol Cell Biol 26:221–229. https://doi.org/10.1128/MCB.26.1.221-229.2006

Köhler S, Delwiche CF, Denny PW, Tilney LG, Webster P, Wilson RJ, Palmer JD, Roos DS (1997) A plastid of probable green algal origin in Apicomplexan parasites. Science 275:1485–1489. https://doi.org/10.1126/science.275.5305.1485

Koncarevic S, Rohrbach P, Deponte M, Krohne G, Prieto JH, Yates J, Rahlfs S, Becker K (2009) The malarial parasite Plasmodium falciparum imports the human protein peroxiredoxin 2 for peroxide detoxification. Proc Natl Acad Sci U S A 106:13323–13328. https://doi.org/10.1073/pnas.0905387106

Laemmli UK (1970) Cleavage of structural proteins during the assembly of the head of bacteriophage T4. Nature 227:680–685. https://doi.org/10.1038/227680a0

Lambros C, Vanderberg JP (1979) Synchronization of Plasmodium falciparum erythrocytic stages in culture. J Parasitol 65:418–420

Lanzer M, Wickert H, Krohne G, Vincensini L, Braun Breton C (2006) Maurer's clefts: a novel multi-functional organelle in the cytoplasm of Plasmodium falciparum-infected erythrocytes. Int J Parasitol 36:23–36. https://doi.org/10.1016/j.ijpara.2005.10.001

Lazarus MD, Schneider TG, Taraschi TF (2008) A new model for hemoglobin ingestion and transport by the human malaria parasite Plasmodium falciparum. J Cell Sci 121:1937–1949. https://doi.org/10.1242/jcs.023150

Leech JH, Barnwell JW, Aikawa M, Miller LH, Howard RJ (1984) Plasmodium falciparum malaria: association of knobs on the surface of infected erythrocytes with a histidine-rich protein and the erythrocyte skeleton. J Cell Biol 98:1256–1264. https://doi.org/10.1083/jcb.98.4.1256

Liu W, Liu Y (2016) Youyou Tu: significance of winning the 2015 Nobel Prize in Physiology or Medicine. Cardiovascular diagnosis and therapy 6:1

Llorà-Batlle O, Michel-Todó L, Witmer K, Toda H, Fernández-Becerra C, Baum J, Cortés A (2020) Conditional expression of PfAP2-G for controlled massive sexual conversion in Plasmodium falciparum. Sci Adv 6:eaaz5057. https://doi.org/10.1126/sciadv.aaz5057

Lüersen K, Walter RD, Müller S (2000) Plasmodium falciparum-infected red blood cells depend on a functional glutathione de novo synthesis attributable to an enhanced loss of glutathione. Biochem J 346 Pt 2:545–552

Maier AG, Matuschewski K, Zhang M, Rug M (2019) Plasmodium falciparum. Trends Parasitol 35:481–482. https://doi.org/10.1016/j.pt.2018.11.010

Mathieu LC, Cox H, Early AM, Mok S, Lazrek Y, Paquet J-C, Ade M-P, Lucchi NW, Grant Q, Udhayakumar V, Alexandre JS, Demar M, Ringwald P, Neafsey DE, Fidock DA, Musset L (2020) Local emergence in Amazonia of Plasmodium falciparum k13 C580Y mutants associated with in vitro artemisinin resistance. Elife 9. https://doi.org/10.7554/eLife.51015

Mbengue A, Bhattacharjee S, Pandharkar T, Liu H, Estiu G, Stahelin RV, Rizk SS, Njimoh DL, Ryan Y, Chotivanich K, Nguon C, Ghorbal M, Lopez-Rubio J-J, Pfrender M, Emrich S, Mohandas N, Dondorp AM, Wiest O, Haldar K (2015) A molecular mechanism of artemisinin resistance in Plasmodium falciparum malaria. Nature 520:683–687. https://doi.org/10.1038/nature14412

McRobert L, Taylor CJ, Deng W, Fivelman QL, Cummings RM, Polley SD, Billker O, Baker DA (2008) Gametogenesis in malaria parasites is mediated by the cGMP-dependent protein kinase. PLoS Biol 6:e139. https://doi.org/10.1371/journal.pbio.0060139

Mehlin C, Boni E, Buckner FS, Engel L, Feist T, Gelb MH, Haji L, Kim D, Liu C, Mueller N, Myler PJ, Reddy JT, Sampson JN, Subramanian E, van Voorhis WC, Worthey E, Zucker F, Hol WGJ (2006) Heterologous expression of proteins from Plasmodium falciparum: results from 1000 genes. Mol Biochem Parasitol 148:144–160. https://doi.org/10.1016/j.molbiopara.2006.03.011

Mohring F, Rahbari M, Zechmann B, Rahlfs S, Przyborski JM, Meyer AJ, Becker K (2017) Determination of glutathione redox potential and pH value in subcellular compartments of malaria parasites. Free Radic Biol Med 104:104–117. https://doi.org/10.1016/j.freeradbiomed.2017.01.001

Mota MM, Rodriguez A (2004) Migration through host cells: the first steps of Plasmodium sporozoites in the mammalian host. Cell Microbiol 6:1113–1118. https://doi.org/10.1111/j.1462-5822.2004.00460.x

Müller S (2015) Role and Regulation of Glutathione Metabolism in Plasmodium falciparum. Molecules 20:10511–10534. https://doi.org/10.3390/molecules200610511

Nagaraj VA, Sundaram B, Varadarajan NM, Subramani PA, Kalappa DM, Ghosh SK, Padmanaban G (2013) Malaria parasite-synthesized heme is essential in the mosquito and liver stages and complements host heme in the blood stages of infection. PLoS Pathog 9:e1003522. https://doi.org/10.1371/journal.ppat.1003522

Nickel C, Rahlfs S, Deponte M, Koncarevic S, Becker K (2006) Thioredoxin networks in the malarial parasite Plasmodium falciparum. Antioxid Redox Signal 8:1227–1239. https://doi.org/10.1089/ars.2006.8.1227

Niz M de, Burda P-C, Kaiser G, Del Portillo HA, Spielmann T, Frischknecht F, Heussler VT (2017) Progress in imaging methods: insights gained into Plasmodium biology. Nat Rev Microbiol 15:37–54. https://doi.org/10.1038/nrmicro.2016.158

Oborník M, Lukeš J (2015) The Organellar Genomes of Chromera and Vitrella, the Phototrophic Relatives of Apicomplexan Parasites. Annu Rev Microbiol 69:129–144. https://doi.org/10.1146/annurev-micro-091014-104449

Oborník M, Modrý D, Lukeš M, Cernotíková-Stříbrná E, Cihlář J, Tesařová M, Kotabová E, Vancová M, Prášil O, Lukeš J (2012) Morphology, ultrastructure and life cycle of Vitrella brassicaformis n. sp., n. gen., a novel chromerid from the Great Barrier Reef. Protist 163:306–323. https://doi.org/10.1016/j.protis.2011.09.001

Olafson KN, Nguyen TQ, Rimer JD, Vekilov PG (2017) Antimalarials inhibit hematin crystallization by unique drug-surface site interactions. Proc Natl Acad Sci U S A 114:7531–7536. https://doi.org/10.1073/pnas.1700125114

Ogwan'g RA, Mwangi JK, Githure J, Were JBO, Roberts CR, Martin SK (1993) Factors affecting exflagellation of in vitro-cultivated Plasmodium falciparum gametocytes. The American journal of tropical medicine and hygiene 49:25–29

Pagola S, Stephens PW, Bohle DS, Kosar AD, Madsen SK (2000) The structure of malaria pigment beta-haematin. Nature 404:307–310. https://doi.org/10.1038/35005132

Paloque L, Ramadani AP, Mercereau-Puijalon O, Augereau J-M, Benoit-Vical F (2016) Plasmodium falciparum: multifaceted resistance to artemisinins. Malar J 15:149. https://doi.org/10.1186/s12936-016-1206-9

Pandey AV, Babbarwal VK, Okoyeh JN, Joshi RM, Puri SK, Singh RL, Chauhan VS (2003) Hemozoin formation in malaria: a two-step process involving histidine-rich proteins and lipids. Biochem Biophys Res Commun 308:736–743. https://doi.org/10.1016/s0006-291x(03)01465-7

Patzewitz E-M, Wong EH, Müller S (2012) Dissecting the role of glutathione biosynthesis in Plasmodium falciparum. Mol Microbiol 83:304–318. https://doi.org/10.1111/j.1365-2958.2011.07933.x

Payne D (1987) Spread of chloroquine resistance in Plasmodium falciparum. Parasitol Today 3:241–246. https://doi.org/10.1016/0169-4758(87)90147-5

Peatey CL, Skinner-Adams TS, Dixon MWA, McCarthy JS, Gardiner DL, Trenholme KR (2009) Effect of antimalarial drugs on Plasmodium falciparum gametocytes. J Infect Dis 200:1518–1521. https://doi.org/10.1086/644645

Perez-Iratxeta C, Andrade-Navarro MA (2008) K2D2: estimation of protein secondary structure from circular dichroism spectra. BMC Struct Biol 8:25. https://doi.org/10.1186/1472-6807-8-25

Peskin AV, Pace PE, Behring JB, Paton LN, Soethoudt M, Bachschmid MM, Winterbourn CC (2016) Glutathionylation of the Active Site Cysteines of Peroxiredoxin 2 and Recycling by Glutaredoxin. J Biol Chem 291:3053–3062. https://doi.org/10.1074/jbc.M115.692798

Prommana P, Uthaipibull C, Wongsombat C, Kamchonwongpaisan S, Yuthavong Y, Knuepfer E, Holder AA, Shaw PJ (2013) Inducible knockdown of Plasmodium gene expression using the glmS ribozyme. PLoS One 8:e73783. https://doi.org/10.1371/journal.pone.0073783

Prudêncio M, Rodriguez A, Mota MM (2006) The silent path to thousands of merozoites: the Plasmodium liver stage. Nat Rev Microbiol 4:849–856. https://doi.org/10.1038/nrmicro1529

Rhee SG, Jeong W, Chang T-S, Woo HA (2007) Sulfiredoxin, the cysteine sulfinic acid reductase specific to 2-Cys peroxiredoxin: its discovery, mechanism of action, and biological significance. Kidney Int Suppl:S3-8. https://doi.org/10.1038/sj.ki.5002380

Rhee SG (2016) Overview on Peroxiredoxin. Mol Cells 39:1–5. https://doi.org/10.14348/molcells.2016.2368

Richard D, Bartfai R, Volz J, Ralph SA, Muller S, Stunnenberg HG, Cowman AF (2011) A genome-wide chromatin-associated nuclear peroxiredoxin from the malaria parasite Plasmodium falciparum. J Biol Chem 286:11746–11755. https://doi.org/10.1074/jbc.M110.198499

Roncalés M, Vidal-Mas J, Leroy D, Herreros E (2012) Comparison and Optimization of Different Methods for the In Vitro Production of Plasmodium falciparum Gametocytes. J Parasitol Res 2012:927148. https://doi.org/10.1155/2012/927148

Rosenthal MR, Ng CL (2020) Plasmodium falciparum Artemisinin Resistance: The Effect of Heme, Protein Damage, and Parasite Cell Stress Response. ACS Infect Dis 6:1599–1614. https://doi.org/10.1021/acsinfecdis.9b00527

Sarma GN, Nickel C, Rahlfs S, Fischer M, Becker K, Karplus PA (2005) Crystal structure of a novel Plasmodium falciparum 1-Cys peroxiredoxin. J Mol Biol 346:1021–1034

Schafer FQ, Buettner GR (2001) Redox environment of the cell as viewed through the redox state of the glutathione disulfide/glutathione couple. Free Radic Biol Med 30:1191–1212. https://doi.org/10.1016/s0891-5849(01)00480-4

Schieber M, Chandel NS (2014) ROS function in redox signaling and oxidative stress. Curr Biol 24:R453-62. https://doi.org/10.1016/j.cub.2014.03.034

Scholz J (2013) A new method to customize protein expression vectors for fast, efficient and background free parallel cloning. BMC biotechnology 13:1–11. https://doi.org/10.1186/1472-6750-13-12

Seesui K, Imtawil K, Chanetmahun P, Laummaunwai P, Boonmars T (2018) An Alternative Method for Extracting Plasmodium DNA from EDTA Whole Blood for Malaria Diagnosis. Korean J Parasitol 56:25–32. https://doi.org/10.3347/kjp.2018.56.1.25

Sharma YD (1991) Knobs, knob proteins and cytoadherence in falciparum malaria. Int J Biochem 23:775–789. https://doi.org/10.1016/0020-711x(91)90061-q

Siddiqui G, Srivastava A, Russell AS, Creek DJ (2017) Multi-omics Based Identification of Specific Biochemical Changes Associated With PfKelch13-Mutant Artemisinin-Resistant Plasmodium falciparum. J Infect Dis 215:1435–1444. https://doi.org/10.1093/infdis/jix156

Siddiqui FA, Boonhok R, Cabrera M, Mbenda HGN, Wang M, Min H, Liang X, Qin J, Zhu X, Miao J, Cao Y, Cui L (2020) Role of Plasmodium falciparum Kelch 13 Protein Mutations in P. falciparum Populations from Northeastern Myanmar in Mediating Artemisinin Resistance. mBio 11. https://doi.org/10.1128/mBio.01134-19

Sienkiewicz N, Daher W, Dive D, Wrenger C, Viscogliosi E, Wintjens R, Jouin H, Capron M, Müller S, Khalife J (2004) Identification of a mitochondrial superoxide dismutase with an unusual targeting sequence in Plasmodium falciparum. Mol Biochem Parasitol 137:121–132. https://doi.org/10.1016/j.molbiopara.2004.05.005

Sies H (1997) Oxidative stress: oxidants and antioxidants. Exp Physiol 82:291–295. https://doi.org/10.1113/expphysiol.1997.sp004024

Simwela NV, Stokes BH, Aghabi D, Bogyo M, Fidock DA, Waters AP (2020) Plasmodium berghei K13 Mutations Mediate In Vivo Artemisinin Resistance That Is Reversed by Proteasome Inhibition. mBio 11. https://doi.org/10.1128/mBio.02312-20

Singh GP (2016) Structural mapping of Kelch13 mutations associated with artemisinin resistance in malaria. Journal of structural and functional genomics:1–6. https://doi.org/10.1007/s10969-016-9205-1

Smilkstein M, Sriwilaijaroen N, Kelly JX, Wilairat P, Riscoe M (2004) Simple and inexpensive fluorescence-based technique for high-throughput antimalarial drug screening. Antimicrob Agents Chemother 48:1803–1806. https://doi.org/10.1128/aac.48.5.1803-1806.2004

Soito L, Williamson C, Knutson ST, Fetrow JS, Poole LB, Nelson KJ (2011) PREX: PeroxiRedoxin classification indEX, a database of subfamily assignments across the diverse peroxiredoxin family. Nucleic Acids Res 39:D332-7. https://doi.org/10.1093/nar/gkq1060

Soldati D (1999) The apicoplast as a potential therapeutic target in and other apicomplexan parasites. Parasitol Today 15:5–7. https://doi.org/10.1016/s0169-4758(98)01363-5

Spielmann T, Gras S, Sabitzki R, Meissner M (2020) Endocytosis in Plasmodium and Toxoplasma Parasites. Trends Parasitol 36:520–532. https://doi.org/10.1016/j.pt.2020.03.010

Staudacher V, Djuika CF, Koduka J, Schlossarek S, Kopp J, Büchler M, Lanzer M, Deponte M (2015) Plasmodium falciparum antioxidant protein reveals a novel mechanism for balancing turnover and inactivation of peroxiredoxins. Free Radic Biol Med 85:228–236. https://doi.org/10.1016/j.freeradbiomed.2015.04.030

Staudacher V, Trujillo M, Diederichs T, Dick TP, Radi R, Morgan B, Deponte M (2018) Redox-sensitive GFP fusions for monitoring the catalytic mechanism and inactivation of peroxiredoxins in living cells. Redox Biol 14:549–556. https://doi.org/10.1016/j.redox.2017.10.017

Stone JR, Yang S (2006) Hydrogen peroxide: a signaling messenger. Antioxid Redox Signal 8:243–270. https://doi.org/10.1089/ars.2006.8.243

Straimer J, Gnädig NF, Witkowski B, Amaratunga C, Duru V, Ramadani AP, Dacheux M, Khim N, Zhang L, Lam S, Gregory PD, Urnov FD, Mercereau-Puijalon O, Benoit-Vical F, Fairhurst RM, Ménard D, Fidock DA (2015) Drug resistance. K13-propeller mutations confer artemisinin resistance in Plasmodium falciparum clinical isolates. Science 347:428–431. https://doi.org/10.1126/science.1260867

Straimer J, Gnädig NF, Stokes BH, Ehrenberger M, Crane AA, Fidock DA (2017) Plasmodium falciparum K13 Mutations Differentially Impact Ozonide Susceptibility and Parasite Fitness In Vitro. mBio 8. https://doi.org/10.1128/mBio.00172-17

Sturm A, Amino R, van de Sand C, Regen T, Retzlaff S, Rennenberg A, Krueger A, Pollok J-M, Menard R, Heussler VT (2006) Manipulation of host hepatocytes by the malaria parasite for delivery into liver sinusoids. Science 313:1287–1290. https://doi.org/10.1126/science.1129720

Sullivan DJ, Gluzman IY, Goldberg DE (1996) Plasmodium hemozoin formation mediated by histidine-rich proteins. Science 271:219–222. https://doi.org/10.1126/science.271.5246.219

Sutherland CJ (2017) Genetic markers of artemisinin resistance in Plasmodium spp. parasites. Emerging Topics in Life Sciences 1:525–531

Suzuki T, Muramatsu A, Saito R, Iso T, Shibata T, Kuwata K, Kawaguchi S-I, Iwawaki T, Adachi S, Suda H, Morita M, Uchida K, Baird L, Yamamoto M (2019) Molecular Mechanism of Cellular Oxidative Stress Sensing by Keap1. Cell Rep 28:746-758.e4. https://doi.org/10.1016/j.celrep.2019.06.047

Tarun AS, Vaughan AM, Kappe SHI (2009) Redefining the role of de novo fatty acid synthesis in Plasmodium parasites. Trends Parasitol 25:545–550. https://doi.org/10.1016/j.pt.2009.09.002

Tilley L, Straimer J, Gnädig NF, Ralph SA, Fidock DA (2016) Artemisinin Action and Resistance in Plasmodium falciparum. Trends Parasitol 32:682–696. https://doi.org/10.1016/j.pt.2016.05.010

Trager W, Jensen JB (1976) Human malaria parasites in continuous culture. Science 193:673–675

Tu Y (2011) The discovery of artemisinin (qinghaosu) and gifts from Chinese medicine. Nat Med 17:1217–1220. https://doi.org/10.1038/nm.2471

Turra GL, Schneider L, Liedgens L, Deponte M (2021) Testing the CRISPR-Cas9 and glmS ribozyme systems in Leishmania tarentolae. Mol Biochem Parasitol 241:111336. https://doi.org/10.1016/j.molbiopara.2020.111336

Uwimana A, Legrand E, Stokes BH, Ndikumana J-LM, Warsame M, Umulisa N, Ngamije D, Munyaneza T, Mazarati J-B, Munguti K, Campagne P, Criscuolo A, Ariey F, Murindahabi M, Ringwald P, Fidock DA, Mbituyumuremyi A, Menard D (2020) Emergence and clonal expansion of in vitro

artemisinin-resistant Plasmodium falciparum kelch13 R561H mutant parasites in Rwanda. Nat Med. https://doi.org/10.1038/s41591-020-1005-2

Vries PJ de (1996) Clinical Pharmacology and Therapeutic Potential of Artemisinin and its Derivatives in the Treatment of Malaria. Drugs 52:818–836. https://doi.org/10.2165/00003495-199652060-00004

Waller RF, Reed MB, Cowman AF, McFadden GI (2000) Protein trafficking to the plastid of Plasmodium falciparum is via the secretory pathway. EMBO J 19:1794–1802. https://doi.org/10.1093/emboj/19.8.1794

Walliker D, Quakyi IA, Wellems TE, McCutchan TF, Szarfman A, London WT, Corcoran LM, Burkot TR, Carter R (1987) Genetic analysis of the human malaria parasite Plasmodium falciparum. Science 236:1661–1666. https://doi.org/10.1126/science.3299700

Wang J, Zhang C-J, Chia WN, Loh CCY, Li Z, Lee YM, He Y, Yuan L-X, Lim TK, Liu M, Liew CX, Lee YQ, Zhang J, Lu N, Lim CT, Hua Z-C, Liu B, Shen H-M, Tan KSW, Lin Q (2015) Haem-activated promiscuous targeting of artemisinin in Plasmodium falciparum. Nat Commun 6:10111. https://doi.org/10.1038/ncomms10111

Wezena CA, Krafczyk J, Staudacher V, Deponte M (2017) Growth inhibitory effects of standard pro- and antioxidants on the human malaria parasite Plasmodium falciparum. Exp Parasitol 180:64–70. https://doi.org/10.1016/j.exppara.2017.02.017

Wiesner J, Jomaa H (2007) Isoprenoid biosynthesis of the apicoplast as drug target. Curr Drug Targets 8:3–13. https://doi.org/10.2174/138945007779315551

Wilson RJ, Denny PW, Preiser PR, Rangachari K, Roberts K, Roy A, Whyte A, Strath M, Moore DJ, Moore PW, Williamson DH (1996) Complete gene map of the plastid-like DNA of the malaria parasite Plasmodium falciparum. J Mol Biol 261:155–172. https://doi.org/10.1006/jmbi.1996.0449

Wirth CC, Pradel G (2012) Molecular mechanisms of host cell egress by malaria parasites. Int J Med Microbiol 302:172–178. https://doi.org/10.1016/j.ijmm.2012.07.003

Witkowski B, Amaratunga C, Khim N, Sreng S, Chim P, Kim S, Lim P, Mao S, Sopha C, Sam B, Anderson JM, Duong S, Chuor CM, Taylor WRJ, Suon S, Mercereau-Puijalon O, Fairhurst RM, Menard D (2013) Novel phenotypic assays for the detection of artemisinin-resistant Plasmodium falciparum malaria in Cambodia: in-vitro and ex-vivo drug-response studies. Lancet Infect Dis 13:1043–1049. https://doi.org/10.1016/S1473-3099(13)70252-4

Wood ZA, Schröder E, Robin Harris J, Poole LB (2003) Structure, mechanism and regulation of peroxiredoxins. Trends Biochem Sci 28:32–40. https://doi.org/10.1016/s0968-0004(02)00003-8

World Health Organization (2020) World Malaria Report 2019. World Health Organization

Xie SC, Dogovski C, Hanssen E, Chiu F, Yang T, Crespo MP, Stafford C, Batinovic S, Teguh S, Charman S, Klonis N, Tilley L (2016) Haemoglobin degradation underpins the sensitivity of early ring stage Plasmodium falciparum to artemisinins. J Cell Sci 129:406–416. https://doi.org/10.1242/jcs.178830

Xie SC, Ralph SA, Tilley L (2020) K13, the Cytostome, and Artemisinin Resistance. Trends Parasitol 36:533–544. https://doi.org/10.1016/j.pt.2020.03.006

Xiong A, Prakash P, Gao X, Chew M, Tay IJJ, Woodrow CJ, Engelward BP, Han J, Preiser PR (2020) K13-Mediated Reduced Susceptibility to Artemisinin in Plasmodium falciparum Is Overlaid on a Trait of Enhanced DNA Damage Repair. Cell Rep 32. https://doi.org/10.1016/j.celrep.2020.107996

Yang T, Yeoh LM, Tutor MV, Dixon MW, McMillan PJ, Xie SC, Bridgford JL, Gillett DL, Duffy MF, Ralph SA, McConville MJ, Tilley L, Cobbold SA (2019) Decreased K13 Abundance Reduces Hemoglobin Catabolism and Proteotoxic Stress, Underpinning Artemisinin Resistance. Cell Rep 29:2917-2928.e5. https://doi.org/10.1016/j.celrep.2019.10.095

Yayon A, Cabantchik ZI, Ginsburg H (1984) Identification of the acidic compartment of Plasmodium falciparum-infected human erythrocytes as the target of the antimalarial drug chloroquine. EMBO J 3:2695–2700

Yeh E, DeRisi JL (2011) Chemical rescue of malaria parasites lacking an apicoplast defines organelle function in blood-stage Plasmodium falciparum. PLoS Biol 9:e1001138. https://doi.org/10.1371/journal.pbio.1001138

Yeoh S, O'Donnell RA, Koussis K, Dluzewski AR, Ansell KH, Osborne SA, Hackett F, Withers-Martinez C, Mitchell GH, Bannister LH, Bryans JS, Kettleborough CA, Blackman MJ (2007) Subcellular discharge of a serine protease mediates release of invasive malaria parasites from host erythrocytes. Cell 131:1072–1083. https://doi.org/10.1016/j.cell.2007.10.049

Zaw MT, Lin Z, Emran NA (2020) Importance of kelch 13 C580Y mutation in the studies of artemisinin resistance in Plasmodium falciparum in Greater Mekong Subregion. J Microbiol Immunol Infect 53:676–681. https://doi.org/10.1016/j.jmii.2019.07.006

Zhang DD, Lo S-C, Sun Z, Habib GM, Lieberman MW, Hannink M (2005) Ubiquitination of Keap1, a BTB-Kelch substrate adaptor protein for Cul3, targets Keap1 for degradation by a proteasome-independent pathway. J Biol Chem 280:30091–30099. https://doi.org/10.1074/jbc.M501279200

Zhao R-Z, Jiang S, Zhang L, Yu Z-B (2019) Mitochondrial electron transport chain, ROS generation and uncoupling (Review). Int J Mol Med 44:3–15. https://doi.org/10.3892/ijmm.2019.4188